

國立交通大學

電子物理研究所

博士論文

脈衝式近紅外人眼安全雷射研究及探討

The Researches and Investigations of Pulsed
Laser in NIR Eye-safe Wavelength

研究生：張漢龍

指導教授：陳永富 教授

中華民國一〇〇年六月

脈衝式近紅外人眼安全雷射研究及探討
The Researches and Investigations of Pulsed Laser in NIR
Eye-safe Wavelength

研究生：張漢龍

Student: Han-Lung Chang

指導教授：陳永富 教授

Advisor: Prof. Yung-Fu Chen

國立交通大學
電子物理研究所
博士論文

A Dissertation
Submitted to Institute and Electrophysics
College of Science
National Chiao Tung University
In partial Fulfillment of the Requirements
for the Degree of
Doctor of Philosophy
In
Electrophysics

June 2011

Hsinchu, Taiwan, Republic of China

中華民國一〇〇年六月

脈衝式近紅外人眼安全雷射研究及探討

研究生：張漢龍

指導老師：陳永富 教授

國立交通大學電子物理研究所博士班

中文摘要

脈衝式人眼安全雷射在醫療、通訊、遙測、以及雷射雷達、尋標、測距等軍事領域上具有相當廣泛的應用。本文研究幾種產生人眼安全雷射的方式，一方面利用新穎的方法提昇雷射轉換效率，另一方面針對不同應用面的需求，本論文研究幾種不同架構的脈衝式人眼安全雷射的輸出特性。

(一)、利用腔內光參數共振腔技術產生數毫焦耳的高脈衝能量人眼安全雷射，並探討被動式 Q 開關下的雷射閾值特性以及脈衝波形受到熱效應的影響所產生的變化；(二)、使用雙端擴散鍵合的自受激拉曼散射雷射晶體，Nd:YVO₄，除本身具雷射增益產生雷射之外，可自行產生受激拉曼散熱將波長轉換至 1525 奈米人眼安全雷射波段，並且有效降低熱累積，使得轉換效率相對一般無擴散鍵合的受激拉曼散射晶體有效提昇 40% 以上；(三)使用一雙包層之摻鉕/鏡離子大口徑光纖搭配新穎材料，鋁鎵銻量子井半導體，來作為飽和吸收體產生 100 毫焦耳的高能量 1560 奈米人眼安全雷射，除優異的散熱特性之外，更能保持高光束品質的輸出。(四)結合光纖雷射散射佳的特性、使用一大口徑摻鏡光子光纖搭配鋁鎵銻量子井半導體高調制深度的優點，產生高脈衝能量雷射，並使用週期性反轉鋁酸鋰晶體透過光參數共振腔產生一波長可調的人眼安全雷射，波長調整範圍超過 80 奈米。(五)使用鋁鎵銻量子井半導體當作雷射增益介質，透過光激發的方式以及面射型的架構下產生一高光束品質的腔外面射型雷射，並且探討由能障區激發及量子井區激發的輸出特性，在量子井區激發架構下，可有效降低熱的產生，將整體轉換效率提昇到 30% 以上。雷射輸出脈衝功率達 500 瓦。

藉由本論文對脈衝式近紅外人眼安全雷射的基礎研究及理論分析，我們可更進一步掌握各架構的特性，並依此優化系統轉換效率及性能，進而滿足各應用面的需求。

The Researches and Investigations of Pulsed Laser in NIR Eye-safe Wavelength

Student: Han-Lung Chang

Advisor: Prof. Yung-Fu Chen

Institute and Department of Electrophysics
National Chiao Tung University

ABSTRACT

Pulsed eye-safe lasers have drawn great interest since their wide potential in kinds of applications such as medical treatment, telecom communication, range-finder, and laser radar, etc. In this thesis, we study several schemes in realizing the NIR eye-safe lasers for different applications by employing novel materials and improving the conversion efficiency.

(a). In an intracavity optical parametric oscillator (OPO), a subnanosecond ten mJ eye-safe laser was demonstrated. We theoretically and experimentally investigated the threshold of an intracavity OPO pumped by a passively Q-switched laser and the dynamics of output pulse influenced by the thermal effect in the gain medium. (b). In the configuration of self stimulated Raman scattering (SRS), we employed a double-end diffusion-bonded Nd:YVO₄ crystal to decrease the accumulated heat. The performance of the self-SRS laser at 1525 nm is found to be nearly 40% higher than that with a conventional Nd:YVO₄ crystal. (c). By employing an AlGaInAs semiconductor saturable absorber in a passively Q-switched Er/Yb codoped large-mode-area fiber laser, we demonstrated a passively Q-switched fiber laser at 1560 nm with output energy up to 100 μJ with high beam quality and good thermal management. (d) A passively Q-switched photonic crystal fiber (PCF) laser with an AlGaInAs saturable absorber was employed as pump source in an external-cavity OPO. By tuning the temperature of nonlinear crystal, periodically poled lithium niobate (PPLN), in the OPO, the tuning range of signal in eye-safe regime up to 80 nm was obtained. (e). An AlGaInAs QW/barrier was used as a gain medium in the external cavity surface emitting laser with high beam quality. The performance of barrier and in-well pumping schemes were investigated. The quantum defect is lower in in-well pumping and consequently the conversion efficiency is enhanced to 30% and a high peak output power up to 500 W was generated.

Based on these fundamental investigations in this thesis, we can know well the characteristics of these configurations of NIR pulsed eye-safe lasers and further expand the researches to meet kinds of applications.

誌謝

Acknowledgement

『你知道我有多少次想像這一刻的到來？想好你和我坐在這裡，要說些什麼話。』當電影"型男飛行日誌"中的主角達到一千萬飛行哩程的時候這麼對機長說著。我也曾這樣想過，想好當這一刻來臨時，要如何對那些在這一路走來不斷給于我幫助以及精神上鼓勵的前輩及朋友們寫出我心中的感謝。但不知道從什麼時候開始，我便不再覺得這一刻是個終點，雖然在這一年來，歷經一連串的低潮及挫折的事件，似乎是要告訴我，想要攻上這座山頭，就是要經歷這一番心智、精神、體力、以及情感上考驗，才足以在往後的道路上直挺地走下去…。這，便是成長的過程。

非常感謝我的指導教授，陳永富老師這幾年來對我的栽培，陳老師是個有大智慧的人，每次在與他的對談之中，總是能在他的隻字片語裡感受到對生命以及對生活上的熱忱以及樂觀態度；在學術上，更是在信手拈來之間，便能發現研究的樂趣以及奧妙，叫人讚佩。老師總是要我別想太多，凡事自有安排，但做事卻要有規劃，才能看得遠、有效率；並且告訴我惟有提昇自己，才能走到哪裡都順遂。簡單扼要，卻受用無窮。

感謝黃凱風老師的指導，是個既和善又具有學術素養的老師，學識淵博，總是能在簡短字語之間就能表達複雜的物理觀念。感謝閻偉中博士，一位既溫文儒雅、又熱心助人的前輩跟主管。在我的博士研究生涯中，他總是不吝伸出他的手，毫無保留地提供他的意見及資源協助我。對他我的心中總是有道不盡的感謝，卻一直無法當面說出口。

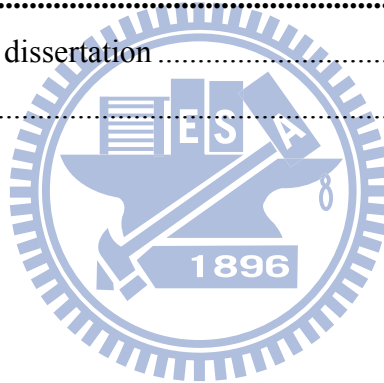
感謝周遭所有朋友們的大力支持，家銘、馬克、阿格西、戴博、還有其他同事，在我情感最脆弱、工作最繁忙的時候，不斷地支援我、開導我，聽我說心事。感謝寵棟以及碩泰，以前共患難的戰友，在畢業後仍不斷地協助我，在他們身上學到了許多對於人生的態度。還有實驗室的學長姐以及學弟妹們，不形於色的老大、不拘小節的小黃、活力四射的興弛、熱心義氣的哲彥、實驗快手依萍、講話如機槍的毅帆、個性溫和的威哲、見解獨到的彥廷、心思細膩的毓捷、來自純樸東台灣的郁仁哥、行事低調的昆毅、對學術充滿熱忱的舜子、實作超強的小江，還有三句話內就能帶動笑聲的易純，雖然我的年紀要大上他們許多，但是與他們相處，總是讓自己感覺更年輕充滿了活力。謝謝善筑，相處時間雖不長，但讓我對生活充滿新的期待。

在此，謹以此文，獻給我最摯愛的雙親及家人。感謝他們的教育之恩以及多年來不帶任何壓力的支持、關懷以及鼓勵。

Contents

中文摘要.....	i
ABSTRACT.....	ii
誌謝.....	iii
目錄.....	iv
表目錄.....	vi
圖目錄.....	vi
Chapter 1 Introduction	1
1.1 Motivation	2
1.2 Optical Parametric Oscillator	4
1.3 Stimulated Raman Scattering (SRS).....	10
1.4 Erbium/Ytterbium Fiber Laser	14
1.5 Optically-pumped Semiconductor Laser (OPSL).....	19
1.6 Overview of this dissertation.....	26
Chapter 2 Passively Q-switched Eye-safe Laser with Optical Parametric Oscillator	31
2.1 Intracavity OPO Pumped with Nd-doped Laser.....	32
2.2 Experimental setup	33
2.2.1 Theoretical analysis of threshold.....	37
2.2.2 Experimental results and discussions	40
2.3 The influence of birefringence on pulse behavior in OPO	44
2.3.1 Theoretical analysis and discussion in birefringence effect	46
2.4 Conclusion	53
Chapter 3 Self-Stimulated Raman Scattering Laser	56
3.1 Self-Stimulated Raman Scattering.....	57
3.2 Experimental setup	59
3.3 Experimental results and discussions	61
3.3.1 Thermal lensing effect in a 1342-nm cavity.....	61
3.4 Conclusion	70
Chapter 4 Passively Q-switched Erbium/Ytterbium Fiber Laser.....	73
4.1 Semiconductor Saturable Absorber	74
4.2 Experimental setup	77
4.3 Results and discussions	81
4.4 Conclusion.....	86

Chapter 5 Widely Tunable Eye-safe Laser with Photonic Crystal Fiber	89
5.1 Experimental setup and results	92
5.1.1 Diode pumped PCF laser with AlGaInAs semiconductor absorber	92
5.1.2 External-cavity OPO.....	99
5.2 Conclusion	104
Chapter 6 Optically Pumped Semiconductor Laser.....	108
6.1 OPSL with barrier-pumping	109
6.1.1 Device fabrication and laser structure	109
6.1.2 Experimental results and discussion.....	113
6.2 OPSL with in-well-pumping.....	120
6.2.1 Device fabrication and experimental setup	120
6.2.2 Experimental results and discussions	126
6.3 Conclusion	132
Chapter 7 Summary	135
7.1 Contribution of this dissertation	136
7.2 Future work.....	139



List of Tables

Table 1.3-1. The parameters of commercial Raman crystals.....	13
Table 5.1-1. The property of Yb doped rod-type PCF.	94

List of Figures

Chapter 1

Fig. 1.1-1. Transmission spectrum of human eyes [4]. The laser radiation after 1400 nm is absorbed by the ocular fluid of eyes and is called as eye-safe laser.....	3
Fig. 1.2-1. An incident field creates a source and then radiates an optical field. The radiated field would have higher order term [5].	5
Fig. 1.2-2. (a) Schematic of three-wave nonlinear process (b) Energy conservation diagram of nonlinear process; (c) Momentum diagram under phase matching condition	7
Fig. 1.2-3. The schematics of (a) External-cavity OPO; NLC: nonlinear crystal. (b) Intra-cavity OPO; GM: gain medium.....	9
Fig. 1.3-1. The schematics of Stimulated Raman Scattering.....	12
Fig. 1.4-1. (a) The absorption spectrum of Er^{3+} and codoped $\text{Er}^{3+}/\text{Yb}^{3+}$; (b) Energy level diagram in codoped $\text{Er}^{3+}/\text{Yb}^{3+}$ fiber.....	15
Fig. 1.4-2. The schematic of double-cladding fiber.....	17
Fig. 1.4-3. Different cladding design for increasing the pump absorption efficiency in cores.....	18
Fig. 1.6-1. Schematic of typical VECSEL device.....	20
Fig. 1.6-2. (a) The lattice constant diagram of semiconductor compounds; (b) The corresponding compounds versus radiated wavelength.....	21
Fig. 1.6-3. Quantum well arrangement: (a) Periodic structure of quantum wells. The separation between successive pairs is designed to be half wavelength. (b) The quantum number as a function of the overlapping of optical intensity of lasing mode and pump mode [21].	23
Fig. 1.6-4. The method of thermal management: (a) Heat minimization by thinning the device or bonding a transparent heat spreader [22]. (b) In-well pumping could have better thermal control than barrier pumping.	24
Fig. 1.7-1. The overall structures of eye-safe lasers reported in this dissertation.....	27

Chapter 2

- Fig. 2.2-1.** Experimental setup for an intracavity OPO pumped by a high-power QCW diode pumped passively Q-switched Nd:YAG laser in a shared resonator. 34
- Fig. 2.2-2.** (a) The schematics of diode power coupled by a lens duct. (b) ~ (d) The simulation result of intensity pattern in the image plane with 5-mm diameter from the exit surface of lens duct, 0.5 mm, 3 mm, and 5 mm respectively. The corresponding transmittance is 91.7 %, 87.9 %, and 68.4 %. 35
- Fig. 2.2-3.** Calculated results for the dependence of the threshold photon density on the output reflectivity R_s 39
- Fig. 2.2-4.** (a) Experimental results for the threshold pump energy versus the OPO output reflectivity. (b) Experimental results for the pulse energy of the signal output versus the OPO output reflectivity 41
- Fig. 2.2-5.** Experimental results for the temporal shapes of the fundamental and the signal pulses..... 42
- Fig. 2.2-6.** Experimental results for the peak power of the signal output versus the OPO output reflectivity..... 43
- Fig. 2.3-1.** The output temporal pulse at 1573 nm for different reflectivity of output couple..... 45
- Fig. 2.3-2.** The schematic of depolarization due to thermally induced birefringence effect. 48
- Fig. 2.3-3.** The temporal pulse of simulation result for the value of $\Gamma = 0$ and 0.03. The result shows the influence of depolarization and the dependence of signal output reflectivity..... 51
- Fig. 2.3-4.** The output energy versus different output signal reflectivity. The solid lines are numerical results of theoretical analysis for different value of Γ . The empty circles with error bar are experimental results..... 52

Chapter 3

- Fig. 3.2-1.** Experimental setup of (a) a diode-end-pumped actively Q-switched Nd:YVO₄ Raman laser; (b) CW operation at 1342 nm for measuring thermal lens effect.60
- Fig. 3.3-1.** (a) The method for measuring the thermal lens by estimating the critical cavity length in a 134-nm cavity. (b) Dependences of thermal lensing power on input pump power for conventional and double-end diffusion-bonded

Nd:YVO ₄ CW laser at 1342 nm.	64
Fig. 3.3-2. Optical spectrum of the diode-pumped actively Q-switch Nd:YVO ₄ self-Raman laser.z.....	65
Fig. 3.3-3. The average output power at 1525 nm with respect to the input pump power at pulse repetition rates of 20 and 40 kHz shown as the down-triangle and circle symbols respectively for the double-end diffusion-bonded Nd:YVO ₄ crystal and that at 20 kHz shown as the square symbol for a conventional Nd:YVO ₄ crystal [1]......	68
Fig. 3.3-4. Temporal characteristics of the fundamental and Raman pulses at a pulse repetition rate of (a) 40 kHz and (b) 20 kHz with a pump power of 17.2W.	69

Chapter 4

Fig. 4.1-1. The energy diagram of (a) InGaAsP QWs/barriers; (b) AlGaInAs QWs/barriers.....	75
Fig. 4.2-1. Transmittance spectrum at room temperature for the AR-coated AlGaInAs/InP SESA device.	79
Fig. 4.2-2. Schematic of the experimental setup for EYDFL comprising a 7-m Er-Yb codoped fiber and an external feedback cavity with a periodic AlGaInAs QW/barrier structure as a saturable absorber. HR, high reflection; HT, high transmission.	80
Fig. 4.3-1. Dependence of the average output power on the incident pump power for the cw and passive Q-switching operations.....	83
Fig. 4.3-2. Pulse repetition rate and the pulse energy versus the incident pump power.	84
Fig. 4.3-3. (a) Oscilloscope traces of a typical Q-switched envelope., (b) Oscilloscope traces of a train of Q-switched pulses.....	85

Chapter 5

Fig. 5.1-1. The experimental setup of external-cavity pumped OPO with PCF fiber.	93
Fig. 5.1-2. (a) The image of cross section of rod-type PCF. (b) The transmission spectrum and structure of AlGaInAs saturable absorber, which consists of 50 groups of three quantum wells.....	96
Fig. 5.1-3. The output power of the passively Q-switched PCF laser versus the 976-nm launched pump power. Inset, the lasing spectrum obtained with 12.5 W of	

pump power.	97
Fig. 5.1-4. Typical oscilloscope traces of output pulses of the passively Q-switched PCF laser. (a) Pulse shape with 6.3 W of pump power. (b) Pulse shape with 13.1 W of pump power.	98
Fig. 5.1-5. The schematics of external-cavity OPO setup. A half-wave plate and polarization beam splitter cube were settled in front of OPO to control the input pump power.	100
Fig. 5.1-6. The output performance of external-cavity OPO. (a) The averaged output power of signal wave versus averaged power of PCF laser. (b) The temporal traces of pump and signal wave.	102
Fig. 5.1-7. The tuning curve of signal wavelength versus different operating temperature. Inset, the conversion efficiency versus operating temperature.	103

Chapter 6

Fig. 6.1-1. (a) Experimental configuration of the high-peak-power AlGaInAs QWs 1570-nm laser pumped by a Q-switched Nd:GdVO ₄ laser; HR: high reflection, HT: high transmission, PR: partial reflection. (b) Actual setup.	111
Fig. 6.1-2. Room-temperature spontaneous emission spectrum of the AlGaInAs QWs pumped by a Q-switched Nd:GdVO ₄ 1064-nm laser.	112
Fig. 6.1-3. Experimental results for the optically pumped AlGaInAs 1570-nm laser operated at the water temperature of 10°C at pump repetition rates of 20, 30, 40, and 60 kHz. Inset shows typical lasing spectrum obtained with 1.0 W of average pump power at a repetition rate of 30 kHz.	114
Fig. 6.1-4. Typical oscilloscope traces of pump and output pulse.	115
Fig. 6.1-5. (a) Experimental results for the peak output power versus peak pump power at a repetition rate of 20 kHz; (b) the transmittance of the gain chip versus the excitation intensity at 1.57 μm.	118
Fig. 6.1-6. Input–output characteristics for the water temperatures of 10, 15, 20, and 25°C at a repetition rate of 30 kHz.	119
Fig. 6.2-1. Schematic explanation of energy diagrams of (a) barrier pumping and (b) in-well pumping.	121
Fig. 6.2-2. The schematic of the AlGaInAs/InP eye-safe laser at 1555 nm. HR: high reflection; HT: high transmission; PR: partial reflection.	124


- Fig. 6.2-3.** (a) The transmission spectrum of AlGaInAs/InP quantum-well/barrier structure. (b) the room-temperature spectrum of photoluminescence pumped by an actively Q-switched Nd:YVO₄ 1342-nm laser. (c) The single pass absorption efficiency of single and double AlGaInAs QW chips..... 125
- Fig. 6.2-4.** The performance of single-chip AlGaInAs 1555-nm laser for 40 kHz and 12°C operation in the scheme of barrier and in-well pumping, respectively. The solid lines are forth order polynomial fitting curves. The in-well pumping scheme exhibits good performance in conversion efficiency..... 127
- Fig. 6.2-5.** Performance of double chips: (a) Experimental results for the optically pumped AlGaInAs eye-safe laser operated at 12 °C for several pulse repetition rates. The repetition rate for optimum performance of conversion efficiency was between 40 kHz and 60 kHz. (b) Typical lasing spectrum at repetition rate of 40 kHz and average pump power of 0.65 W. 128
- Fig. 6.2-6.** (a) The output characteristics of double chips in in-well pumping (50 kHz) and of single chip in barrier pumping (30 kHz) were measured for the operation of different temperature. (b) The output peak power of double-chip in-well pumping AlGaInAs laser at the repetition rate of 20 kHz. 130
- Fig. 6.2-7.** The typical pump and output pulse train and the expanded pulse shape of a single pulse. 131

Chapter 7

- Fig. 7.2-1.** (a) The concept of narrow-linewidth tunable eye-safe laser. (b) The simulated result of signal output wavelength pumped by tunable PCF laser..... 140

Chapter 1

Introduction



1.1 Motivation

The motivation for this thesis started with the intention to develop a range finder with high pulse energy up to several milli-joules. The range between the target and the observer is obtained by measuring the time of flight of laser pulse. Most commercial products of range finder are with the wavelength around $1.5\mu\text{m}$ for the requirement of eye-safe regulations. The radiation around $1.5\mu\text{m}$ within eye-safe region is absorbed mainly in the ocular fluid of the eye before the retina such that the damage threshold of the eye is greatly increased (Fig. 1.1-1). With the increasing requirements in different applications and operating modes, for example, a hand-held range finder in the battle field requires high pulse energy with repetition rate in the 0.2~10 Hz level while a laser radar requires pulses with high repetition rate in the range of kHz to tens kHz. On the other hand, due to the fact that high-peak-power lasers operated at the eye-safe region near 1.5-1.6 μm have been attracting versatile interesting applications including telecom communication, 3D image, medical treatment, gas sensing, range-finder, designator, laser radar, and laser target [1]-[3], we expand the investigations to kinds of laser sources in different schemes.

In this thesis I report the present progress of my investigations and researches in realizing NIR eye-safe laser sources: (a) Optical parametric oscillators (OPO) pumped by high peak power neodymium (Nd) lasers operating at the 1064-nm line. (b) Self-stimulated Raman scattering (SRS) lasers pumped by pulsed Nd lasers operating at the 1340-nm lines. (c) Utilizing Erbium/Ytterbium (Er:Yb) ion-doped double cladding fiber as gain materials for generating 1.54- μm radiation. (d) A tunable laser with photonic crystal fiber (PCF). And (e) optically pumped semiconductor lasers with AlInGaAs Qw/barrier materials. Each method possesses different optical characteristics but one common issue that affects the performance is the thermal effect. The influence of thermal effect in those configurations will be taken care and the output performance will be investigated and discussed in the following chapters. In this dissertation, I will focus on the development of pulsed laser generation in NIR eye-safe region and on the investigations of the technology and physics.

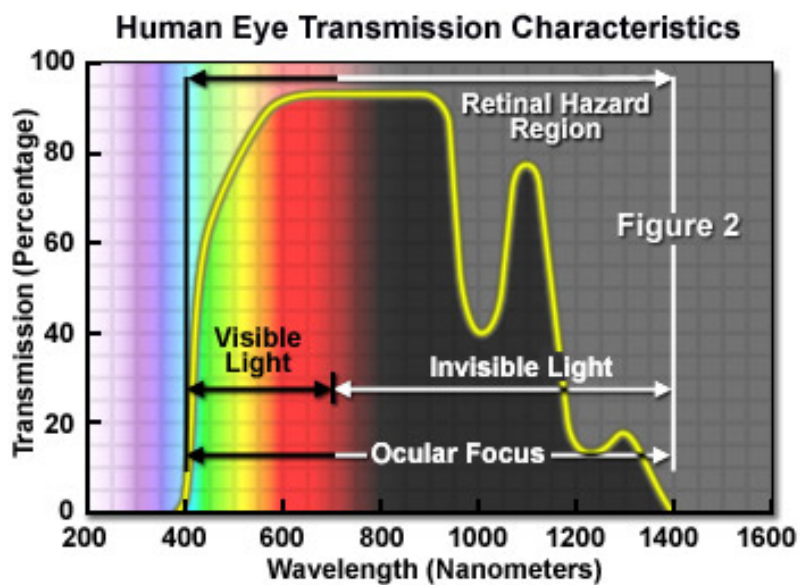


Fig. 1.1-1. Transmission spectrum of human eyes [4]. The laser radiation after 1400 nm is absorbed by the ocular fluid of eyes and is called as eye-safe laser.

1.2 Optical Parametric Oscillator

When an electromagnetic field with angular frequency ω_1 is incident on a dielectric material, the dipoles inside the atoms react by starting to oscillate. Such an oscillation will radiate a new field. Nonlinear wavelength conversion process is a result of higher order of dipole response (Fig. 1.2-1). Dipole response is frequency related but usually considered as linear with incident electric field under low intensity. If a nonlinear crystal, however, is illuminated with high intensity, the dipole response and then radiated light would contain higher order term which means the radiated field has higher order frequency.

$$\begin{aligned}
 P(z,t) &= \varepsilon_0 \chi^{(1)} E(z,t) + \varepsilon_0 \chi^{(2)} E^2(z,t) + \varepsilon_0 \chi^{(3)} E^3(z,t) + \dots \\
 &= \underbrace{P^{(1)}(z,t)}_{\text{Linear}} + \underbrace{P^{(2)}(z,t) + P^{(3)}(z,t) + \dots}_{\text{Nonlinear}}
 \end{aligned} \tag{1-1}$$

When the 2nd-order dipole response ($P^{(2)}(z,t)$) is considered, which means only three waves are involved (Fig. 1.2-2(a)), the pump source with frequency ω_1 can be regarded providing gain via the nonlinear crystal to the other two radiated waves with frequency ω_2 and ω_3 (Fig. 1.2-2(b)). To finish the process, these three frequency components have to satisfy energy conservation and momentum conservation:

$$\begin{cases} \omega_1 = \omega_2 + \omega_3 \\ \vec{k}_1 = \vec{k}_2 + \vec{k}_3 \end{cases} \tag{1-2}$$

Since materials are always dispersive, only under specific condition the above equations could be held simultaneously. That is,

$$\begin{cases} \frac{1}{\lambda_1} = \frac{1}{\lambda_2} + \frac{1}{\lambda_3} \\ \frac{2\pi}{\lambda_1} n_1(\lambda_1) = \frac{2\pi}{\lambda_2} n_2(\lambda_2) + \frac{2\pi}{\lambda_3} n_3(\lambda_3) \end{cases} \tag{1-3}$$

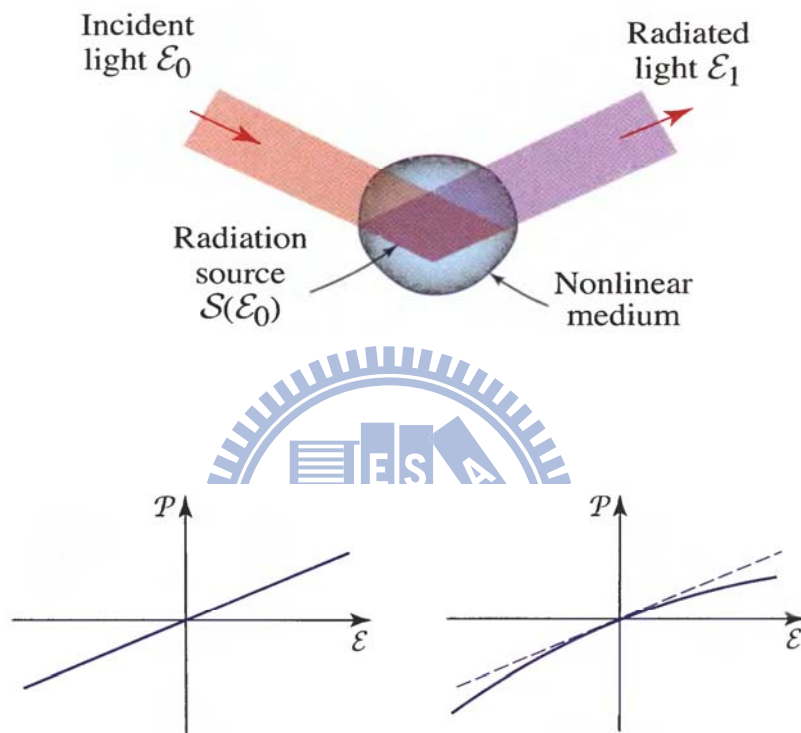


Fig. 1.2-1. An incident field creates a source and then radiates an optical field. The radiated field would have higher order term [5].

where λ_i is the corresponding wavelength and n_i is the corresponding refractive index. We can derive the relationship of involved three electric fields, E_{ω_1} , E_{ω_2} , and E_{ω_3} , from Maxwell's equations and obtain the following coupled wave equations of derivatives of fields along propagation direction,

$$\begin{cases} \frac{\partial E_{\omega_1}}{\partial z} = -j \frac{\omega_1 d_{eff}}{c_0 n_{\omega_1}} E_{\omega_2} E_{\omega_3} e^{j\Delta k z} \\ \frac{\partial E_{\omega_2}}{\partial z} = -j \frac{\omega_2 d_{eff}}{c_0 n_{\omega_2}} E_{\omega_1} E_{\omega_3}^* e^{-j\Delta k z} \\ \frac{\partial E_{\omega_3}}{\partial z} = -j \frac{\omega_3 d_{eff}}{c_0 n_{\omega_3}} E_{\omega_1} E_{\omega_2}^* e^{-j\Delta k z} \end{cases} \quad (1-4)$$

where d_{eff} is the 2nd-order nonlinear coefficient of material, c_0 light of speed, and $\Delta \vec{k} = \vec{k}_{\omega_1} - \vec{k}_{\omega_2} - \vec{k}_{\omega_3}$. When $\Delta \vec{k} = \vec{k}_{\omega_1} - \vec{k}_{\omega_2} - \vec{k}_{\omega_3} = 0$ is termed as phase matching condition and could be diagramed as Fig. 1.2-2(c).

From the coupled wave equations, we can see that if the phase matching condition is not satisfied ($\Delta \vec{k} \neq 0$), the amplitude of field will oscillate with $e^{j\Delta k z}$ and can not grow up. On the contrary, when the condition is satisfied, the field will have an exponential gain under the situation of non-depleted pump source. Since the energy level between ω_2 and ω_3 is a virtual level, we could design an appropriate condition to obtain output light with desired frequency and this nonlinear wavelength conversion process is referred to as optical parametric process.

If an additional oscillator is added to store energy of radiated waves in the parametric process, this is referred to as optical parametric oscillator (OPO). The first OPO was demonstrated in 1965 by Giordmaine and Miller and operated around 1 μm [6]. Depending on the choice of mirrors, different types of OPOs can be constructed. For example, it is possible to let one or two or three waves be resonated in the OPO, resulting in singly resonant (SRO), doubly resonant OPOs (DRO), or triply resonant OPOs (TRO). If one of the phases of three waves is fixed, for example, the phase of pump source in an external-cavity OPO

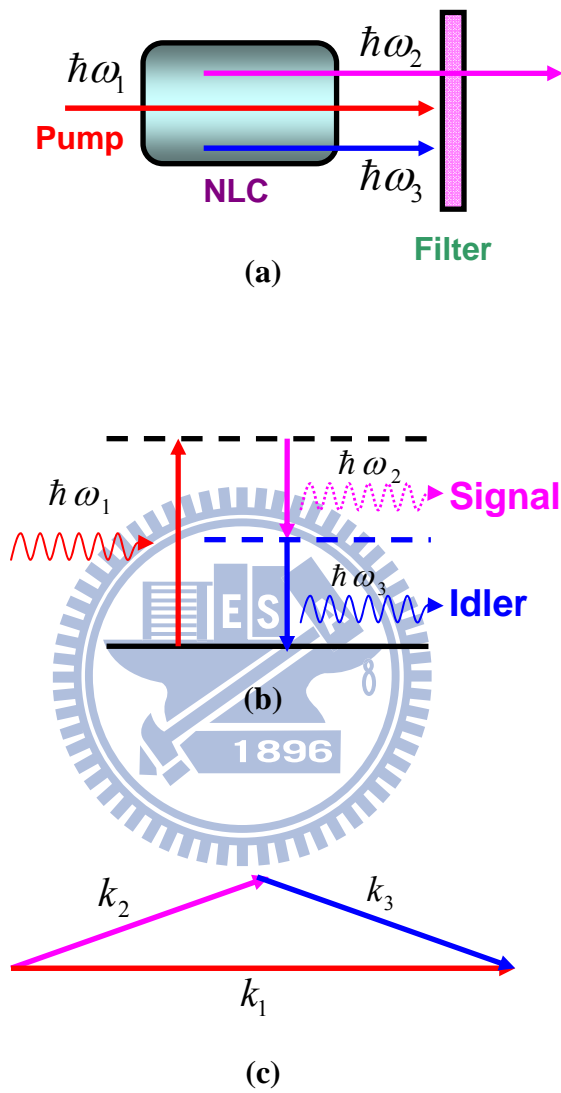
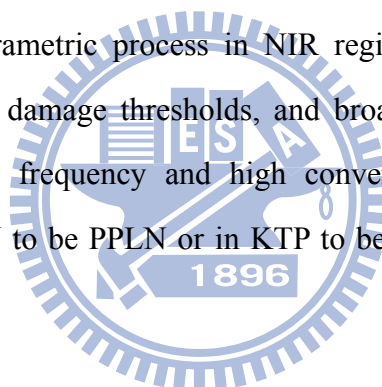


Fig. 1.2-2. (a) Schematic of three-wave nonlinear process (b) Energy conservation diagram of nonlinear process; (c) Momentum diagram under phase matching condition

configuration, the alignment of a DRO cavity is more stringent than a SRO in order to simultaneously satisfy the phase matching condition and cavity phase. As a result, the most frequently used setup is the SRO, in which only the signal or idler is resonated.

Typically a wavelength-conversion system consists of a separated pump laser and an OPO configuration. This is referred to as external cavity OPO (Fig. 1.2-3(a)). An alternative configuration is the intracavity OPO, where the OPO is inserted into the laser cavity (Fig. 1.2-3(b)). In a nonlinear parametric process, the small-gain coefficient is proportional to laser intensity. Therefore, compared with the configuration of external cavity OPO, the intracavity OPO takes the advantage of higher laser intensity within the pump laser cavity to lower threshold and increase overall conversion efficiency.

At the present day, KTiOPO_4 (KTP) and LiNbO_3 (LN) are the most popular nonlinear crystals used in optical parametric process in NIR region due to the advantages of high nonlinear coefficients, high damage thresholds, and broad transmission spectrum. To have more flexibility of tunable frequency and high conversion efficiency, the technique of quasi-phase matching in LN to be PPLN or in KTP to be PPKTP has been attracting lots of interest.



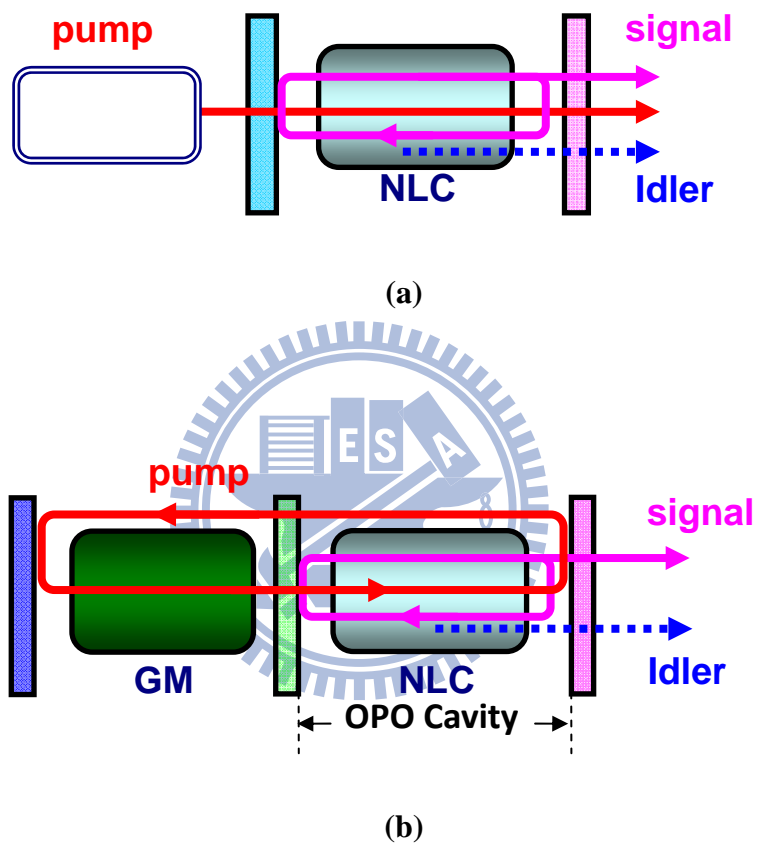


Fig. 1.2-3. The schematics of (a) External-cavity OPO; NLC: nonlinear crystal. (b) Intra-cavity OPO; GM: gain medium.

1.3 Stimulated Raman Scattering (SRS)

Unlike optical parametric process, Raman scattering is a 3rd-order nonlinear and inelastic scattering process where the incident light reacts with the vibrational mode of crystal lattice and losses energy or gets energy from the lattice. The first spontaneous scattering effect was first discovered by C. V. Raman in 1928. Raman scattering results in a frequency shift equal to phonon vibration frequency ω_v and called as Raman shift. When the incident photon losses phonon energy, it is referred to as Stoke process and the photon becomes Stoke photon. On the contrary, it is referred to as anti-Stoke process if the incident photon obtains phonon energy. For both conditions, additional peak from pump incident photon in the spectrum will be observed.

Stimulated Raman scattering occurs when a stoke photon is incident together with a pump photon, the pump photon will transfer into another stoke photon and be stimulated to be coherent with the incident stoke photon (Fig. 1.3-1). Pump beam can be regarded to provide gain via the Raman crystal to the Stoke photons and amplify the incident photons. This can be achieved by introducing an oscillator to the Raman active medium. The mirrors of the oscillator are coated with high reflectivity or partial reflectivity in the frequency of the Stoke photons. The Stokes field will experience gain and if the Raman active medium is placed between two mirrors and the gain is strong enough to overcome the cavity's losses, oscillation at Stokes frequency will occur.

Though stimulated Raman scattering process is a 3rd-order nonlinear or four-wave mixing process, there are only two photons involved, ω_p and ω_s . And the Raman shift does not depend on the pump laser wavelength, nor requires phase matching condition. Therefore, for generating eye-safe laser with SRS, only the pump source with proper wavelength and the Raman gain medium have to be considered. In order to provide enough gain, high pump intensity is required since the Raman gain is proportional to pump intensity. As intracavity OPO, an intracavity SRS also have the merits of decreasing the lasing threshold and increase the conversion efficiency.

Recently, the discovery of new Raman materials gives birth to the laser sources at new wavelengths. In the recent years, eye-safe lasers from SRS frequency conversion have been successfully demonstrated in several Raman materials such as $\text{Ba}(\text{NO}_3)_2$, YVO_4 , GdVO_4 , SrWO_4 , KGWO_4 , BaWO_4 , and PbWO_4 [7]-[12]. Some of the Raman materials and their relative parameters are listed as Table 1.3-1. . Those materials are favored because they possess high Raman gain, high cross section, narrower linewidth, and high damage threshold. By incorporating the pump source and corresponding Raman gain medium, it is much practicable to realize an eye-safe laser. During those crystals, YVO_4 or GdVO_4 are attracting more interest since they perform not just only as Raman crystals but also laser gain materials after doping with active ions such as neodymium (Nd). In the later chapter, I will discuss such materials can be used as both Raman crystals and laser gain materials simultaneously which is called as Self-SRS.



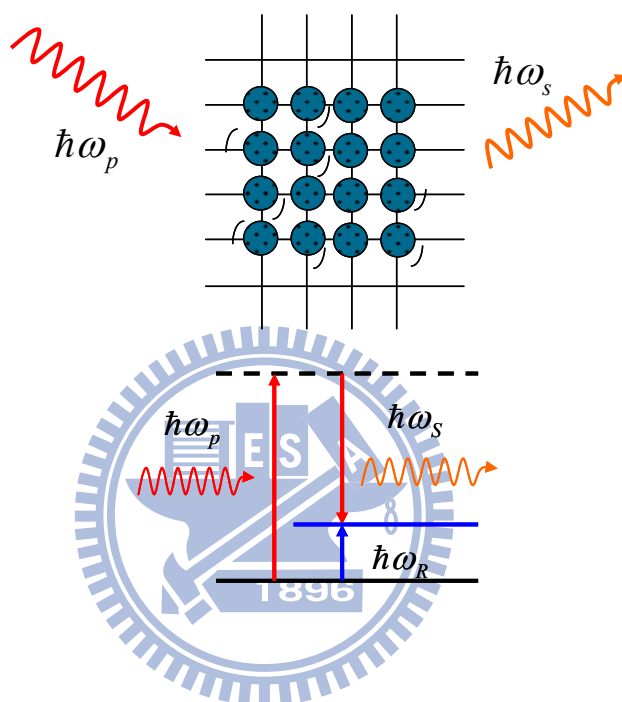


Fig. 1.3-1. The schematics of Stimulated Raman Scattering.

Material	Raman shift (cm ⁻¹)	Raman linewidth (cm ⁻¹)	Cross section (arb. Units)	Raman gain (cm/GW)	Damage threshold (GW/cm ²)
Ba(NO ₃) ₂	1047	0.4	21	11	~ 0.4
BaWO ₄	924	1.6	52	8.5	~ 5
KGd(WO ₄) ₂	768	6.7	59	4.4	~ 10
	901	5.7	54	3.3	
YVO ₄	890	2.6	92	> 4.5	~ 1
GdVO ₄	882	3	92	> 4.5	~ 1

Table 1.3-1. The parameters of commercial Raman crystals.

1.4 Erbium/Ytterbium Fiber Laser

Fiber was firstly proposed to be doped with rare-earth elements such as erbium (Er), ytterbium (Yb), neodymium (Nd), praseodymium (Pr), and thulium (Tm), to be an active fiber since 1985. Such a fiber has been used to provide gain and amplify signal in a laser system. The doped element will decide the wavelength of fluorescence region. For eye-safe region, Nd^{3+} [13], Tm^{3+} [9] and Pr^{3+} [10] are mostly used to generate light source with high pulse energy and high peak power owing to their large cross section. Similar to bulk solid-state lasers, the gain fiber purely doped with Er^{3+} ions to lase at $1.54 \mu\text{m}$ has the problem of weak absorption. Therefore, doping with Yb^{3+} ions to sensitize Er^{3+} can greatly enhance the absorption at all room temperature since Yb^{3+} has a broad absorption from 0.9 to $1 \mu\text{m}$ (Fig. 1.4-1(a)). On the other hand, it can reduce the clustering of Er^{3+} ions, and allow for higher Er^{3+} concentrations without strong quenching effects. In the codoped Er/Yb fiber, radiation from a laser diode pumps the strong $2\text{F}_{7/2}-2\text{F}_{5/2}$ transition in Yb^{3+} (Fig. 1.4-1(b)). The excited Yb^{3+} ions transfer energy to the $4\text{I}_{11/2}$ level of Er^{3+} owing to the good overlap between the upper states of Yb^{3+} and Er^{3+} . The erbium ions then relax to the upper laser level $4\text{I}_{13/2}$ and lasing occurs down to the $4\text{I}_{15/2}$ manifold.

A single mode fiber (SMF) is designed to follow the rule of V-number under the value of 2.405. That is,

$$V = \frac{2\pi a}{\lambda} \sqrt{(n_1^2 - n_2^2)} = \frac{2\pi a}{\lambda} NA < 2.405 \quad (1-5)$$

where a is the core diameter, λ is the propagation wavelength, n_1 and n_2 are the refractive index of core, and cladding, respectively. NA demotes numerical aperture. Equation 1-5 shows that the single mode fiber has to be designed to keep the source into single mode signal. However, suffering from the high NA value of inner cladding, the skew rays of pump light enter the fiber off the fiber axis and zigzag down the fiber without crossing the axis. Those skew rays are regards as higher order modes guiding in the fiber. Those higher order modes possess poor mode overlapping with the core region of fiber such that the pump light can not

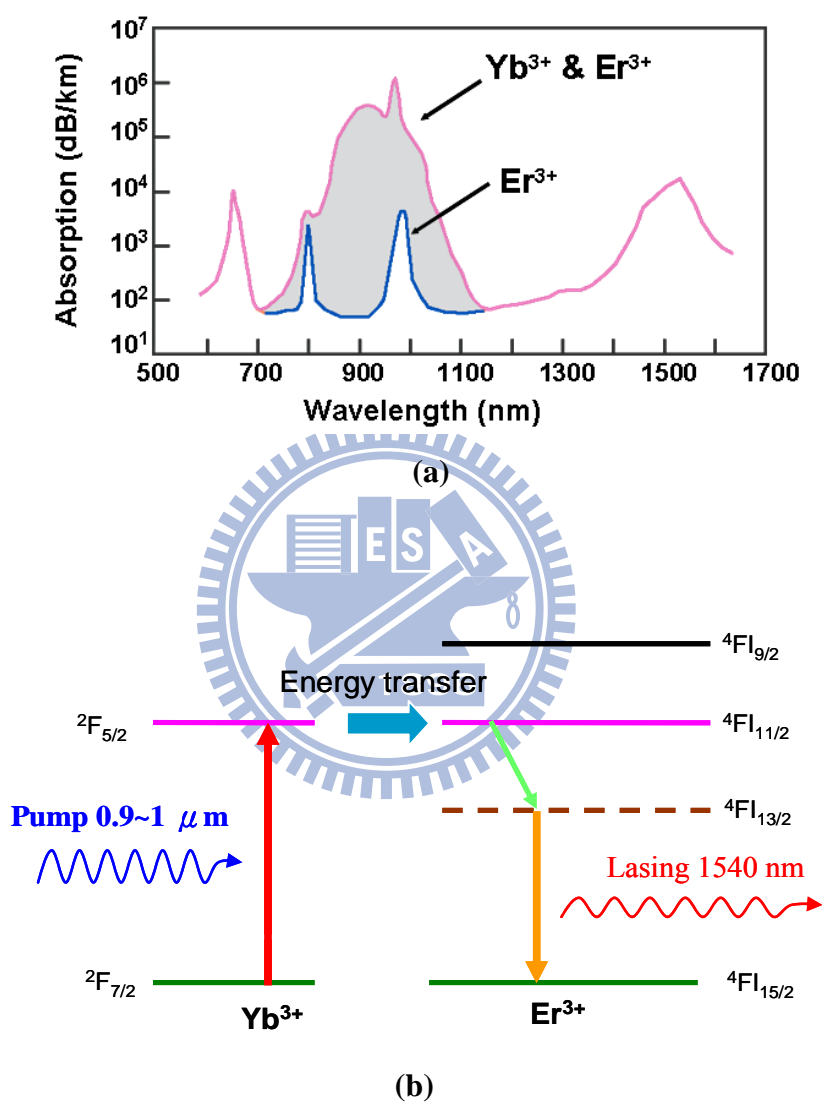


Fig. 1.4-1. (a) The absorption spectrum of Er^{3+} and codoped $\text{Er}^{3+}/\text{Yb}^{3+}$; (b) Energy level diagram in codoped $\text{Er}^{3+}/\text{Yb}^{3+}$ fiber.

be effectively absorbed. To overcome the limitation, consequently, a longer fiber length or an ingenious clad-design for higher absorption is needed to achieve an efficient fiber laser. Especially, a fiber with circular symmetry would have the worst coupling efficiency. As a result, there are a variety of designs of double-clad fibers to reduce symmetry of inner-cladding. For example, by designing the shape of core in an asymmetry type such as D-shape, rectangular shape, elliptic shape or petal structure (Fig. 1.4-3) the absorption efficiency can be greatly enhance up to 100 times than in a fiber with a symmetrically circular core shape.

Because of the merits of high spatial beam quality, low thermal lensing and their properties of beam confinement combined with excellent heat dissipation, double-clad fiber lasers are getting popular and competitive to conventional bulk solid-state lasers with regard to high-power applications.



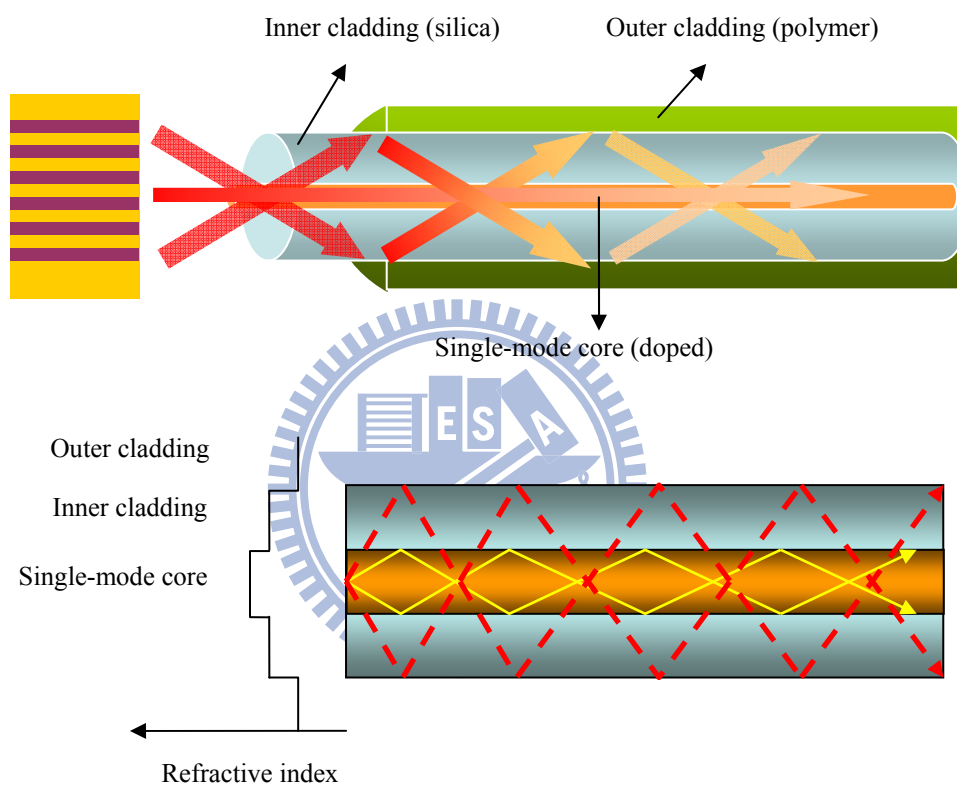


Fig. 1.4-2. The schematic of double-cladding fiber.

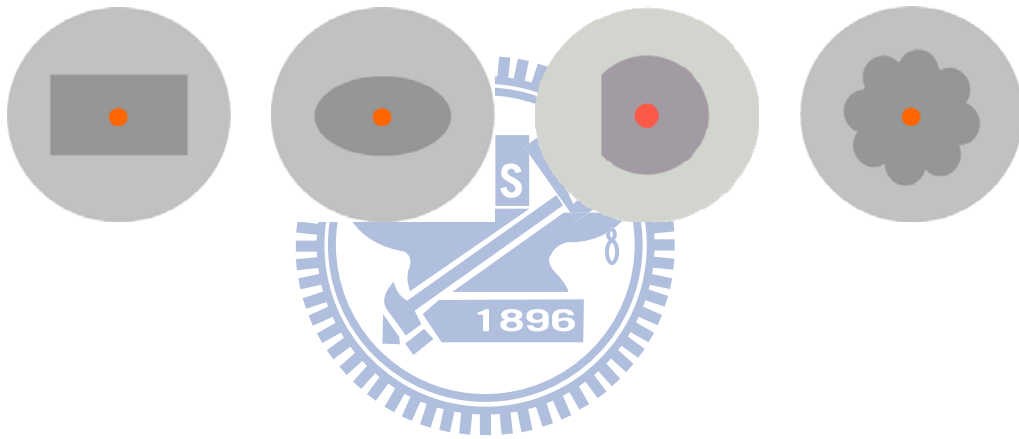


Fig. 1.4-3. Different cladding design for increasing the pump absorption efficiency in cores.

1.5 Optically-pumped Semiconductor Laser (OPSL)

Vertical-external-cavity surface-emitting-laser (VECSEL), which is a small laser similar to vertical-cavity surface-emitting-laser (VCSEL) but without two high reflectors on the device, is grown with series of quantum wells to be an active layer incorporated with a Bragg reflector layer on semiconductor substrate (Fig. 1.5-1). The concept of using an external cavity enables integration of additional elements to improve the performance and flexibility in cavity design. Such a laser has the cavity axis along the direction of carrier flow instead of perpendicular to the flow as in conventional edge-emitting laser diodes and the radiation emerges from the surface of the cavity. Since the active region length is very short compared with the lateral dimensions, it is easier to obtain single longitudinal mode due larger mode spacing. On the other hand, unlike normal edge-emitting semiconductor laser, owing to the large emitting surface, it can generate a near diffraction-limited laser beam with single symmetrically transverse mode.

The quantum wells could be arranged in periodic or aperiodic way and covered by a window layer to prevent oxidation and surface recombination. These processes can be accomplished by MEMs techniques such as metal-organic chemical vapor deposition (MOCVD), or molecular beam epitaxy (MBE). The materials of quantum well/barrier and substrate are variety depending on the required wavelength. The composition of semiconductor compounds could be selected to from a new alloy from the engineered lattice constant diagram according to Vegard's law (Fig. 1.5-2 (a)). In eye-safe region, GaInNAs/GaAs, InGaAsP/InP, and AlGaInAs/InP are popularly utilized [17]-[19] (Fig. 1.5-2 (b)) since high quality multilayer structures to be grown are allowed.

Optically pumped vertical-external-cavity surface-emitting-lasers (OP-VECSEL) belong to an emerging class of semiconductor lasers that combine high output power with a diffraction limited output beam. It is also referred to as OPSL. In parallel with the impressive characteristics of those electrically-driven devices, the advantages of OPSL compared with electrically-driven semiconductor laser are the availability of uniform and high-power

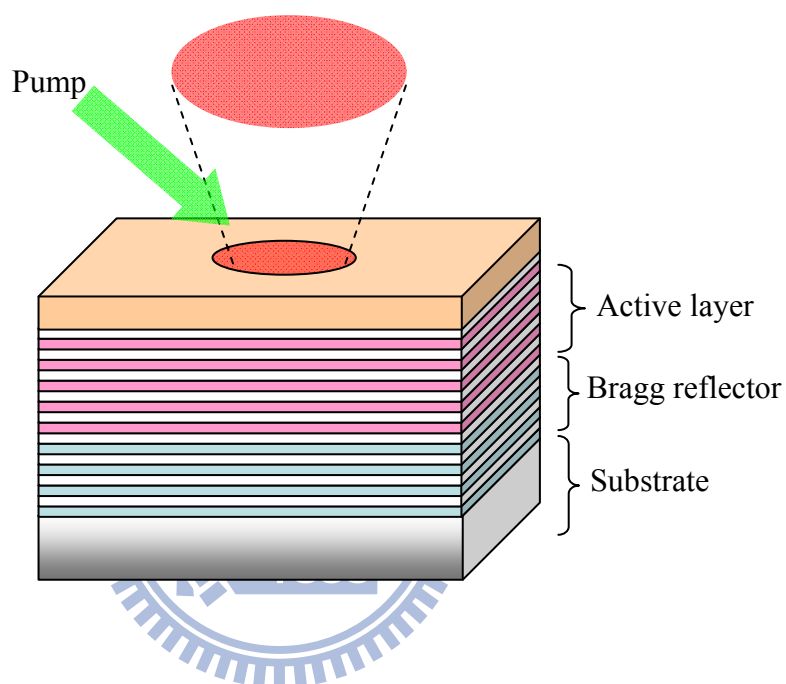


Fig. 1.5-1. Schematic of typical VECSEL device

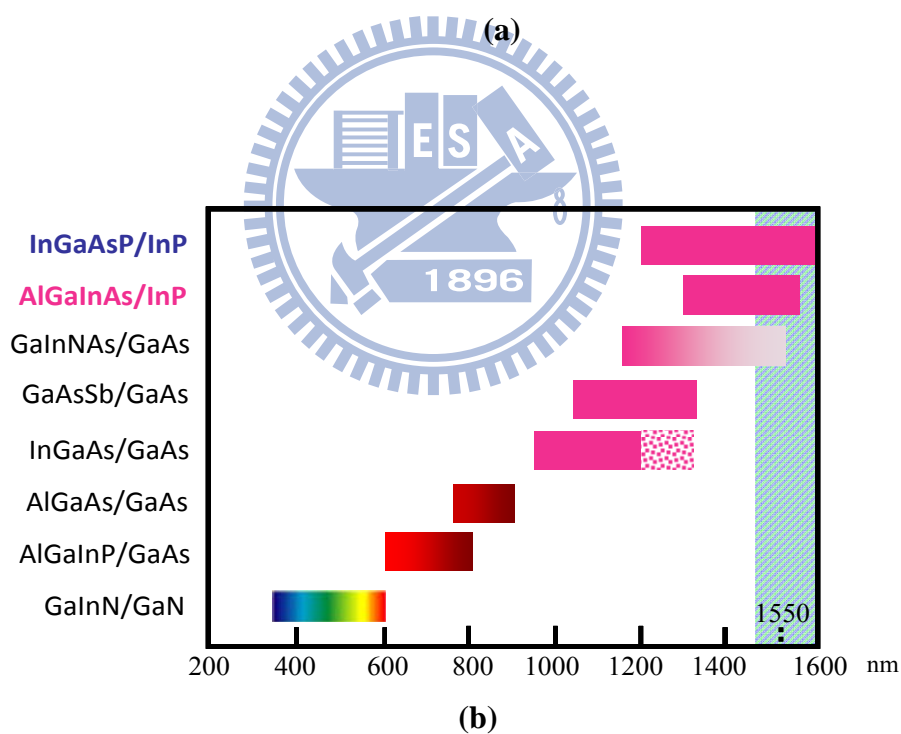
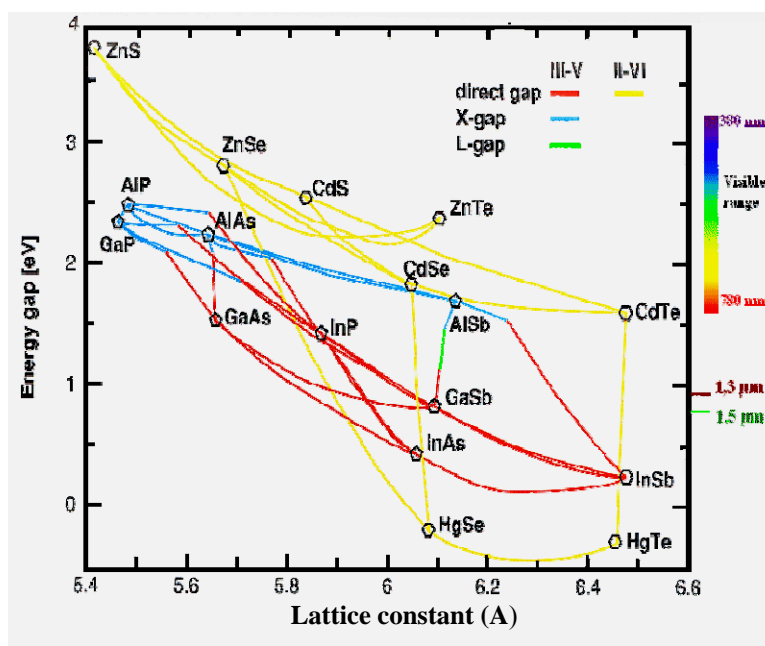


Fig. 1.5-2. (a) The lattice constant diagram of semiconductor compounds; (b) The corresponding compounds versus radiated wavelength.

pumping as well as larger cavity mode size. This result in a good mode matching and single transverse mode with high output power, wavelength controllable and fast dynamics.

Since quantum wells in the active layer offers gain and they are laid onto the wafer during the growth process, their thickness and position in the structure can be optimized. Quantum wells are stacked perpendicular to the optical propagation axis and spaced by barriers. The fluorescence radiated from each quantum well is feed back by the oscillator and resonates in the cavity. In order to obtain resonant periodic gain, the quantum wells are usually centrally designed to be located at the antinodes of the lasing mode of the micro-cavity standing wave, or to have intervals of half-wavelength separated by barriers [19], [20]. Hence, gain locates where it is most accessible and only where it is required thus eliminating saturation effects and spatial hole burning. The technique was used to improve the efficiency of surface emitting lasers and is known as Resonant Periodic Gain (RPG). In addition to a periodic structure, more complex structure has ever been proposed with dynamic number of quantum wells to have good overlapping of intensity between pumping mode and lasing mode simultaneously [21].

Typically, the structure of VCSEL contains several parts: The gain region containing quantum wells, distributed Bragg reflector (DBR), and substrate. Regarding a single-mode OPSL, the output power is inhibited by induced thermal and usually limited to some milli-watts. The main sources of heat generation are from the active region, DBR, and substrate. For high power operation of OPSL, the efficient thermal management or heat removal has become an issue and has to be treated considerably. Conventionally, there are two methods to minimize the temperature rise of VCSEL. One is to reduce the heat generation from the internal structure of VCSEL. This could be achieved by thinning the thickness of DBR and substrate [22]. Moreover, the DBR could be eliminated and replaced by an external cavity. The other one is thermal removal by bonding a transparent thermally conductive dielectric material or adhering a heat sink such as copper or diamond to the device. Such a materials act as heat spreaders.

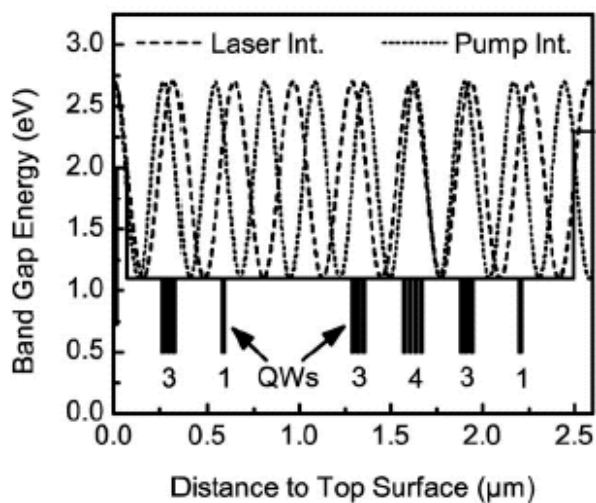
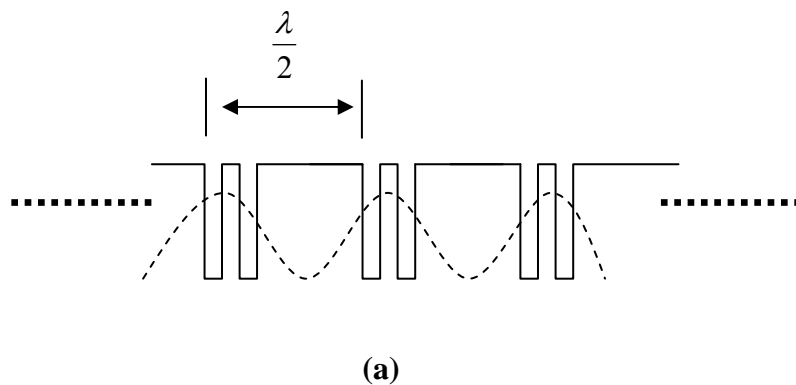


Fig. 1.5-3. Quantum well arrangement: (a) Periodic structure of quantum wells. The separation between successive pairs is designed to be half wavelength. (b) The quantum number as a function of the overlapping of optical intensity of lasing mode and pump mode [21].

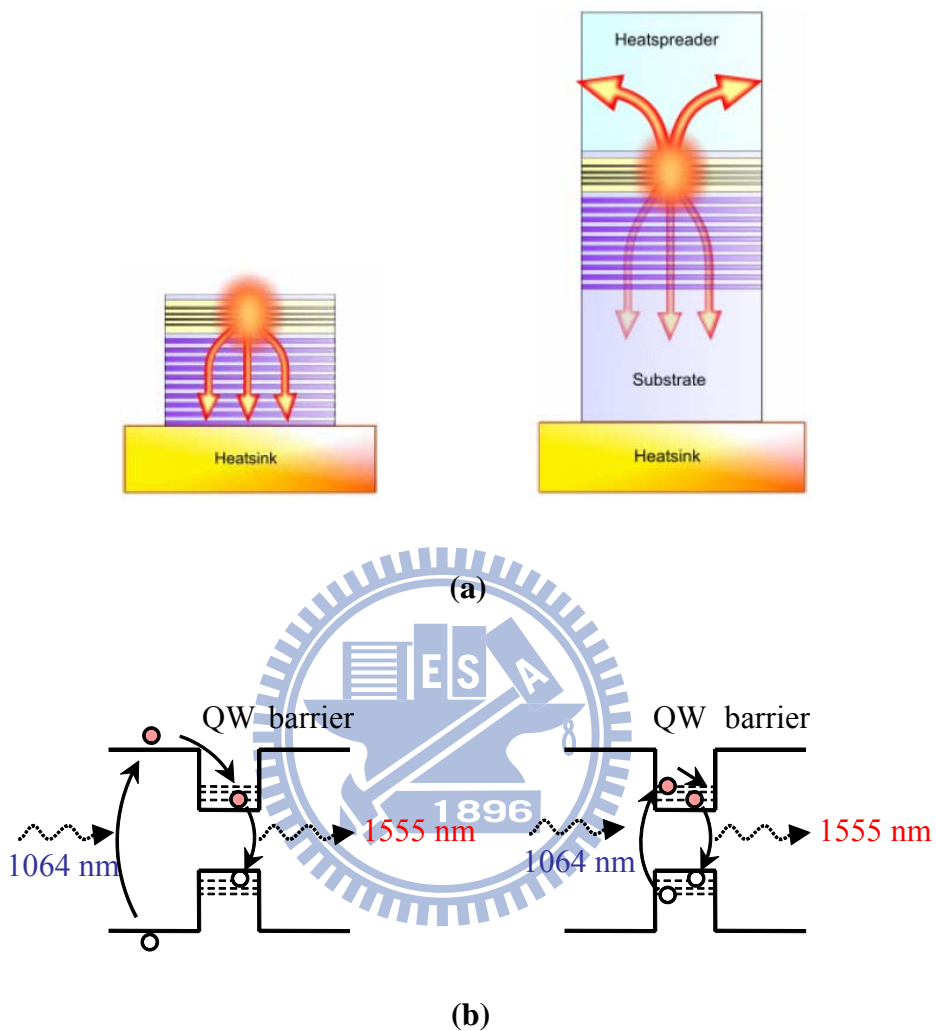
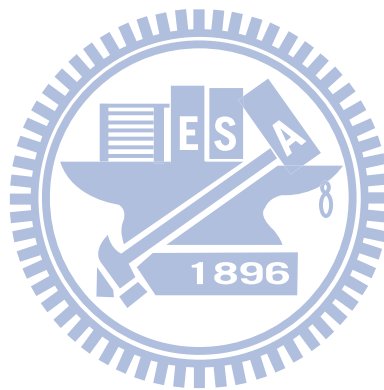


Fig. 1.5-4. The method of thermal management: (a) Heat minimization by thinning the device or bonding a transparent heat spreader [22]. (b) In-well pumping could have better thermal control than barrier pumping.

The main heat source comes from the quantum deficit, the energy difference between a pump and a laser photon, in the active region. The required pumping energy from ground state to excited state for carriers is lower in the quantum well than in the barrier region. Therefore, in addition to the thermal alleviation from DBR and substrate, the heat could be also reduced from the active region by in-well pumping rather than barrier pumping [23]-[25].



1.6 Overview of this dissertation

The accomplishments of this dissertation are the novel investigations in the realization of eye-safe lasers and the thermal management to improve the performance. The overall structures of the eye-safe lasers in this dissertation are summarized in Fig. 1.6-1. The organization of this dissertation is mainly as follows. Chapter 2 describes a high-pulse-energy eye safe laser up to ten mJ in the repetition rate of 1 ~ 20 Hz via optical parametric oscillator and the investigation of pulse dynamics under the thermally induce birefringence effect. Chapter 3 shows an idea of diffusion-bond Raman crystal employed in the self-SRS to improve the thermal effect and then the performance. Chapter 4 shows a passively Q-switched Er/Yb doped double cladding fiber laser with a novel AlGaInAs quantum well structure to be a saturable absorber. Chapter 5 describes a widely tunable laser accomplished with an OPO pumped by a passively Q-switched PCF laser with AlGaInAs quantum well structure to be a saturable absorber. Chapter 6 shows high-power AlGaInAs OPSLs with barrier pumping and in-well pumping and the investigations of thermal management via different pumping scheme. Chapter 7, I list the contributions of this dissertation and the future work in the following researches.

Based on the gain mediums, there are three categories in laser types: solid-state lasers, fiber lasers, and vertical external cavity surface emitting laser (semiconductor disk laser). Three pumping modes: continues-wave (CW), quasi-continuous-wave (QCW), and pulsed mode. The lasers are Q-switched in two ways to generate short pulse: passively and actively (Acoustic optical, AO). For the passively Q-switching, Cr⁴⁺:YAG and AlGaInAs QW/barrier are used as saturable absorblers. The overall structures of pulsed eye-safe laser reported in this dissertation are summarized in Fig. 1.6-1.

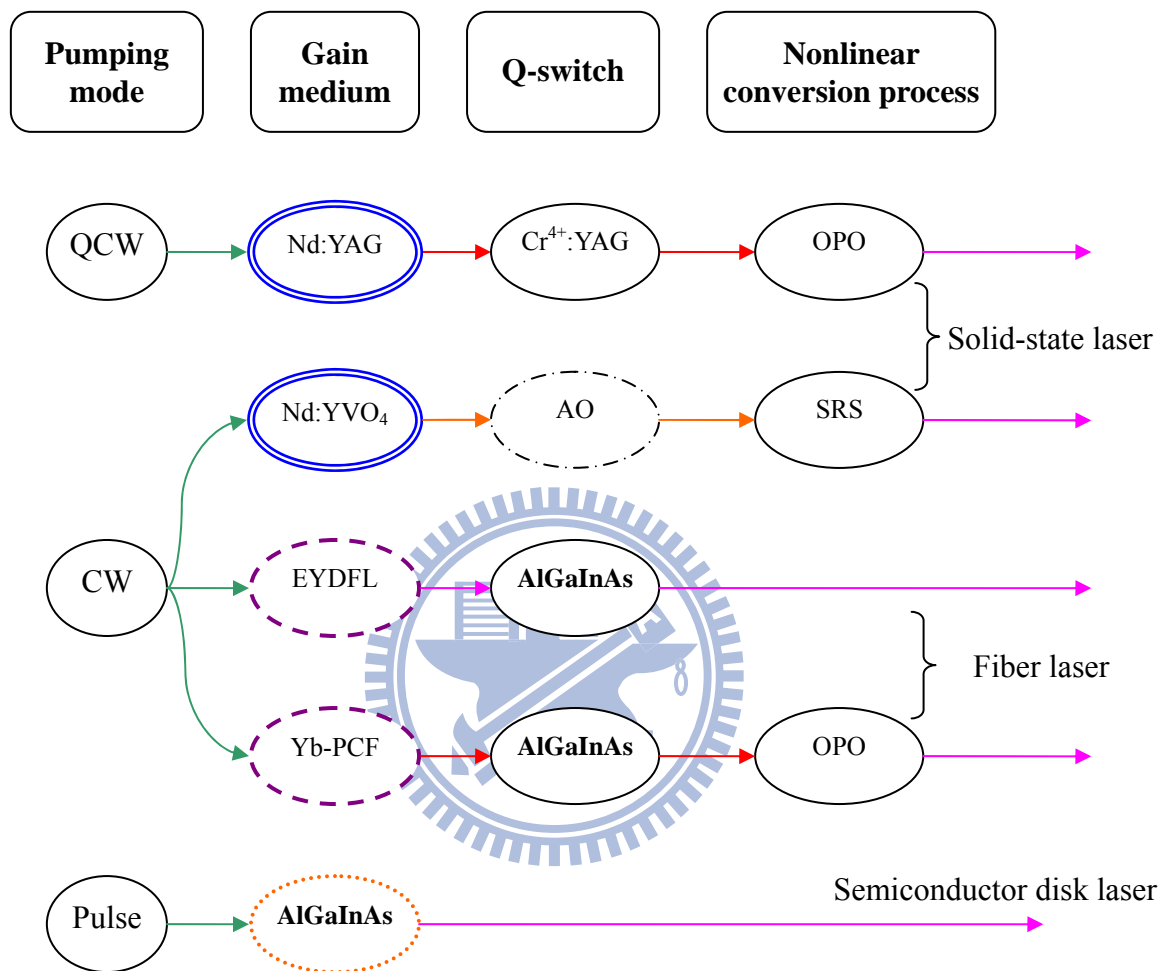


Fig. 1.6-1. The overall structures of eye-safe lasers reported in this dissertation.

References

- [1]. S. M. Spuler and S. D. Mayer, "Raman shifter optimized for lidar at a 1.5 μm wavelength," *Appl. Opt.* **46**, 2990-2995 (2007).
- [2]. G. S. Mecherle, Ed., Free-Space Laser Communication Technologies XIII, San Jose, CA, 24 to 25 January 2001, *Proc. SPIE* **4272** (2001).
- [3]. A. J. McGrath, J. Munch, G. Smith, and P. Veitch, "Injection-Seeded, Single-Frequency, Q-Switched Erbium:Glass Laser for Remote Sensing," *Appl. Opt.* **37**, 5706-5709 (1998).
- [4]. <http://www.microscopyu.com/print/articles/fluorescence/lasersafety-print.html>
- [5]. Bahaa E. A. Saleh, Malvin Carl Teich, "Fundamentals of photonics", Chap 19, John Wiley & Sons, New York (2001).
- [6]. J. A. Giordmaine and R. C. Miller, "Tunable Coherent Parametric Oscillation in LiNbO_3 at Optical Frequencies," *Phys. Rev. Lett.* **14**, 973 (1965)
- [7]. G. M. A. Gad, H. J. Eichler, and A. A. Kaminskii, "Highly efficient 1.3- μm second-Stokes PbWO_4 Raman laser," *Opt. Lett.* **28**, 426-428 (2003).
- [8]. A. A. Kaminskii, K. Ueda, H. J. Eichler, Y. Kuwano, H. Kouta, S. N. Bagaev, T. H. Chyba, J. C. Barnes, G.M. A. Gad, T. Murai, and J. Lu, "Tetragonal vanadates YVO_4 and GdVO_4 – new efficient $\chi^{(3)}$ -materials for Raman lasers," *Opt. Commun.* **194**, 201-206 (2001).
- [9]. S. H. Ding, X. Y. Zhang, Q. P. Wang, F. F. Su, P. Jia, S. T. Li, S. Z. Fan, J. Chang, S. S. Zhang, and Z. J. Liu, "Theoretical and experimental study on the self-Raman laser with Nd:YVO_4 crystal," *IEEE J. Quantum Electron.*, **42**, 927-933 (2006).
- [10]. Y. F. Chen, "High-power diode-pumped actively Q-switched Nd:YVO_4 self-Raman laser: influence of dopant concentration," *Opt. Lett.*, **29**, 1915-1917 (2004).
- [11]. F. F. Su, X. Y. Zhang, Q. P. Wang, S. H. Ding, P. Jia, S. T. Li, S. Z. Fan, C. Zhang, and B. Liu "Diode pumped actively Q-switched Nd:YVO_4 self-Raman laser," *J. Phys. D: Appl. Phys.*, **39**, 2090-2093 (2006).

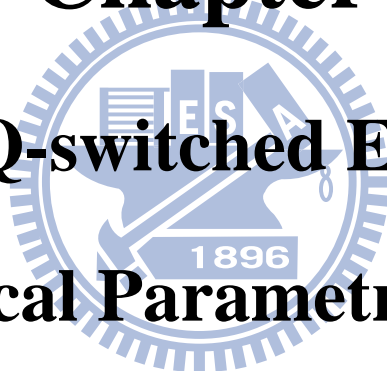
- [12]. F. Hanson, "Improved laser performance at 946 and 473 nm from a composite Nd:Y₃Al₅O₁₂ rod," Appl. Phys. Lett., **66**, 3549-3551 (1995).
- [13]. Etienne Rochat, Karim Haround, and René Dändliker, "High-power Nd-doped fiber amplifier for coherent intersatellite links," IEEE J. Quantum Electron., **35**, 1419-1423 (1999).
- [14]. Tadashi Sakamoto, Makoto Shimizu, Makoto Yamada, Terutoshi Kanamori, Yasutake Ohishi, Yukio Terunuma, and Shoichi Sudo, "35-dB gain Tm-doped ZBLAN fiber amplifier operating at 1.65 μm ," IEEE Photon. Technol. Lett., **8**, 349-351 (1996).
- [15]. Makoto Yamada, Terutoshi Kanamori, Yasutake Ohishi, Makoto Shimizu, Yukio Terunuma, and Shoichi Sudo, "Pr³⁺-doped fluoride fiber amplifier module pumped by a fiber coupled master oscillator/power amplifier laser diode," IEEE Photon. Technol. Lett., **9**, 321-323 (1997)
- [16]. E. Snitzer et al., "Double-clad, offset-core Nd fiber laser," proc.conf. Optical fiber Sensors, Postdeadline paper PD5 (1988).
- [17]. C. E. Zah, R. Bhat, B. N. Pathak, F. Favire, W. Lin, M. C. Wang, N. C. Andreadakis, D. M. Hwang, M. A. Koza, T. P. Lee, Z. Wang, D. Darby. Flanders, and J. J. Hsieh, "High-performance uncooled 1.3- μm AlGaInAs/InP strained-layer quantum-well lasers for subscriberloop applications," IEEE J. Quantum Electron. **30**, 511-521 (1994).
- [18]. J. Minch, S. H. Park, J. Minch, and S. L. Chuang, "Theory and Experiment of InGaAsP and InGaAlAs long-wavelength strained quantum-well lasers," IEEE J. Quantum Electron. **35**, 771-782 (1999)
- [19]. M. Y. A. Raja, S. R. J. Brueck, M. O. Scully, C. Lee, "Resonant Periodic Gain Surface-Emitting Semiconductor Lasers," Phys. Rev. A. **44**, 4599-4607 (1991).
- [20]. S. W. Corzine, R. S. Geels, J. W. Scott, R. H. Yan, L. A. Coldran, "Design of Fabry-Perot Surface-Emitting Lasers with a Periodic Gain Structure," IEEE Quantum Electronics. **25**, 1513-1524 (1989).
- [21]. N. Schulz, M. Rattunde, et.al., "Resonant optical in-well pumping of an (AlGaIn)(AsSb)-based vertical-external-cavity surface-emitting laser emitting at 2.35 μm ," Appl. Phys. Lett. **91**, 091113 (2007)

- [22]. J.M. Hopkins, S. Calvez, A. J. Kemp, J. E. Hastie, et al., "High-power vertical external-cavity surface-emitting lasers," Phys. Stat. Sol. 3, No. 3, 308-385 (2006)
- [23]. M. Schmid, S. Benchabane, F. T. Goudarzi, R. Abram, A. I. Ferguson, and E. Riis, "Optical in-well pumping of a vertical-external-cavity surface-emitting laser," Appl. Phys. Lett. **84**, 4860-4862 (2004)
- [24]. J. Wagner, N. Schulz, M. Rattunde, C. Ritzenthaler, C. Manz, C. Wild, and K. Köhler, "Barrier- and in-well pumped GaSb-based 2.3 μm VECSELs," Phys. Status Solidi **4**, No 5, 1594-1600 (2007).
- [25]. H. L. Chang, S. C. Huang, Yi-Fan Chen, K. W. Su, Y. F. Chen, and K. F. Huang, "Efficient high-peak-power AlGaInAs eye-safe wavelength disk laser with optical in-well pumping," Opt. Express **17**, 11409-11414 (2009).



Chapter 2

Passively Q-switched Eye-safe Laser with Optical Parametric Oscillator



2.1 Intracavity OPO Pumped with Nd-doped Laser

Intracavity optical parametric oscillator (OPO) is one of the most promising approaches for high-peak-power eye-safe laser sources since it can greatly reduce the lasing threshold due to the high pump intensity in the cavity. The advent of high damage threshold nonlinear crystals and diode-pumped Nd-doped lasers leads to a renaissance of interest in intracavity OPO's. In recent years, a number of efficient eye-safe intracavity OPOs pumped by actively [1]-[3] or passively [4]-[6] Q-switched Nd-doped lasers have been demonstrated to produce pulse energies of tens of μJ with pulse peak powers of 1-100 kW.

The intracavity OPOs are mostly constructed with the coupled cavity configuration in which the resonators for the signal and fundamental wave fields are separate. Recently, it was found [7], [8] that the shared cavity configuration in which the pump and signal beams share the same resonator provides a substantially superior amplitude stability, in comparison with the coupled cavity configuration. Even so, the maximum peak power in a shared cavity is usually several times lower than that in a coupled cavity under the circumstance of the same output coupler. Therefore, it is a practical interest to explore an intracavity OPO in a shared resonator in quest of optimal pulse energies and peak powers.

In this chapter, I will report a ten-mJ eye-safe laser with an intracavity OPO pumped in a shared resonator. We first confirm that the threshold of an intracavity OPO pumped by a passively Q-switched laser is essentially determined by the bleach of the saturable absorber not by the signal output reflectivity. On the other hand, we numerically analyze and experimentally demonstrate the pulse behavior is affected by the birefringence induced from thermal effect in active medium.

2.2 Experimental setup

Figure 2.2-1 shows the experimental setup for an intracavity OPO pumped by a high-power quasi-continuous-wave (QCW) diode-pumped passively Q-switched Nd:YAG laser in a shared resonator. The fundamental laser cavity was formed by a coated Nd:YAG crystal and an output coupler. The OPO cavity entirely overlapped with the fundamental laser cavity. The pump source is a high-power QCW diode stack (Quantel Laser Diodes) that consists of three 10-mm-long diode bars generating 130 W per bar, for a total of 390 W at the central wavelength of 808 nm. The diode stack is designed with 0.4 mm spacing between the diode bars so the overall area of emission is approximately 10 mm (slow axis) \times 0.8 mm (fast axis). The full divergence angles in the fast and slow axes are approximately 35° and 10°, respectively. A lens duct was exploited to couple the pump light from the diode stack into the laser crystal. The lens duct has the benefits of simple structure, high coupling efficiency, and unaffected by slight misalignment. The geometric parameters of a lens duct include r , L , H_1 , H_2 , and H_3 , where r is the radius of the input surface, L is the length of the duct, H_1 is the width of the input surface, H_2 is the width of the output surface, and H_3 is the thickness of the duct [9], [10]. Here a lens duct with the parameters of $r = 10$ mm, $L = 32$ mm, $H_1 = 12$ mm, $H_2 = 2.7$ mm, and $H_3 = 2.7$ mm was manufactured and used in the experiment. The coupling effect and the intensity distribution of intensity in exit surface of lens duct was simulated with commercial optical engineering software, the Advanced Systems Analysis Program (ASAP), as depicted in Fig. 2.2-2. The coupling efficiency of this lens duct was measured to be approximately 90 % and is in good agreement with simulation results.

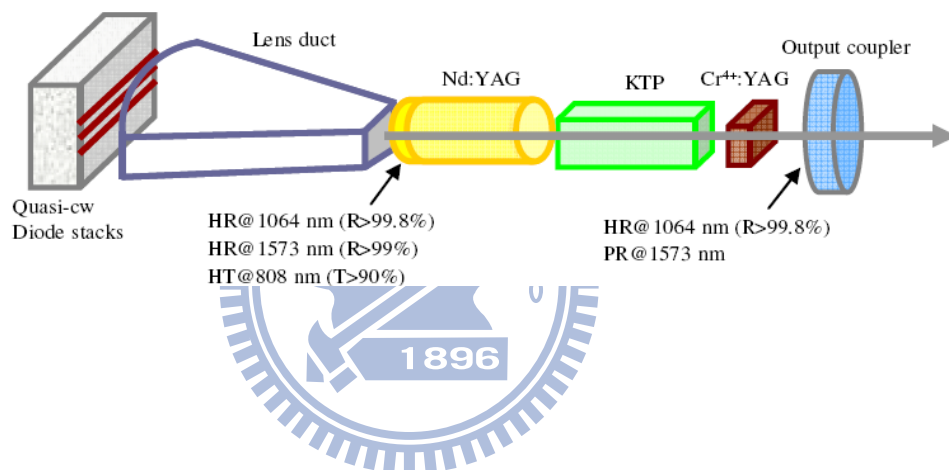


Fig. 2.2-1. Experimental setup for an intracavity OPO pumped by a high-power QCW diode pumped passively Q-switched Nd:YAG laser in a shared resonator.

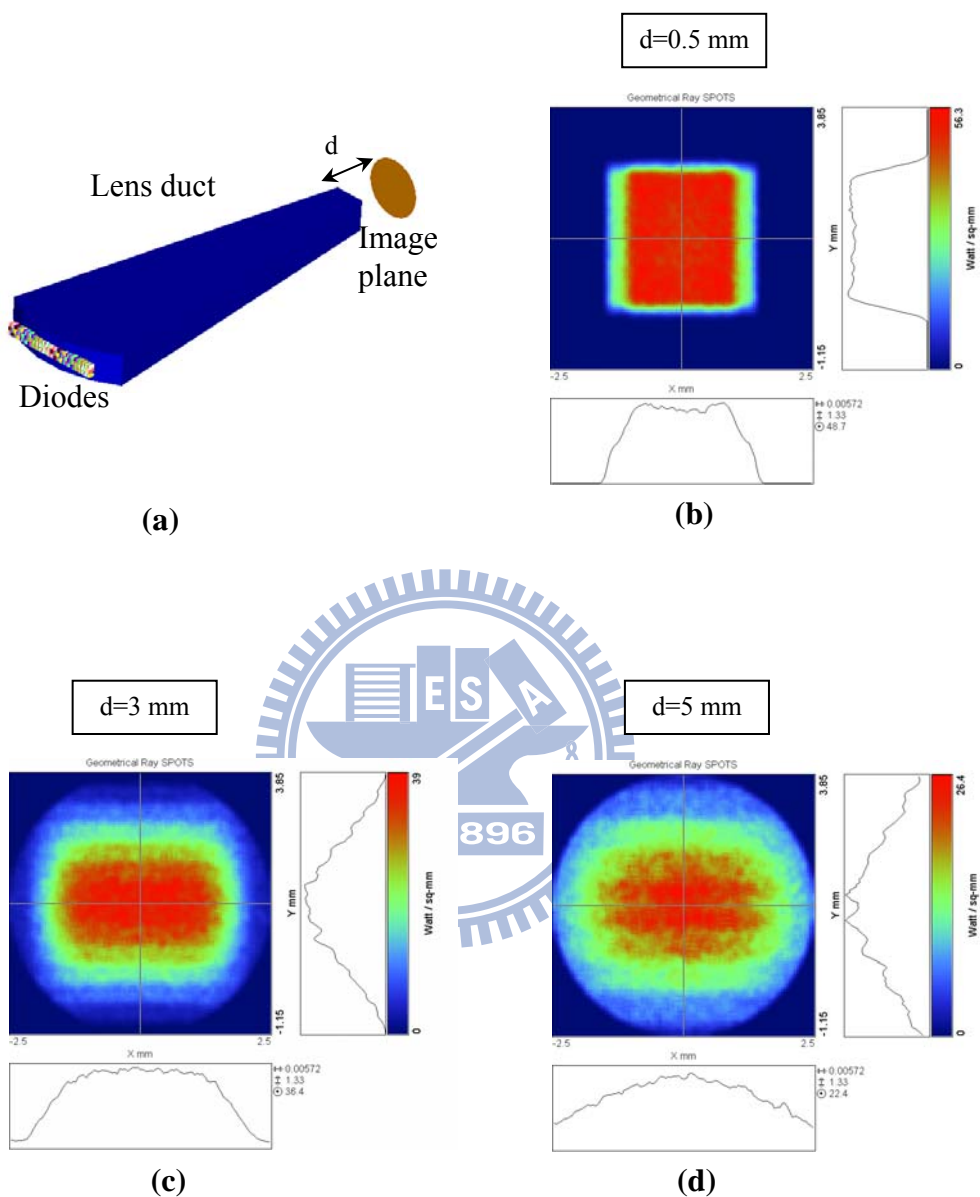


Fig. 2.2-2. (a) The schematics of diode power coupled by a lens duct. (b) ~ (d) The simulation result of intensity pattern in the image plane with 5-mm diameter from the exit surface of lens duct, 0.5 mm, 3 mm, and 5 mm respectively. The corresponding transmittance is 91.7 %, 87.9 %, and 68.4 %.

The gain medium was a 1.0 at. % Nd:YAG crystal with a diameter of 5 mm and a length of 10 mm. The incident surface of the laser crystal was coated to be highly reflective at 1064 nm and 1573 nm ($R > 99.8\%$) and highly transmitted at the pump wavelength of 808 nm ($T > 90\%$). The other surface of the laser crystal was coated to be antireflective at 1064 nm and 1573 nm ($R < 0.2\%$). The nonlinear material for the intracavity OPO was an *x*-cut KTP crystal with a size of $4 \times 4 \times 20$ mm³. The saturable absorber for the passive Q-switching was a Cr⁴⁺:YAG crystal with a thickness of 3 mm and an initial transmission of 60% at 1064 nm. Both surfaces of the KTP and Cr⁴⁺:YAG crystals were coated for antireflection at 1573 nm and 1064 nm. All crystals were wrapped with indium foil and mounted in conductively cooled copper blocks. The output coupler had a dichroic coating that was highly reflective at 1064 nm ($R > 99.8\%$) and partially reflective at 1573 nm. Several output couplers with different reflectivities ($10\% \leq R_s \leq 70\%$) at 1573 nm were used in the experiment to investigate the output optimization. The total cavity length was approximately 5.5 cm. The pulse temporal behavior at 1063 nm and 1571 nm was recorded by a LeCroy digital oscilloscope (Wavepro 7100; 10 G samples/sec; 1 GHz bandwidth) with a fast InGaAs photodiode. The spectral information was monitored by an optical spectrum analyzer (Advantest Q8381A) that employs a diffraction grating monochromator to measure high speed light pulses with the resolution of 0.1 nm. In all investigations, the diode stack was driven to emit optical pulses 250 μ s long, at a repetition rate less than 40 Hz, with a maximum duty cycle of 1%.

2.2.1 Theoretical analysis of threshold

The advantage of the intracavity OPO mainly consists in the exploit of high photon density of the fundamental wave. First of all, we analyze the maximum value of the intracavity photon density for the fundamental wave in a passively Q-switched laser. Next, we verify that the intracavity photon density of the present laser cavity can generally exceed the threshold of a singly resonant intracavity OPO by far, even though the reflectivity of the output mirror at the signal wavelength is nearly zero. In a passively Q-switched laser with a fast Q-switching condition, the maximum value of the intracavity photon density of the fundamental wave can be expressed as [11]

$$\phi_{f,\max} = \frac{l_{gm}}{l_{cav}} \left\{ n_i - n_t \left[1 + \left(\frac{n_i}{n_t} \right) \right] \right\} \quad (2.1-1)$$

where $n_i = \frac{1}{2\sigma l_{gm}} [\ln(1/T_0^2) + \ln(1/R) + L]$; $n_t = \frac{1}{2\sigma l_{gm}} [\beta \ln(1/T_0^2) + \ln(1/R) + L]$; $\beta = \frac{\sigma_{es}}{\sigma_{gs}}$; n_i is the initial population density in the gain medium; σ is the stimulated emission cross section of the gain medium; l_{gm} is the length of the gain medium; l_{cav} is the cavity length; T_0 is the initial transmission of the saturable absorber; σ_{gs} and σ_{es} are the ground-state and excited state absorption cross sections in the saturable absorber, respectively; R is the reflectivity of the output mirror at the fundamental wavelength; and L is the nonsaturable intracavity roundtrip loss. With the properties of the Nd:YAG and Cr⁴⁺:YAG crystals and the typical cavity parameters: $\sigma = 2.8 \times 10^{-19} \text{ cm}^2$, $\sigma_{gs} = 8.7 \times 10^{-19} \text{ cm}^2$, $\sigma_{es} = 2.2 \times 10^{-19} \text{ cm}^2$, $l_{cav} = 5.5 \text{ cm}$, $R = 99.8\%$, $T_0 = 0.6$, and $L = 0.01$, it can be found that $\phi_{f,\max}$ can be up to $1.56 \times 10^{17} \text{ cm}^{-3}$.

With Brosnan and Byer's equation [12], the threshold photon density for the double-pass pumped, single resonant OPO is derived to be given by

$$\phi_{f,th}(R_s) = \frac{1.12}{Gg_s(1+\gamma)^2} \left[33 \frac{l_{cav}}{c\tau_p} + \ln \left(\frac{1}{\sqrt{R_s}} \right) + L_s + \ln 4 \right]^2 \quad (2.1-2)$$

with the gain coefficient

$$G = \frac{2\hbar\omega_1\omega_2\omega_3 d_{eff}^2 l_{nl}^2}{n_1 n_2 n_3 \epsilon_0 c^2} \quad (2.1-3)$$

where g_s is the mode coupling coefficient, γ is the ratio of backward to forward pump amplitude in the cavity; ω_1 , ω_2 and ω_3 are the signal, idler and pump frequencies, respectively; n_2 and n_3 are the refractive indices at the signal, idler and pump wavelengths, respectively; τ_p is the FWHM of the pump pulse; d_{eff} is the effective non-linear coefficient; ϵ_0 is the vacuum permittivity; c is the speed of light; l_{nl} is the length of the nonlinear crystal; L_s is the round-trip signal wave intensity loss in the cavity; and R_s is the output reflectivity at the signal wavelength.

Figure 2.2-3 depicts the calculated results for the dependence of the threshold photon density $\phi_{f,th}(R_s)$ on the output reflectivity R_s with the properties of the KTP crystal and the typical cavity parameters: $\omega_1 = 1.198 \times 10^{15} \text{ sec}^{-1}$, $\omega_2 = 5.712 \times 10^{14} \text{ sec}^{-1}$, $\omega_3 = 1.865 \times 10^{19} \text{ J}$, $d_{eff} = 3.64 \text{ pm/V}$, $l_{nl} = 20 \text{ cm}$, $n_1 = 1.737$, $n_2 = 1.771$, $n_3 = 1.748$, $\epsilon_0 = 8.854 \text{ pF/m}$, $L_s = 0.01$, $\gamma = 0.9$, $g_s = 0.9$, $\tau_p = 10 \text{ ns}$ and $c = 3 \times 10^8 \text{ m/s}$. It can be seen that the threshold photon density $\phi_{f,th}(R_s)$ increases from $6 \times 10^{15} \text{ cm}^{-3}$ to $6 \times 10^{16} \text{ cm}^{-3}$ for the reflectivity R_s varying from 99.9% to 0.1%. As analyzed earlier, the obtainable intracavity photon density of the fundamental wave generally exceeds 10^{17} cm^{-3} . Therefore, the intracavity OPO for any value of R_s can be promisingly generated in the shared cavity, as long as the pump energy can excite the fundamental wave to bleach the saturable absorber and to overcome the lasing threshold.

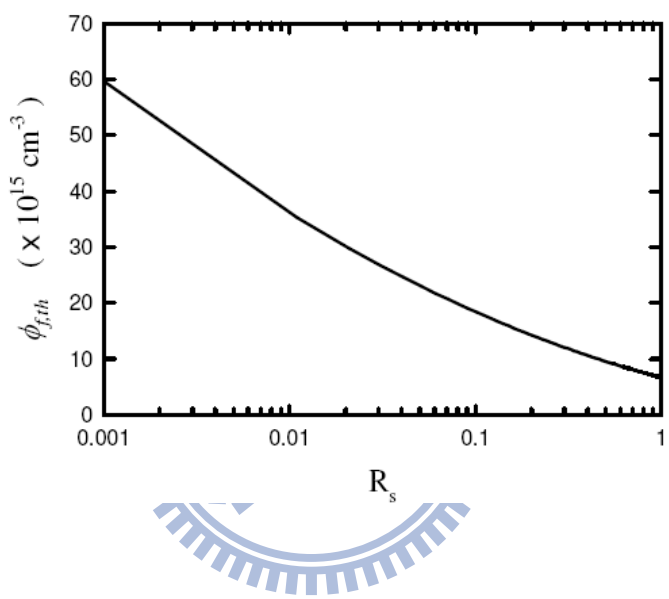
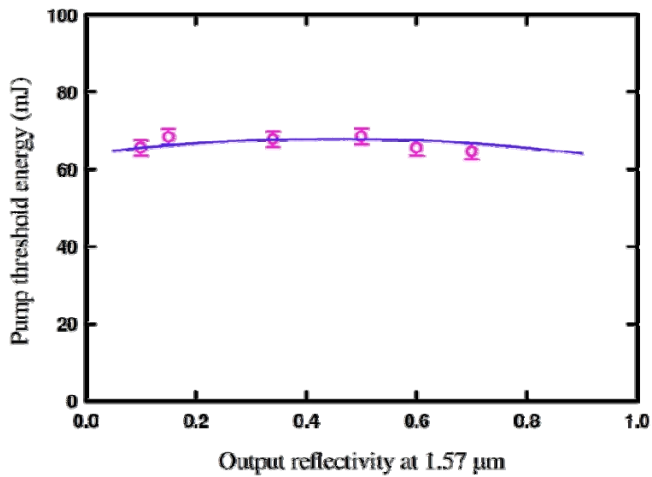


Fig. 2.2-3. Calculated results for the dependence of the threshold photon density on the output reflectivity R_s .

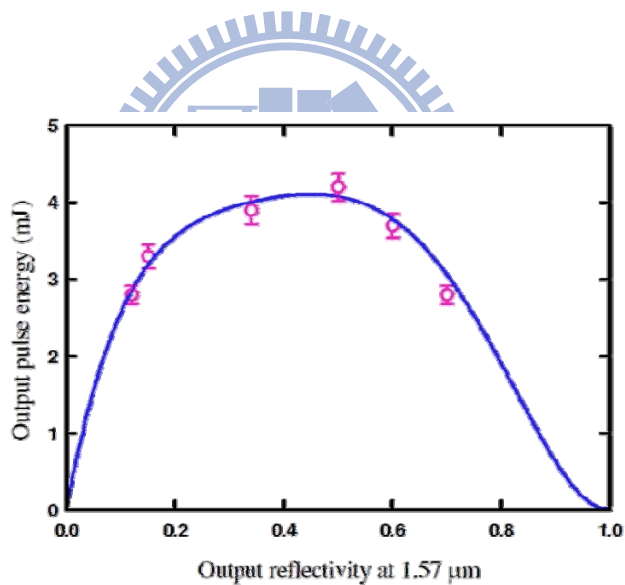
2.2.2 Experimental results and discussions

Figure 2.2-4 (a) shows the experimental results for the threshold pump energy versus the OPO output reflectivity. Experimental results confirm that the threshold pump energy is determined by the bleach of the saturable absorber not by the signal output reflectivity. Consequently, a wide range of the signal output reflectivity can be used to optimize the output performance. Figure 2.2-4 (b) depicts the experimental results for the pulse energy of the signal output versus the signal output reflectivity. The optimal output reflectivity for the output pulse energy can be found to be within $R_s = 40\sim 50\%$. With the optimum output coupler, the conversion efficiency from the diode input energy to the signal output energy is approximately 7%, which is slightly superior to the efficiency of 4~6% obtained in a coupled cavity [13].

Figure 2.2-5 (a)-(c) show the experimental results for the temporal shapes of the fundamental and the signal pulses obtained with three different output couplers. It can be seen that the pulse durations of the signal output are 4.4 ns, 2.1 ns, and 0.85 ns for $R_s = 60\%$, 50%, and 15%, respectively. The pulse width obtained with $R_s = 15\%$ is 2.4 times shorter than that obtained with $R_s = 50\%$; however, the pulse energy is only 20% less than the maximum value. In other words, the peak power reached with $R_s = 15\%$ can be nearly two times higher than that obtained with $R_s = 50\%$. To be more accurate, the output peak was calculated with the experimental pulse energy and the numerical integration of the measured temporal pulse profile. Figure 2.2-6 depicts the experimental results for the peak power of the signal output versus the OPO output reflectivity. The optimal output reflectivity for the output peak power can be found to be within $R_s = 10\sim 20\%$. With the optimum output coupler, the maximum peak power can be up to 1.5 MW.



(a)



(b)

Fig. 2.2-4. (a) Experimental results for the threshold pump energy versus the OPO output reflectivity. (b) Experimental results for the pulse energy of the signal output versus the OPO output reflectivity

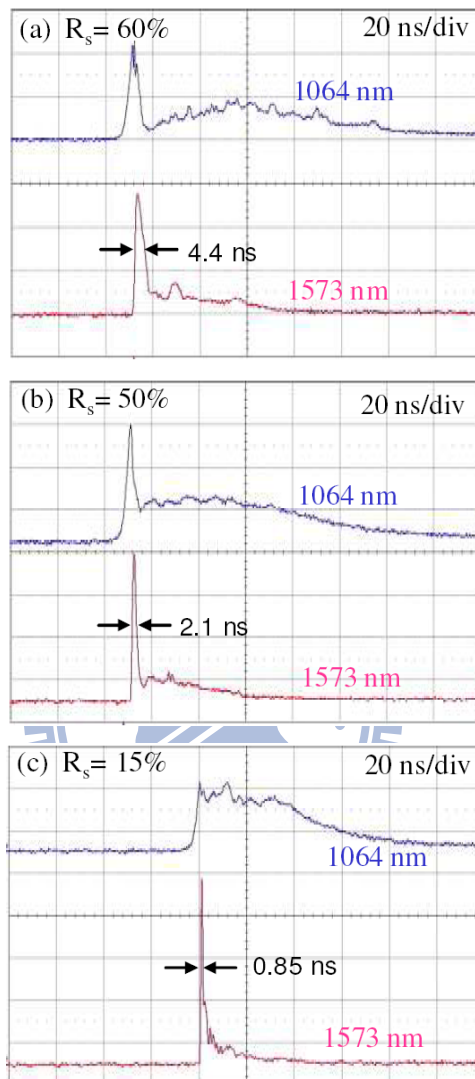


Fig. 2.2-5. Experimental results for the temporal shapes of the fundamental and the signal pulses

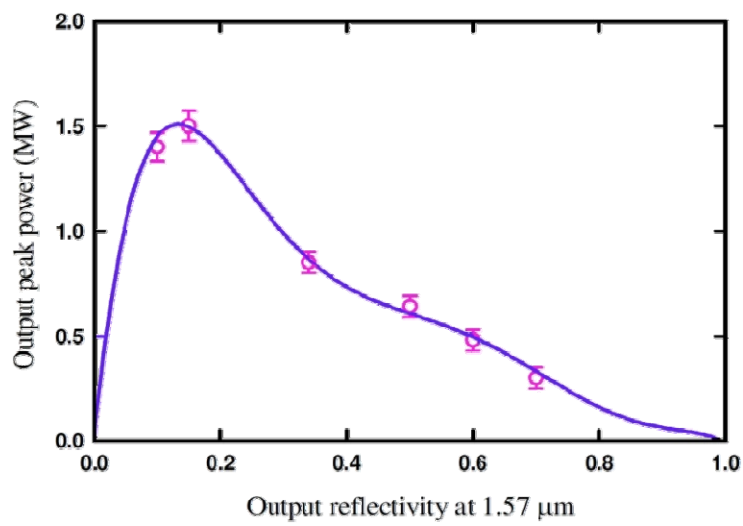


Fig. 2.2-6. Experimental results for the peak power of the signal output versus the OPO output reflectivity.

2.3 The influence of birefringence on pulse behavior in OPO

In order to obtain higher output pulse energy, we enlarged the cross section of end surface of lens duct to $3.3 \times 3.3 \text{ mm}^2$ and the diameter of Nd:YAG rod to 6 mm in the setup of Fig. 2.2-1. The initial transmission of saturable absorber, Cr^{4+} :YAG, is designed to be 51%. The QCW pump diode stack consists of six 10-mm-long diode bars generating 130 W per bar, for a total of 780 W at the central wavelength of 808 nm. The coupling efficiency of the lens duct was measured to be approximately 88%. Several output couplers with different reflectivity were used to investigate the output performance and characteristics. Figure 2.3-1 shows the experimental result about the output pulse temporal behavior at 1573 nm for different reflectivity of output coupler, $R=9, 16, 34,$ and 50% , respectively (Wave pro 7100, 10G samples/sec, 1 GHz bandwidth). The output pulse energy ranges from 11 to 9 mJ corresponded to increasing reflectivity. As shown in Fig. 2.3-1, in addition to the first transient peak, another longer pulse was generated adjacent to first one in the cases of reflectivity higher than 16%. With higher output reflectivity, the ratio of second pulse is higher. This is rarely seen in the configuration of external cavity OPO since the generation of fundamental pulse and signal pulse are separated. I will demonstrate in next section that the satellite pulse is resulted from the depolarized fields in the resonator during the process of pulse formation by rate equations. The depolarization is caused by the Nd:YAG rod which acts as a birefringence element under high pump power. The electric fields between the phase-matching direction and the other orthogonal direction couple mutually after each round trip propagation. The energy transformation between two axes exhibits a perturbation in the Q-switch and OPO process. Consequently, the decline and growth of energy in the phase matching direction gives rise to an adjacent parasitical pulse.

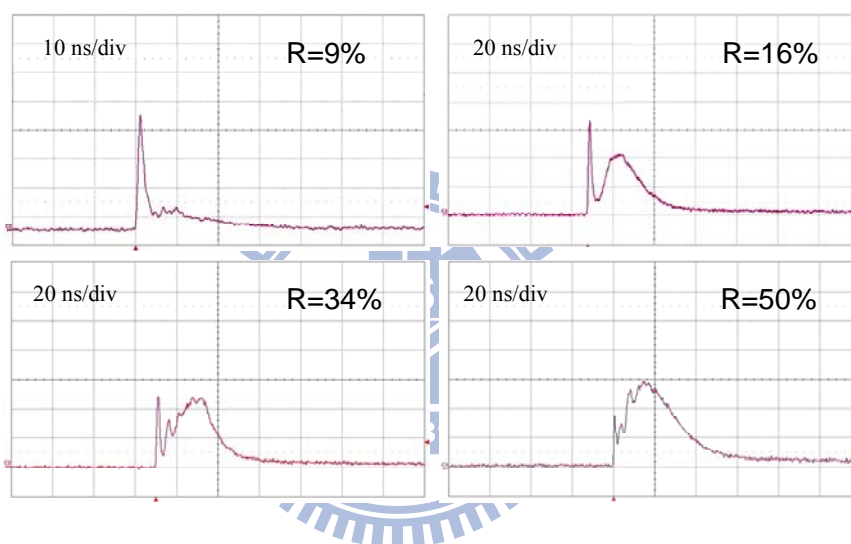


Fig. 2.3-1. The output temporal pulse at 1573 nm for different reflectivity of output couple

2.3.1 Theoretical analysis and discussion in birefringence effect

Figure 2.3-2 depicts the typical thermally induced birefringence effect in a Nd:YAG rod with [111] crystal orientation [15]. The principle axes of the induced birefringence are radially and tangentially directed at each point in the rod cross section. In the propagation of electric field along the rod orientation, a linearly polarized field would suffer a phase difference between radial and tangential direction and turn into elliptically polarized. When a linearly polarized field is along y -axis of the rod cross section, it will be gradually depolarized after propagation and resolved into two components along x - and y -axis. This depolarization indicates an energy coupling and transformation between two axes. If the resonator contains a polarizing element to maintain the polarization of fields on y -axis, the field depolarized into x -axis would be filtered out and becomes a depolarization loss. Without any polarizing element in the resonator, on the contrary, the energy will flow back after multiple round trips. The proportion of energy transformation, Γ , between two orthogonal axes after a round trip could be estimated from the phase difference δ given by [15]

$$\delta(r) = \frac{2\pi}{\lambda} \int \Delta n(r) \cdot 2l_{cr} dl \quad (2.1-4)$$

$$\Gamma = \int_0^{2\pi} \int_0^{r_0} \sin^2(2\varphi) \sin^2\left(\frac{\delta}{2}\right) r dr d\varphi \quad (2.1-5)$$

where λ denotes the optical wavelength, Δn is the difference of refractive index changes between tangential (Δn_ψ) and radial (Δn_r) direction, l_{cr} is the length of Nd:YAG rod, r and ϕ are the radius and azimuth angle of any interesting point in the cylindrical coordinate system of the rod cross section as depicted in Fig. 2.3-2, and the upper limit r_0 of integral about r is confined to the beam radius of wave in the crystal. The difference of refractive changes is mainly related to the deposited heat in the crystal. For Nd:YAG, it could be expressed as [15]

$$\Delta n(r) = \Delta n_\phi - \Delta n_r = (3.2 \times 10^{-4}) \cdot Q(l)r^2, \quad (2.1-6)$$

where Q is the heat deposited in the crystal per unit volume in the dimension of watts per cubic meter and r is in the dimension of meters. For an end-pumped scheme in our experiment,

Q is an exponential-decay function along the axis of rod because of the exponential absorption of pump radiation.

To investigate the influence of polarization transformation, we start from the modified rate equations of Q-switched intracavity OPO modeled by Y.F. Chen et al. [16]. Since the oscillator only resonates fundamental and signal fields, the evolution equation of the idler field was eliminated. In the following analyses, y -axis is set to be the ordinary-wave direction which is the phase-matching direction of fundamental and signal wave. By concerning the depolarization term, the rate equations for the four-level Q-switched laser are re-modified as below:

$$\frac{dn}{dt} = -c\sigma n(\varphi_{p,x} + \varphi_{p,y}) \quad (2.1-7)$$

$$\frac{d\varphi_{p,y}}{dt} = \left[\frac{\varphi_{p,x}}{t_r} \Gamma + \frac{\varphi_{p,y}}{t_r} (1-\Gamma) \right] \left[2\sigma n l_{cr} - \left(\ln \left(\frac{1}{R_p} \right) + L_p \right) \right] - \frac{\varphi_{p,y}}{t_r} \cdot (1-\Gamma) \cdot (2\sigma_{opo} \varphi_{s,y} l_{nl}) \quad (2.1-8)$$

$$\frac{d\varphi_{p,x}}{dt} = \left[\frac{\varphi_{p,x}}{t_r} (1-\Gamma) + \frac{\varphi_{p,y}}{t_r} \Gamma \right] \left[2\sigma n l_{cr} - \left(\ln \left(\frac{1}{R_p} \right) + L_p \right) \right] \quad (2.1-9)$$

$$\frac{d\varphi_{s,y}}{dt} = \frac{l_{nl}}{l_{ca}} c\sigma_{opo} \varphi_{p,y} (\varphi_{s,y} + \Delta\varphi_{s,y}) - \frac{\varphi_{s,y}}{t_r} \left(\ln \left(\frac{1}{R_s} \right) + L_s \right) \quad (2.1-10)$$

where N and φ are the population inversion density and photon density; the subscript p , s , and x , y stand for the fundamental wave, signal wave on x - and y -axis, respectively; t_r is the roundtrip transit time of light in the resonator; σ is the stimulated emission cross section of gain medium and l_{cr} is the length of gain medium; l_{ca} is the effective cavity length; $\Delta\varphi_{s,y}$ is the signal intensity of vacuum noise along y -axis; Γ is the transformation ratio of photon density between two orthogonal axes in a round trip resulted from depolarization; R_s is the signal output reflectivity and L is the roundtrip dissipative optical loss; σ_{opo} is the OPO effective cross section and can be derived from small parametric gain coefficient and is given by

$$2\sigma_{opo} l_{nl} = \frac{8\omega_s \omega_i d_{eff}^2 l_{nl}^2}{n_p n_s n_i c^2 \epsilon_0} \frac{A_p}{A_p + A_s} \quad (2.1-11)$$

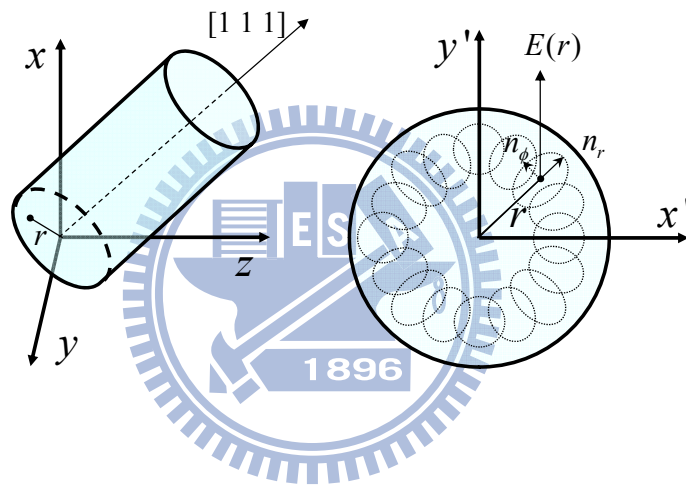


Fig. 2.3-2. The schematic of depolarization due to thermally induced birefringence effect.

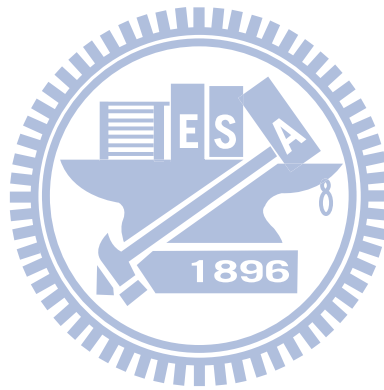
where the subscript i stands for idler wave, ω is the angular frequency, n is the refractive indices, c is the speed of light, d_{eff} is the effective nonlinear coefficient, A_p and A_s are the mode areas of fundamental and signal wave, respectively, and ϵ_0 is the vacuum permittivity. The second terms in the right hand sides of Eq. (5) and (6) represent the losses induced from optical parametric process. There are two assumptions in the modified equations. First, the saturable absorber, Cr^{4+} :YAG, is nearly transparent due to sufficiently high intensity in intracavity OPO scheme and the transmission is set to be unity when the lasing threshold is achieved. Secondly, in the Eq. (7), since the photon density of fundamental wave in the resonator is much higher than the signal wave, we neglect the influence of transformation of signal photons and only consider the signal photons in phase-matching direction (y -axis). From numerical results, these two assumptions have been demonstrated acceptable.

Figure 2.3-3 depicts the calculated results of the temporal pulse behavior of signal wave at 1573 nm for the dependence of output reflectivity according to Eq. (2.1-7)-(2.1-11). The cavity parameters are used with the following value: $\omega_s = 1.198 \times 10^{15} \text{ sec}^{-1}$, $\omega_i = 5.733 \times 10^{15} \text{ sec}^{-1}$, $d_{eff} = 3.1 \text{ pm/V}$, $\sigma = 2.8 \times 10^{-19} \text{ cm}^2$, $l_{cr} = 2 \text{ cm}$, $l_{nl} = 2 \text{ cm}$, $l_{ca} = 9 \text{ cm}$, $n_p = 1.748$, $n_s = 1.737$, $n_i = 1.771$, $R_p = 0.998$, $L_p = 0.01$, $L_s = 0.03$, $\Gamma = 0.03$, $A_p = 0.5\pi \times (1.6 \text{ mm})^2$, $A_s = 0.5\pi \times (1.6 \text{ mm})^2$. It can be seen that under the existence of depolarization induced energy transformation, Γ , the value of OPO output reflectivity will greatly influence the satellite pulse behavior. This can be explained as below. The parasitic pulse results from the energy transformation. With higher output reflectivity, higher component of photons on x -axis is stored in the resonator. Therefore, more conspicuous pulse compared with first peak could be obtained. For $\Gamma = 0.03$, the numerical results show good agreement with the experimental results in temporal pulses. This indicates that the theoretical model is successful in predicting the dynamic behavior of signal pulse.

Figure 2.3-4 shows the theoretical and experimental result of the signal output energy versus output reflectivity for different value of Γ from 0.02 to 0.05. The theoretical curve of signal energy E_s was obtained according to Eq. (2.1-12) given as:

$$E_s = \frac{A_s \cdot h\nu_s l_{ca}}{t_r} \ln\left(\frac{1}{R_s}\right) \int_0^\infty \varphi_{s,y}(t) dt \quad (2.1-12)$$

where $h\nu_s$ is the photon energy of signal wave. It is noted that with higher value of Γ , the higher output energy could be obtained. With the increasing of output reflectivity from 9% to 50%, the experimental output pulse energy varies from 11 mJ to 9 mJ. On the other hand, with lower signal output reflectivity of 9% to reduce the influence of birefringence effect, the effective pulse width is narrower and an output peak power up to 2.5 MW was obtained.



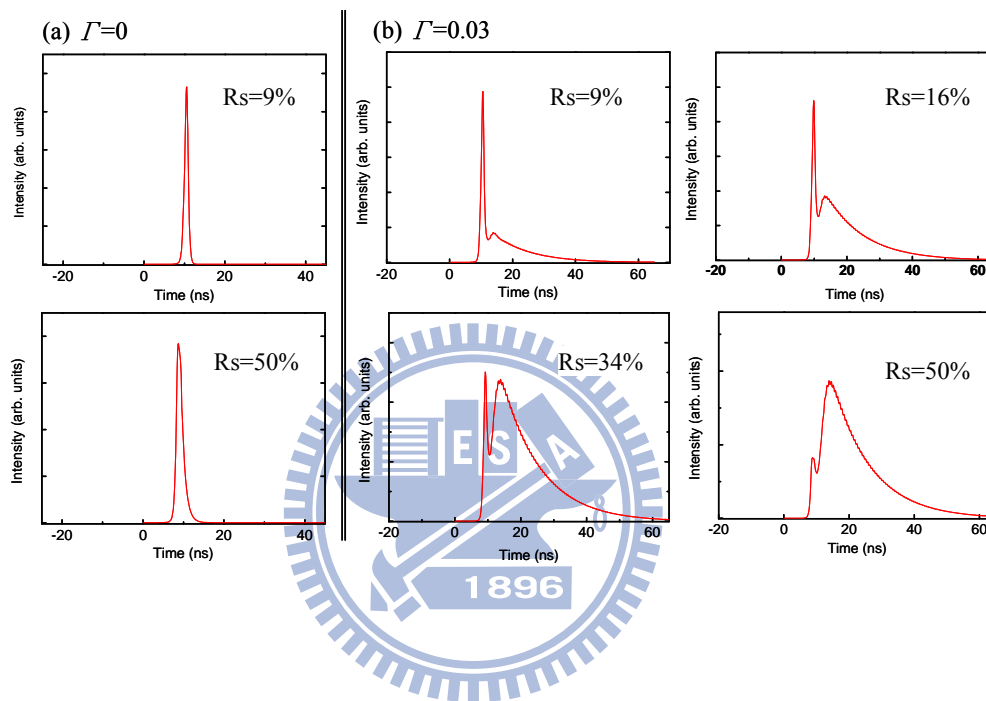


Fig. 2.3-3. The temporal pulse of simulation result for the value of $\Gamma = 0$ and 0.03 . The result shows the influence of depolarization and the dependence of signal output reflectivity.

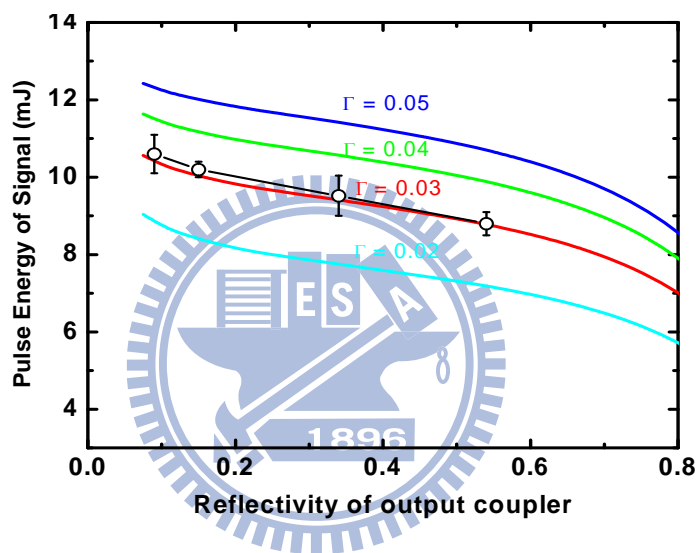
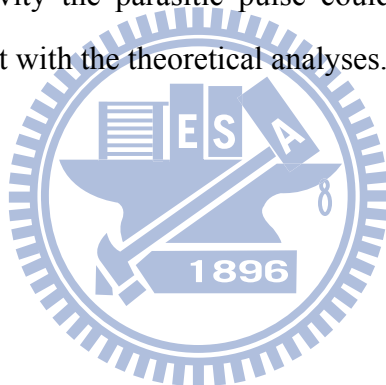


Fig. 2.3-4. The output energy versus different output signal reflectivity. The solid lines are numerical results of theoretical analysis for different value of Γ . The empty circles with error bar are experimental results.

2.4 Conclusion

In summary, I have theoretically and experimentally explored the output performance of an intracavity OPO in a shared cavity configuration. The threshold of an intracavity OPO pumped by a passively Q-switched Nd:YAG laser has been verified to be utterly controlled by the bleach of the saturable absorber not by the signal output reflectivity. Based on thorough experimental studies, we found that an efficient subnanosecond eye-safe laser with 3.3 mJ pulse energy and 1.5 MW peak power could be achieved with a signal output reflectivity of 15%. On the other hand, the pulse behavior is affected by the birefringence induced from thermal effect in the active medium. The depolarization induced energy transformation resulted from birefringence effect would give rise to a multi-peaks pulse in time domain. With lower signal output reflectivity the parasitic pulse could be eliminated. The experimental results are in good agreement with the theoretical analyses.



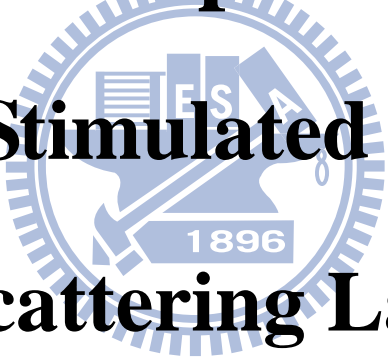
References

- [1]. Z. Liu, Q. Wang, X. Zhang, Z. Liu, J. Chang, H. Wang, S. Fan, W. Sun, G. Jin, X. Tao, S. Zhang, and H. Zhang, "Efficient acoustic-optically Q-switched intracavity Nd:YAG/KTiOAsO₄ parametric oscillator," *Appl. Phys. B* **92**, 37-41 (2008).
- [2]. H. T. Huang, J. L. He, X. L. Dong, C. H. Zuo, B. T. Zhang, G. Qiu, and Z. K. Liu, "High-repetition-rate eye-safe intracavity KTA OPO driven by a diode-end-pumped Q-switched Nd:YVO₄ laser," *Appl. Phys. B* **90**, 43-45 (2008).
- [3]. Y. F. Chen, S. W. Chen, S. W. Tsai, and Y. P. Lan, "High repetition-rate eye-safe optical parametric oscillator intracavity pumped by a diode-pumped Q-switched Nd:YVO₄ laser," *Appl. Phys. B* **76**, 263–266 (2003).
- [4]. J. Miao, J. Peng, B. Wang, H. Tan, and H. Bian, "Compact low threshold Cr:YAG passively Q-switched intracavity optical parametric oscillator," *Opt. Commun.* **281**, 2265–2270 (2008).
- [5]. Y. F. Chen, S. W. Chen, Y. C. Chen, Y. P. Lan, and S. W. Tsai, "Compact efficient intracavity optical parametric oscillator with a passively Q-switched Nd:YVO₄/Cr⁴⁺:YAG laser in a hemispherical cavity," *Appl. Phys. B* **77**, 493-495 (2003).
- [6]. Y. F. Chen, S. W. Chen, L. Y. Tsai, Y. C. Chen, and C. H. Chien, "Efficient subnanosecond intracavity optical parametric oscillator pumped with a passively Q-switched Nd:GdVO₄ laser," *Appl. Phys. B* **79**, 823–825 (2004).
- [7]. Y. F. Chen and L. Y. Tsai, "Comparison between shared and coupled resonators for passively Q-switched Nd:GdVO₄ intracavity optical parametric oscillators," *Appl. Phys. B* **82**, 403–406 (2006).
- [8]. Y. F. Chen, K. W. Su, Y. T. Chang, and W. C. Yen, "Compact efficient eye-safe intracavity optical parametric oscillator with a shared cavity configuration," *Appl. Opt.* **46**, 3597-3601 (2007).
- [9]. R. J. Beach, "Theory and optimization of lens ducts," *Appl. Opt.* **35**, 2005-2015 (1996).

- [10]. R. Fu, G. Wang, Z. Wang, E. Ba, G. Mu, and X. Hu, “Design of efficient lens ducts,” *Appl. Opt.* **37**, 4000-4003 (1998).
- [11]. J. J. Degnan, “Optimization of passively Q-switched lasers,” *IEEE J. Quantum Electron.*, **vol. 31**, pp. 1890–1901, 1995.
- [12]. S. J. Brosnan and R. L. Byer, “Optical parametric oscillator threshold and linewidth studies,” *IEEE J. Quantum Electron.*, **vol. 15**, pp. 415–431, 1979.
- [13]. B. W. Schilling, S. R. Chinn, A. D. Hays, L. Goldberg, and C. W. Trussell, “End-pumped 1.5 μm monoblock laser for broad temperature operation,” *Appl. Opt.* **45**, 6607-6615 (2006).
- [14]. R. Dabu, Constantin Fenic, and A. Stratan, “Intracavity pumped nanosecond optical parametric oscillator emitting in the eye-safe range,” *Appl. Opt.* **40**, 4334-4340 (2001).
- [15]. W. Koechner, *Solid-state laser engineering*, Chap 7, Springer (Optical Sciences), New York, 2005
- [16]. Y. F. Chen, S. W. Chen, S. W. Tsai, Y. P. Lan, “Output optimization of a high-repetition-rate diode-pumped Q-switched intracavity optical parametric oscillator at 1.57 μm .” *Appl. Phys. B* **77**, 505-508 (2003)

Chapter 3

Self-Stimulated Raman Scattering Laser



3.1 Self-Stimulated Raman Scattering

In Chapter 2, I introduce an intracavity pumped OPO with a QCW pumping laser diode in the repetition of single shot to tens Hz. In this section, I will introduce another nonlinear wavelength conversion process, stimulated Raman scattering, with CW pumping source to achieve a multi-kHz eye-safe wavelength laser by means of active Q-switch.

Recently, it has been reported that the laser crystal simultaneously serving as a Raman crystal can provide the advantage of compactness and simplicity for an intracavity SRS laser [1]. The laser emission at wavelengths of 1176 and 1525 nm based on self-SRS action in 1064- and 1342-nm actively Q-switched Nd:YVO₄ laser have been demonstrated, respectively [2]-[4]. As a laser gain crystal, though Nd:YVO₄ has a large stimulated emission cross section, the low thermal conductivity prevents good heat dissipation. The heat accumulated in the crystal not just only affects the stability of cavity but also decreases the Raman gain such that the overall performance is limited to scaling up to the operation to high power. Raman gain coefficient in the cavity can be represented as below

$$g_s = \frac{\lambda_p \lambda_s^2 N}{\hbar c \pi n_s^2} \left(\frac{d\sigma/d\Omega}{\Delta\nu_R} \right) \quad (3-1)$$

where λ_p , λ_s are the wavelength of pump and Raman scattering, respectively. n_s is the refractive index of Raman scattering wave. $d\sigma/d\Omega$ stands for the differential Raman cross section where σ is the Raman cross section and Ω is the solid angle. $\Delta\nu_R$ is the half-maximum Raman linewidth and related to the temperature:

$$\Delta\nu_R(T) = \Delta\nu_R(0) \left[1 + \frac{2}{\exp((\hbar\omega_0/2k_B T) - 1)} \right] \quad (3-2)$$

Equation (3-2) shows that the linewidth of Raman gain will increase with increasing the temperature of Raman crystal and then the gain coefficient will be reduced. Therefore, the performance will be hindered by the thermal effects with increasing temperature above room temperature [3]. To improve the thermal effects in the gain medium is critically important for

developing self-Raman solid-state lasers.

In the past few years, the thermal effects have been verified to be efficiently improved by using the so-called composite crystal as a gain medium. The composite crystal is fabricated by the diffusion bonding of a doped crystal to an undoped crystal with the same cross section [5]-[11]. Based on the philosophy, in this chapter, I will report how to employ a double-end diffusion-bonded Nd:YVO₄ crystal to investigate the output performance of the self-Raman laser at 1525 nm. Compared with the conventional self-SRS crystal, the following results will show that by utilizing a double-end diffusion-bonded Nd:YVO₄ to be a self-SRS crystal, the lasing threshold will be reduced significantly. And the conversion efficiency, the critical output power, as well as the maximum average output power are greatly increased.



3.2 Experimental setup

The experimental setup of a diode-pumped actively Q-switched eye-safe Raman laser employing a composite Nd:YVO₄ crystal is shown in Fig. 3.2-1(a). The laser crystal is an *a*-cut 4 mm × 4 mm × 20 mm double-end diffusion-bonded Nd:YVO₄ crystal bounded with one 2-mm-long undoped YVO₄ end at the pumped facet of 0.3-at.% Nd³⁺-doped Nd:YVO₄ crystal and one 8-mm-long undoped YVO₄ end at the other facet. With the 1342-nm fundamental pump wavelength, the wavelength of the first-Stokes component for the YVO₄ Stokes shift at 890-cm⁻¹ can be calculated to be around 1525 nm. The front and output coupler are designed for the first-Stokes generation. Both sides of the laser crystal are coated for antireflection at 1330-1530 nm (R<0.2%). In addition, the laser crystal is wrapped with indium foil and mounted in a water-cooled copper block. The water temperature was maintained at 22 °C. The front mirror is a 500-mm radius-of-curvature concave mirror with antireflection coating at 808 nm on the entrance face (R<0.2%), high-transmission (HT) coating at 808 nm (T>90%), and high-reflection (HR) coating at 1342 and 1525 nm on the other face (R>99.8%). The output coupler is a flat mirror with high-reflection coating at 1342 nm and partial-reflection (PR) coating at 1525 nm (R=65%). The pump source is an 808-nm fiber-coupled laser diode with a core diameter of 600 μm, a numerical aperture of 0.16, and a maximum power of 17.2 W. The pump beam is reimaged at the laser active medium and the waist radius is nearly 250 μm. The 30-mm-long acousto-optic Q-switcher (NEOS Technologies) had anti-reflectance coatings at 1342 nm on both faces and was driven at a 27.12-MHz center frequency with 15.0 W of RF power. The overall laser cavity length is 75 mm.

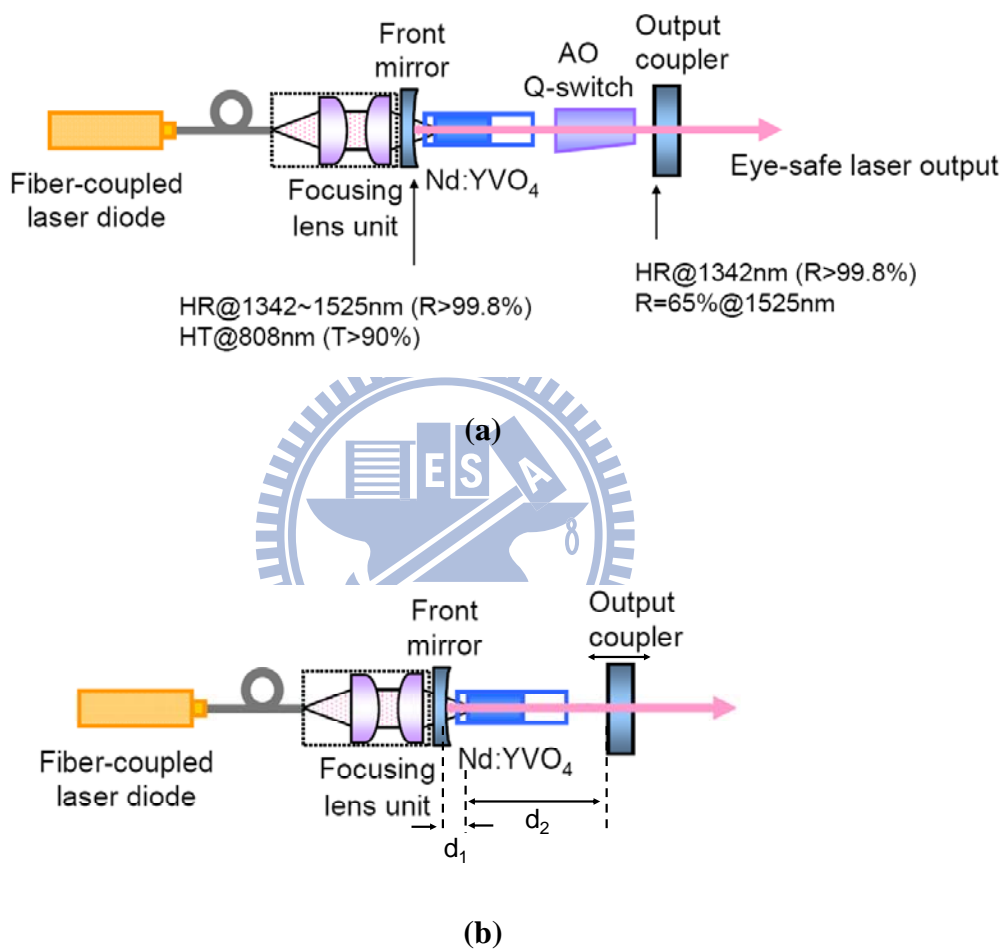


Fig. 3.2-1. Experimental setup of (a) a diode-end-pumped actively Q-switched Nd:YVO₄ Raman laser; (b) CW operation at 1342 nm for measuring thermal lens effect.

3.3 Experimental results and discussions

3.3.1 Thermal lensing effect in a 1342-nm cavity

We firstly used a simple laser setup for CW operation at 1342 nm to investigate the improvement of the thermal lensing effect in a double-end diffusion-bonded Nd:YVO₄ crystal [12], as depicted in Fig. 3.2-1(b). For this investigation an output coupler with partial reflection at 1342 nm was used instead of the above-mentioned Raman cavity output coupler. The optimum reflectivity of the output coupler was found to be approximately 92–94%. The effective focal lengths of the thermal lens were estimated based on the fact that the laser system would start unstable for a cavity length longer than the critical length related to the thermal lensing. Even though the absolute accuracy is not easily achieved, this method is confirmed to provide the high relative accuracy for the effective focal lengths of the thermal lens [12].

The thermal lens is assumed to be a thin lens located in the center of the gain medium. The focal length of thermal lens is inversely proportional to the pump intensity and the relationship can be represented as below.

$$f_{th} = \frac{\pi K \omega_p^2}{\xi P_{in} (dn/dT)} \left[\frac{1}{1 - \exp(-\alpha l_a)} \right] = C \frac{\omega_p^2}{P_{in}} \quad (3-1)$$

where f_{th} is the effective focal length of thermal lens, K is the thermal conductivity of gain medium, ω_p is the pump radius inside the gain medium, P_{in} is the pump power, ξ is the fractional thermal loading, dn/dT is the thermal-optical coefficient of refractive index, T is the temperature of gain medium, n is the refractive index, l_a is the length of gain medium, α is the absorption coefficient, C is a constant.

The characteristics of the beam light propagating in the resonator of cavity can be represented in the form of round-trip propagation matrix.

$$\begin{aligned} \begin{bmatrix} A & B \\ C & D \end{bmatrix} &= \begin{bmatrix} 1 & 0 \\ -\frac{2}{r} & 1 \end{bmatrix} \begin{bmatrix} 1 & d_1 + \frac{l_a}{2n} \\ 0 & 1 \end{bmatrix} \begin{bmatrix} 1 & 0 \\ -\frac{1}{f} & 1 \end{bmatrix} \begin{bmatrix} 1 & (d_2 - l_a) + \frac{l_a}{2n} \\ 0 & 1 \end{bmatrix} \\ & \begin{bmatrix} 1 & 0 \\ 0 & 1 \end{bmatrix} \begin{bmatrix} 1 & (d_2 - l_a) + \frac{l_a}{2n} \\ 0 & 1 \end{bmatrix} \begin{bmatrix} 1 & 0 \\ -\frac{1}{f} & 1 \end{bmatrix} \begin{bmatrix} 1 & d_1 + \frac{l_a}{2n} \\ 0 & 1 \end{bmatrix} \end{aligned} \quad (3-2)$$

where r is the radius curvature of the rear mirror. The criteria for a stable cavity is $\frac{|A+D|}{2} \leq 1$

and it turns out an simplified expression from (3-2) as below

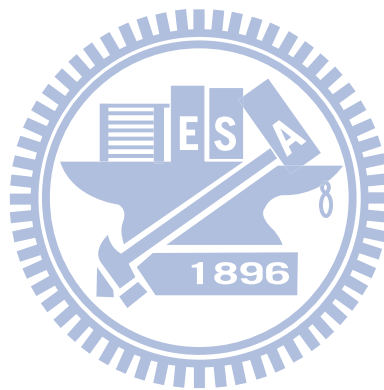
$$\frac{1}{f_{th}} = \frac{1}{d_2 + l_a \left(\frac{1}{n} - 1 \right)} - \frac{1}{d_1} \quad (3-3)$$

According to (3-3), we can find out the focal length of thermal lens by tuning the cavity length from the stable region into the marginal region of cavity, that is and observing the status of output power abruptly decreased. 80% of maximum power was taken as the critical point of stable cavity, as depicted in Fig. 3.3-1(a) which shows the result under the pump power of 7.61W. We can obtain a focal length for a certain pump power after the critical cavity length is estimated. And then the relationship between the pump power and diopter (reciprocal of focal length) can be obtained and fitted for a series of pump power.

Figure 3.3-1(b) shows the experimental data and fitted lines of thermal lensing power in a conventional crystal and a double-end diffusion-bonded crystal with the same dopant concentration. It can be seen that the effective focal length in a double-end diffusion-bonded crystal is nearly 1.6 times that in a conventional Nd:YVO₄ crystal. As a result, the thermal effects can be substantiated to be significantly reduced in a double-end diffusion-bonded crystal.

When the Raman cavity output coupler was used in the laser cavity, the pumping threshold for the Raman laser output was found to be 2–3 W for the pulse repetition rates within 20-40 kHz. The beam quality factor was found to be better than 1.5 over the entire operating region. The spectrum of laser output was measured by an optical spectrum analyzer with a resolution of 0.1 nm. As shown in Fig. 3.3-2, the optical spectrum for the actively

Q-switched self-Raman output displayed that the fundamental laser emission was at 1342 nm and the Stokes component was at 1525 nm. The frequency shift between Stokes and laser lines is in good agreement with the optical vibration modes of tetrahedral VO_4^{3-} ionic groups (890 cm^{-1}) [1].



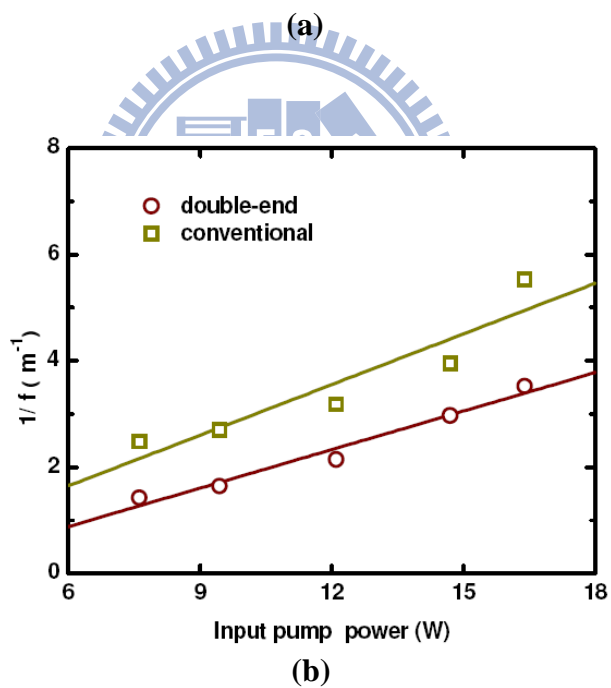
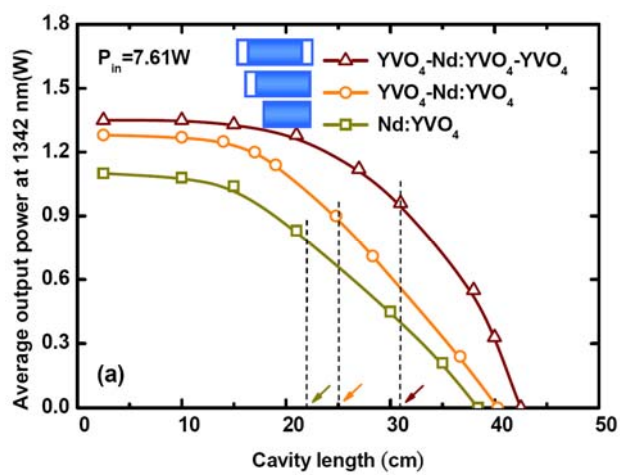


Fig. 3.3-1. (a) The method for measuring the thermal lens by estimating the critical cavity length in a 134-nm cavity. (b) Dependences of thermal lensing power on input pump power for conventional and double-end diffusion-bonded Nd:YVO₄ CW laser at 1342 nm.

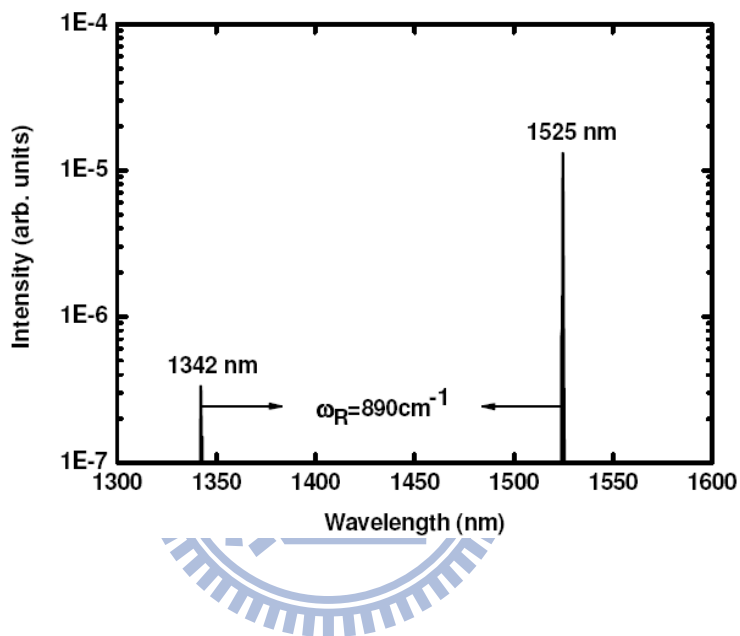


Fig. 3.3-2. Optical spectrum of the diode-pumped actively Q-switch Nd:YVO₄ self-Raman laser.

Figure 3.3-3 shows the experimental results of the average output power at 1525 nm with respect to the input pump power for the present self-Raman laser at pulse repetition rates of 20 and 40 kHz. For comparison, the previous results obtained by Chen [2] with a conventional 0.2%-doped Nd:YVO₄ crystal at a repetition rate of 20 kHz is also depicted in the same figure. Note that there were no experimental data for a conventional 0.2%-doped Nd:YVO₄ crystal at a pulse repetition rate of 40 kHz because of the high lasing threshold. It can be seen that the Raman lasing threshold for a double-end diffusion-bonded Nd:YVO₄ crystal is approximately 2.0 W that is substantially lower than the lasing threshold of 8.5 W for a conventional Nd:YVO₄ crystal at the repetition rate of 20 kHz. Moreover, the lasing threshold at a pulse repetition rate of 40 kHz for present self-Raman laser is below 3.0 W. A rather low lasing threshold for high pulse repetition rates comes from the fact that the undoped part of the composite crystal increases the interaction length and then enhances the Raman gain.

It has been experimentally evidenced that the maximum output power for a conventional self-Raman laser is limited by the critical pump power that induces a large temperature gradient in the gain medium to lead to the Raman gain lower than the cavity losses [3]. Consequently, the output power begins to saturate when the pump power exceeds the critical pump power. As shown in Fig. 3.3-3, the critical pump power for the self-Raman laser with a double-end diffusion-bonded Nd:YVO₄ crystal can exceed 17.2 W that is limited by the available pump power and is considerably greater than the critical pump power of 13.5 W with a conventional Nd:YVO₄ crystal. As a result, the self-Raman laser with a double-end diffusion-bonded Nd:YVO₄ crystal can generate the maximum average output power up to 1.72 W that is approximately 43% higher than the result with a conventional 0.2 %-doped Nd:YVO₄ crystal [1]. At a repetition rate of 40 kHz, the maximum power at 1525 nm is even up to 2.23 W with an input pump power of 17.2 W, corresponding to a conversion efficiency of 13%. To the best of our knowledge, this is the highest average power for diode-pumped eye-safe self-Raman laser.

The temporal traces for the fundamental and Raman pulses are recorded by a LeCroy

digital oscilloscope (Wavepro 7100, 10 Gsamples/s, 1-GHz bandwidth) with two fast p-i-n photodiodes. At a repetition rate of 40 kHz the pulse energy is up to 56 μJ with an input pump power of 17.2 W and the pulse width is measured to be approximately 3.2 ns, as shown in Fig. 3.3-4 (a). The corresponding peak power is higher than 17 kW. At the pulse repetition rate of 20 kHz, the maximum pulse energy is up to 86 μJ . Figure 3.3-4 (b) shows the pulse width at a pulse repetition rate of 20 kHz with a pump power of 17.2 W. It can be seen that although a second tiny Raman pulse usually follows the main first peak, its contribution is rather limited. Consequently the peak power can be generally higher than 22 kW. Since the fundamental energy is remained after first Raman pulse, the sub-pulse of fundamental wave is formed shown as Fig. 3.3-4 (a) and (b). At a pulse repetition rate of 20 kHz, the remaining energy is sufficient to reach Raman gain and a second tiny Raman pulse is produced shown as Fig. 3.3-4 (b). The sub-pulse would not be generated if the reflectivity of output coupler was lowered.



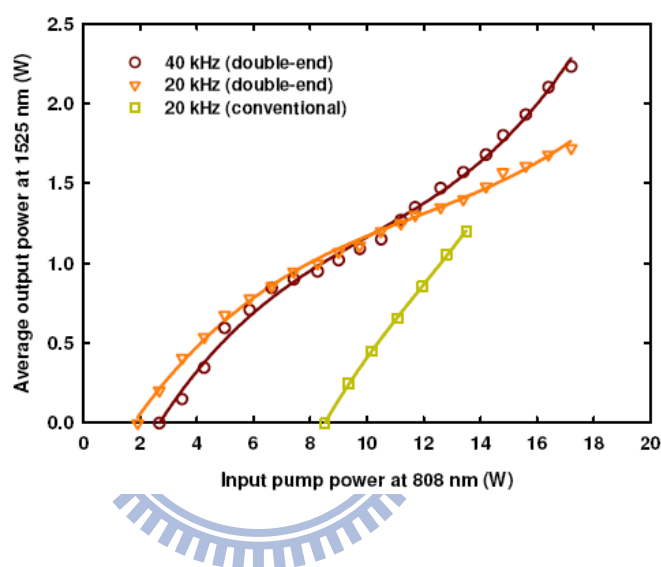
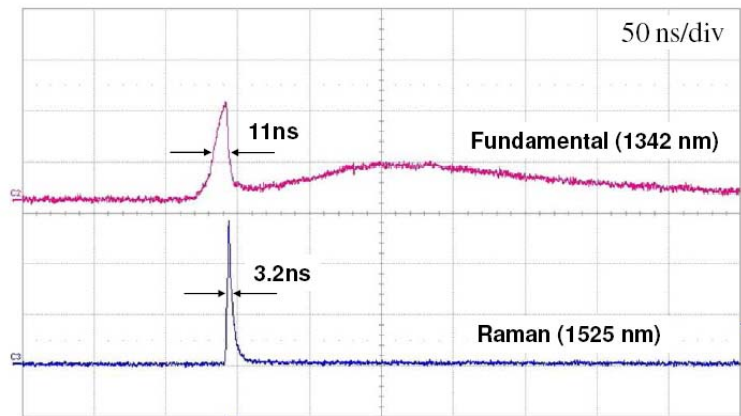
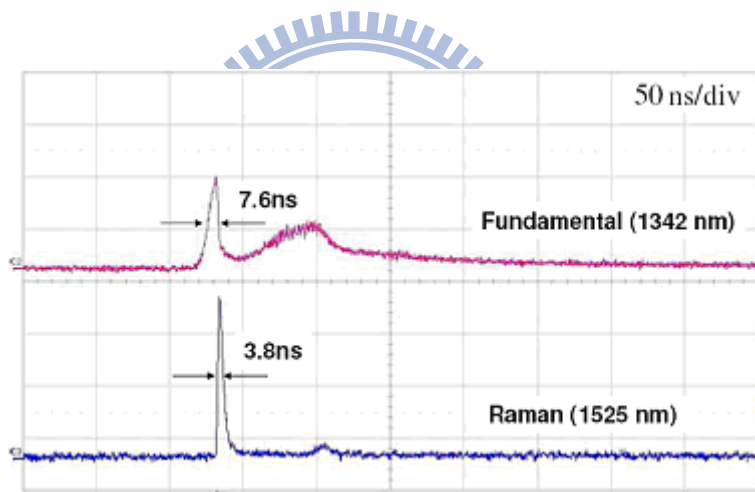


Fig. 3.3-3. The average output power at 1525 nm with respect to the input pump power at pulse repetition rates of 20 and 40 kHz shown as the down-triangle and circle symbols respectively for the double-end diffusion-bonded Nd:YVO₄ crystal and that at 20 kHz shown as the square symbol for a conventional Nd:YVO₄ crystal [1].



(a)



(b)

Fig. 3.3-4. Temporal characteristics of the fundamental and Raman pulses at a pulse repetition rate of (a) 40 kHz and (b) 20 kHz with a pump power of 17.2W.

3.4 Conclusion

A compact efficient high-power diode-pumped actively Q-switched self-Raman laser at 1525 nm is demonstrated by employing a double-end diffusion-bonded Nd:YVO₄ crystal. Experimental results reveal that the composite crystal can reduce the thermal effects to reach a higher critical pump power. More importantly, the undoped part plays a critical role in lowering the lasing threshold at high pulse repetition rates because of the increase of the Raman interaction length. The maximum average output power of 2.23 W at first-Stokes wavelength of 1525 nm is generated at a pulse repetition rate of 40 kHz, and the pulse width of Raman pulse is about 3.2 ns with an input pump power of 17.2 W. The corresponding conversion efficiency and peak power are approximately 13% and 17.4 kW, respectively.

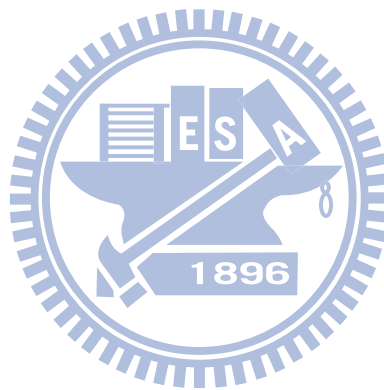


References

- [1]. A. A. Kaminskii, K. Ueda, H. J. Eichler, Y. Kuwano, H. Kouta, S. N. Bagaev, T. H. Chyba, J. C. Barnes, G.M. A. Gad, T. Murai, and J. Lu, "Tetragonal vanadates YVO_4 and GdVO_4 – new efficient $\chi(3)$ -materials for Raman lasers," Opt. Commun. **194**, 201-206 (2001).
- [2]. Y. F. Chen, "Compact efficient all-solid-state eye-safe laser with self-frequency Raman conversion in a Nd:YVO₄ crystal," Opt. Lett. **29**, 2172-2174 (2004).
- [3]. Y. F. Chen, "High-power diode-pumped actively Q-switched Nd:YVO₄ self-Raman laser: influence of dopant concentration," Opt. Lett. **29**, 1915-1917 (2004).
- [4]. F. F. Su, X. Y. Zhang, Q. P. Wang, S. H. Ding, P. Jia, S. T. Li, S. Z. Fan, C. Zhang, and B. Liu "Diode pumped actively Q-switched Nd:YVO₄ self-Raman laser," J. Phys. D: Appl. Phys. **39**, 2090-2093 (2006).
- [5]. F. Hanson, "Improved laser performance at 946 and 473 nm from a composite Nd:Y₃Al₅O₁₂ rod," Appl. Phys. Lett. **66**, 3549-3551 (1995).
- [6]. R. Weber, B. Neuenschwander, M. M. Donald, M. B. Roos, and H. P. Weber, "Cooling schemes for longitudinally diode laser-pumped Nd:YAG rods," IEEE J. Quantum Electron. **34**, 1046-1053 (1998).
- [7]. M. Tsunekane, N. Taguchi, T. Kasamatsu, and H. Inaba, "Analytical and experimental studies on the characteristics of composite solid-state laser rods in diode-end-pumped geometry," IEEE J. Sel. Top. Quantum Electron. **3**, 9-18 (1997).
- [8]. M. Tsunekane, N. Taguchi, and H. Inaba, "Improvement of thermal effects in a diode-end-pumped, composite Tm:YAG rod with undoped ends," Appl. Opt. **38**, 1788-1791 (1999).
- [9]. M. P. MacDonald, Th. Graf, J. E. Balmer, and H. P. Weber, "Reducing thermal lensing in diode-pumped laser rods," Opt. Commun. **178**, 383-393 (2000).
- [10]. J. Šulc, H. Jelínková, V. Kubeček, K. Nejezchleb, and K. Blažek, "Comparison of different composite Nd:YAG rods thermal properties under diode pumping," Proc. SPIE

4630, 128-134 (2002).

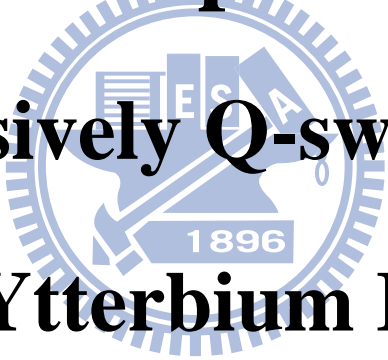
- [11]. Z. Zhuo, T. Li, X Li, and H. Yang, "Investigation of Nd:YVO₄/YVO₄ composite crystal and its laser performance pumped by a fiber coupled diode laser," Opt. Commun. **274**, 176-181 (2007).
- [12]. Y. T. Chang, Y. P. Huang, K. W. Su, and Y. F. Chen, "Comparison of thermal lensing effects between single-end and double-end diffusion-bonded NdYVO₄ Crystals for 4F_{3/2} → 4I_{11/2} and 4F_{3/2} → 4I_{13/2} transitions," Opt. Express **16**, 21155-21160 (2008)



Chapter 4

Passively Q-switched

Erbium/Ytterbium Fiber Laser

The logo of the University of South Alabama is a circular seal. It features a central shield with a book, a quill, and a scale. The letters 'E', 'S', and 'A' are arranged around the shield. Below the shield is a banner with the year '1896'. The entire seal is surrounded by a gear-like border.

4.1 Semiconductor Saturable Absorber

In Chapter 2 and Chapter 3 I report the investigations of the eye-safe laser by means of nonlinear wavelength conversion. In these investigations, we individually utilized a passive saturable absorber (Cr^{4+} :YAG) and AO Q-switch to generate short pulses. To obtain eye-safe lasers, the most direct method is to employ a gain medium doped with the active ions with the radiation in the range of eye-safe regime such as Er^{3+} , Tm^{3+} , or Ho^{3+} . For a radiation in the regime of $1.5\ \mu\text{m}$, Er^{3+} has been the most popular active ions up to date. However, the corresponding laser substrates have been an issue in the thermal management.

Q-switched Erbium-doped fiber (EDF) lasers have been realized with active modulation methods, including acousto-optic modulators, electro-optic modulators, or a piezoelectric device. But all these need active modulation elements, which not only increase the complexity of the lasers but also introduce extra loss to the lasers. Alternatively, passive Q switching by use of a saturable absorber is a simple, convenient, and efficient way to achieve high-peak-power pulses. Various schemes have been utilized to realize passively Q-switching, such as using of semiconductor quantum dots dispersed in glass bulk [1], doped bulky crystals [2]-[5]. In addition to the transition metal-doped crystals, the semiconductor saturable-absorber mirror (SESAM) [6] is an alternative material for the passively Q-switched eye-safe laser. However, the pulse energy with the SESAM has been limited to $17\ \mu\text{J}$ due to the small dynamic transmittance.

Mostly, the semiconductor saturable-absorber materials for passively Q-switched fiber lasers in the range of 1.5 - $1.6\ \mu\text{m}$ are based on the InGaAsP thick layer [6] and the InGaAs quantum-well (QW) structure [7]. Recently, an AlGaInAs material with a periodic QW/barrier structure has been used as a saturable absorber to achieve an efficient passively Q-switched $1.06\text{-}\mu\text{m}$ laser [8][10]. Compared with InGaAsP materials, the AlGaInAs quaternary alloy with a larger conduction band offset can provide a better electron confinement covering the same wavelength region [9]-[11] (Fig. 4.1-1). Therefore, AlGaInAs/InP QWs could possess larger absorption cross section and higher modulation depth. However, AlGaInAs/InP QWs

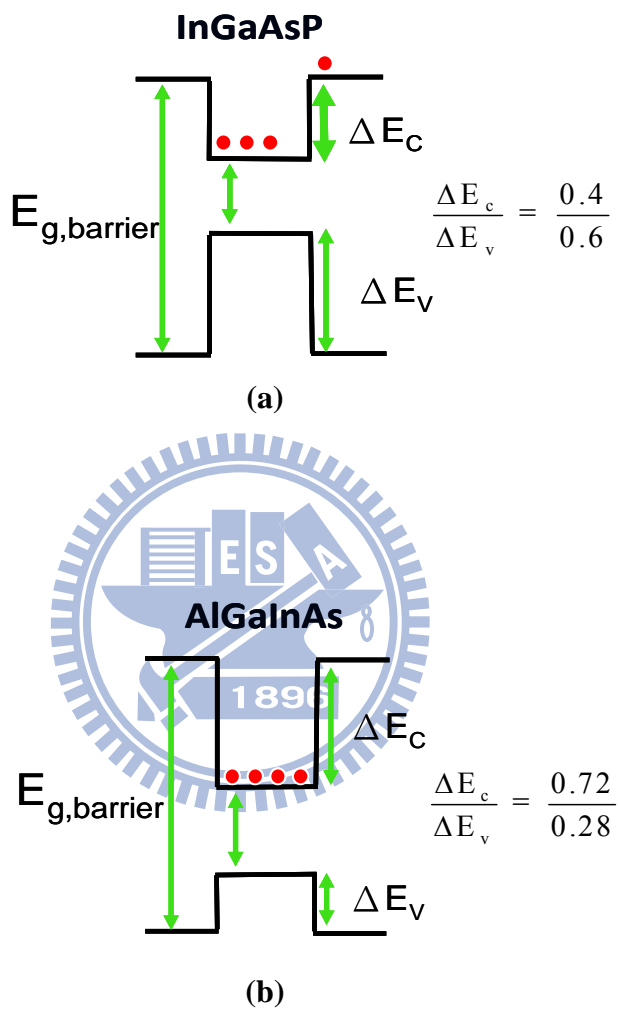


Fig. 4.1-1. The energy diagram of (a) InGaAsP QWs/barriers; (b) AlGaInAs QWs/barriers.

has not been developed to be saturable absorbers in eye-safe lasers. Therefore, it is of practical importance to employ AlGaInAs QWs as saturable absorbers for high-power Q-switched eye-safe lasers.

In this chapter, I report a passively Q-switched EYDFL with a periodic AlGaInAs QW/barrier structure as a saturable absorber. As the result of the rather low nonsaturable loss, the overall Q-switching efficiency could be up to 84%. With an incident pump power of 13.5 W, the passively Q-switched fiber laser, operating at 12 kHz, produces an average output power up to 1.26 W with a pulse energy of 100~110 μJ . The maximum peak power is generally higher than 500 W.



4.2 Experimental setup

An AlGaInAs QW/barrier structure was grown on a Fe-doped InP substrate by metalorganic chemical-vapor deposition. The region of the saturable absorber consists of 30 groups of two QWs with the luminescence wavelength around 1560 nm, spaced at half-wavelength intervals by AlGaInAs barrier layers with the band-gap wavelength around 1070 nm. Note that the structure of the semiconductor saturable absorber (SESA) was essentially similar to that used in the passively Q-switched 1.06- μm laser reported in Ref. [10]. However, the composition for the AlGaInAs alloy has been changed to design the band gap from 1.17 eV (1.06 μm) to 0.79 eV (1.56 μm) for the QWs. Even so, there is very little difference in the fluorescence efficiency and response time for these two saturable absorbers. Compared to a conventional SESAM structure, the missing DBR considerably simplifies the structure of growth. Since the cavity modes with lower losses always dominate the lasing output, the lasing modes are naturally the modes with the electric field minima in the vicinity of the periodic QWs. In other words, the barrier layers are used not only to confine the carriers but also to locate the QW groups nearby the region of the nodes of the lasing standing wave [10]. Consequently, damage to the absorber can be effectively avoided by the periodic QW/barrier structure. An InP window layer was deposited on the QW/barrier structure to avoid surface recombination and oxidation. The backside of the substrate was mechanically polished after growth. The both sides of the semiconductor saturable absorber were antireflection (AR) coated to reduce back reflections and the couple-cavity effects. The total residual reflectivity of the AR-coated sample is approximately 8%.

Figure 4.2-1 shows the transmittance spectrum at room temperature for the AR-coated AlGaInAs/InP SESA device. It can be seen that the strong absorption of the AlGaInAs QWs leads to the initial transmission at the wavelength of 1560 nm to be approximately 40%. A pulsed semiconductor laser at 1.56 μm was used to measure the modulation depth of the QW saturable absorber with the z-scan method. The pump pulse energy and pulse width were 3 μJ and 50 ns, respectively. The pump radius was varied from 0.1 to 1 mm. Therefore, the pump fluence was in the range of 0.1~10 mJ/cm^2 and was comparable to the intra-cavity fluence in

the present fiber laser. Experimental results revealed that the maximum transmission was up to 90%. Consequently, the modulation depth was deduced to be approximately 50% in a single pass. Considering the 8% residual reflectivity of the AR-coating, the total nonsaturable loss introduced by the SESA was estimated to be approximately 2%. In the z-scan experiment, there are no noticeable nonlinear index modifications to be observed except for amplitude effects.

Figure 4.2-2 depicts the schematic of the experimental setup for EYDFL that comprises a 7-m Er-Yb codoped fiber and an external feedback cavity with a periodic AlGaInAs QW/barrier structure as a saturable absorber. The fiber has an absorption coefficient of 3.0 dB/m at 976 nm and a double-clad structure with a diameter of 450- μm octagonal outer cladding, diameter of 300- μm octagonal inner cladding with a numerical aperture (NA) of 0.46, and 25- μm circular core with a NA of 0.07. Note that the large mode area (LMA) fiber featuring a unique low NA core design is used to achieve the nearly single-mode output beam quality with high pulse energies. The external Q-switch part consists of a focusing lens of 25-mm focal length to focus the fiber output into the SESA device and a highly reflective mirror for feedback. The focusing lens was arranged to have a beam waist of 50 μm inside the SESA. The SESA was mounted in a copper block without active cooling. The pump source was a 16-W 976-nm fiber-coupled laser diode with a core diameter of 400 μm and a NA of 0.22. A focusing lens with 25 mm focal length and 85% coupling efficiency was used to re-image the pump beam into the fiber through a dichroic mirror with high transmission (>90%) at 976 nm and high reflectivity (>99.8%) at 1560 nm. The pump spot radius was approximately 200 μm . The fiber end on the pump side was perpendicularly cleaved, which acted as the cavity output coupler with about 4% Fresnel reflection.

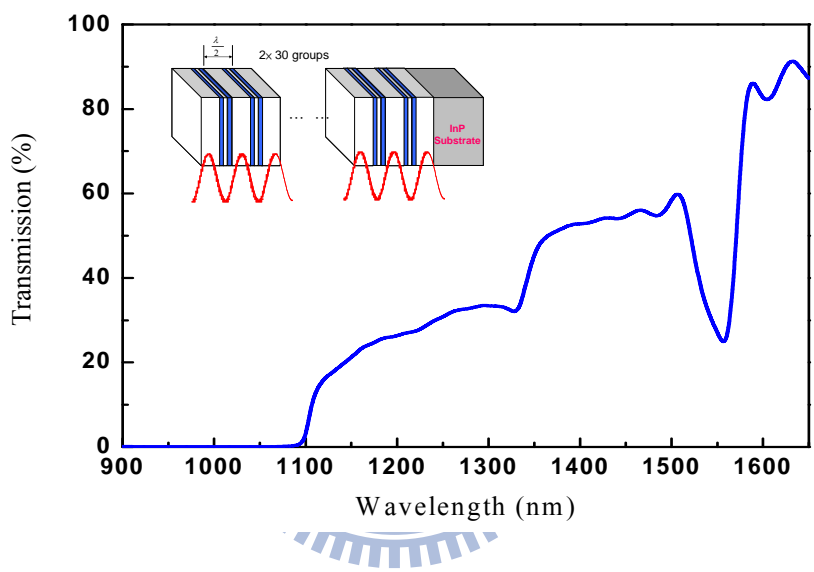


Fig. 4.2-1. Transmittance spectrum at room temperature for the AR-coated AlGaInAs/InP SESA device.

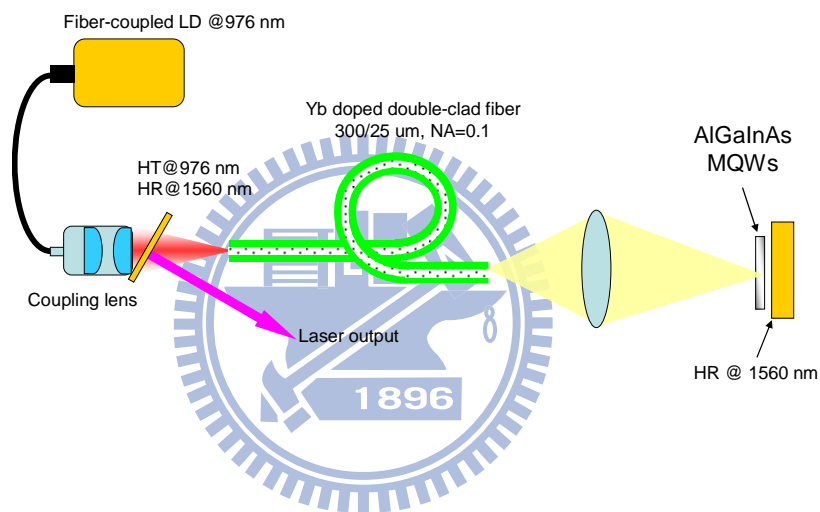


Fig. 4.2-2. Schematic of the experimental setup for EYDFL comprising a 7-m Er-Yb codoped fiber and an external feedback cavity with a periodic AlGaInAs QW/barrier structure as a saturable absorber. HR, high reflection; HT, high transmission.

4.3 Results and discussions

Figure 4.3 -1 shows the average output powers at 1560 nm with respect to the incident pump power in cw and passively Q-switching operations. The cw performance at 1560 nm provides the baseline for evaluating the passively Q-switched efficiency. Without the SESA in the cavity, the cw laser at 1560 nm had an output power of 1.50 W at an incident pump power of 13.5 W. In the passively Q-switching regime, an average output power of 1.26 W was obtained at an incident pump power of 13.5 W. As a consequence, the Q-switching efficiency (ratio of the Q-switched output power to the cw power at the maximum pump power) was found to be as high as 84%. This Q-switching efficiency is significantly superior to those of eye-safe lasers with Co^{2+} or Cr^{2+} doped crystals as saturable absorbers up to 50%. The M^2 beam-quality factor was measured to be <1.5 over the complete output power range. On the other hand, no damage to the fiber was observed over several hours of operation, and the laser performance was reproducible on a day-to-day basis.

The pulse temporal behavior was recorded by a LeCroy digital oscilloscope (Wavepro 7100; 10G samples/sec; 1 GHz bandwidth) with a fast InGaAs photodiode. Figure 4.3-2 shows the pulse repetition rate and the pulse energy versus the incident pump power. The pulse repetition rate increases monotonically with the pump power up to 12 kHz. Like typical passively Q-switched lasers, the pulse energy is almost unrelated to the pump power and its value is 105 μJ on average.

Figure 4.3-3(a) shows the temporal shape of a single Q-switched pulse envelope, which was recorded at the maximum pump power. It can be seen that the self-mode-locking effect [12]-[13] leads to the formation of the mode-locked pulses inside the Q-switched pulse envelope. The separation of the mode-locked pulses was found to be 80 ns, which matched exactly with the cavity roundtrip time and corresponded to a repetition rate of 12.4 MHz. The estimated energy of the highest pulse inside envelope was found to be close to 17 μJ . The expanded oscilloscope traces reveal that the mode-locked pulse width is approximately 33 ns. As a result, the peak power can be found to be greater than 500 W. A typical oscilloscope

trace of Q-switched pulse train is shown in Fig. 4.3-3(b). With the optimum alignment, the pulse-to-pulse stability was found to be approximately $\pm 10\%$ for the pump power higher than 8 W. The pulse-to-pulse instability mainly arises from the modelocking effect, even though this effect can enhance the output peak power. Experimental results reveal that slightly tilting the SESA (10-30 mrad) or inserting an etalon can usefully suppress the mode-locking effect.



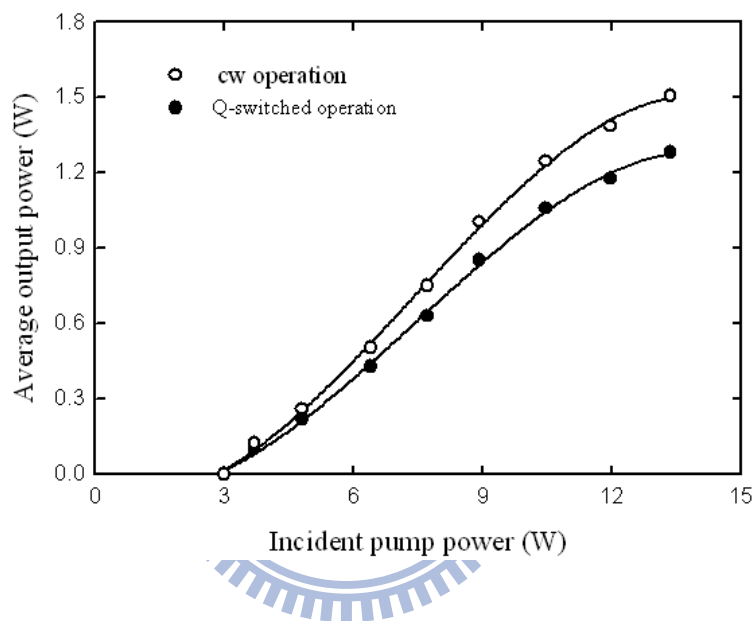


Fig. 4.3-1. Dependence of the average output power on the incident pump power for the cw and passive Q-switching operations.

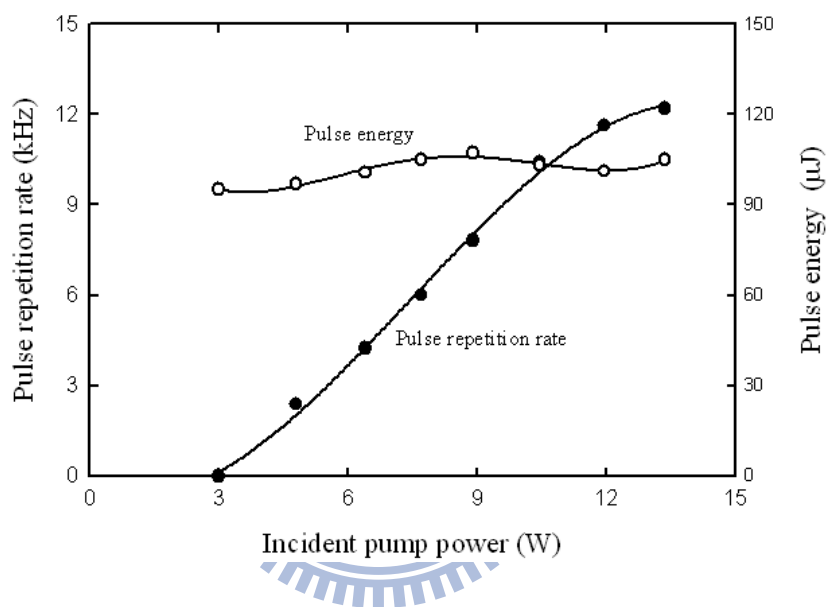


Fig. 4.3-2. Pulse repetition rate and the pulse energy versus the incident pump power.

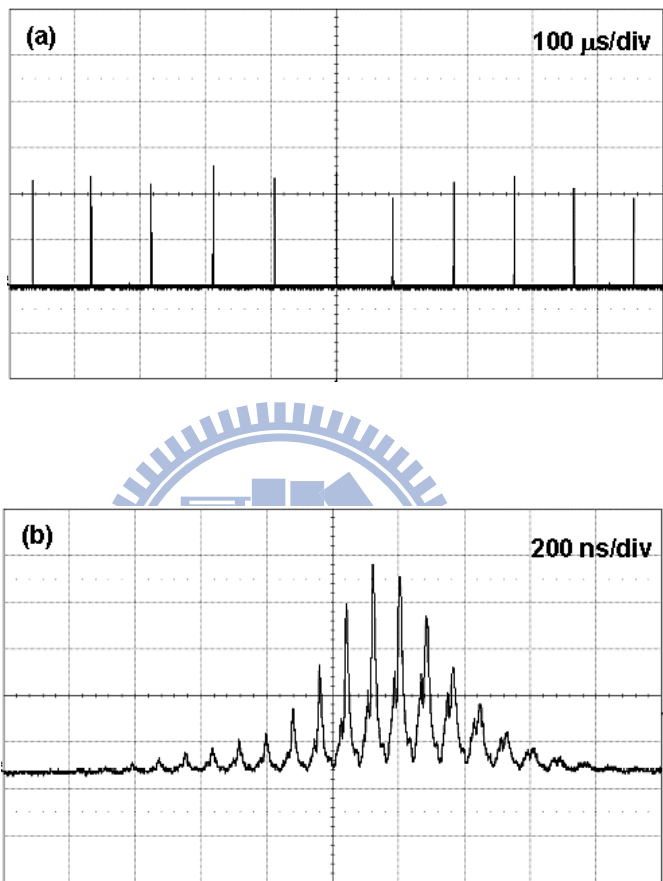


Fig. 4.3-3. (a) Oscilloscope traces of a typical Q-switched envelope., (b) Oscilloscope traces of a train of Q-switched pulses

4.4 Conclusion

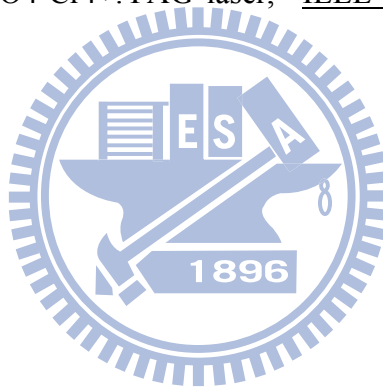
In summary, we have demonstrated an efficient passively Q-switched EYDFL at 1560 nm with a periodic AlGaInAs QW/barrier structure as a saturable absorber in an external Q-switch configuration. Greater than 1.26 W of an average output power at a repetition rate of 12 kHz was generated with a 13.5-W diode pump power. The maximum peak power is higher than 500 W. The remarkable performance confirms the prospect of using AlGaInAs QWs as saturable absorbers in passively Q-switched eye-safe lasers. Moreover, the present result indicates that the output peak power can be significantly enhanced by using a fiber with a larger core size and a saturable absorber with a lower initial transmission.



References


- [1]. A.M. Malyarevich, V.G. Savitski, P.V. Prokoshin, N.N. Posnov, K.V. Yumashev, E. Raaben, and A.A. Zhilin, Glass doped with PbS quantum dots as a saturable absorber for 1- μm neodymium lasers,” *J Opt. Soc. Am. B* **19**, pp. 28–32, (2002).
- [2]. V. N. Filippov, A. N. Starodumov, and A. V. Kir’yanov, “All-fiber passively Q-switched low-threshold erbium laser,” *Opt. Lett.*, **26**, 343–345 (2001).
- [3]. V. N. Philippov, A. V. Kir’yanov, and S. Unger, “Advanced configuration of erbium fiber passively Q-switched laser with Co :ZnSe crystal as saturable absorber,” *IEEE Photon. Technol. Lett.*, **16**, No.1, 57–59, Jan. 2004.
- [4]. M. Laroche, A. M. Chardon, J. Nilsson, D. P. Shepherd, and W. A. Clarkson, “Compact diode-pumped passively Q-switched tunable Er–Yb double-clad fiber laser,” *Opt. Lett.*, **27**, 1080–1082, (2002).
- [5]. V. N. Philippov, J. Nilsson, W. A. Clarkson, A. Abdolvand, V. E. Kisel, V. G. Shcherbitsky, N. V. Kuleshov, V. I. Konstantinov, and V. I. Levchenko, “Passively Q-switched Er–Yb double-clad fiber laser with Cr :ZnSe and Co :MgAl O as a saturable absorber,” *Proc. SPIE*, Vol. **5335**, 8–15, (2004).
- [6]. R. Paschotta, R. Häring, E. Gini, H. Melchior, U. Keller, H. L. Offerhaus, and D. J. Richardson, “Passively Q-switched 0.1 mJ fiber laser system at 1.53 μm ,” *Opt. Lett.* **24**, 388-390 (1999).
- [7]. J.-B. Lecourt, G. Martel, M. Guezo, C. Labbe, and S. Loualiche, “Erbium-doped fiber laser passively Q-switched by an InGaAs/InP multiple quantum well saturable absorber,” *Opt. Commun.*, **263**, 71-83 (2006).
- [8]. S. C. Huang, S. C. Liu, A. Li, K. W. Su, Y. F. Chen, and K. F. Huang, “AlGaInAs quantum-well as a saturable absorber in a diode-pumped passively Q-switched solid-state laser,” *Opt. Lett.* **32**, 1480–1482 (2007).
- [9]. K. Alavi, H. Temkin, W. R. Wagner, and A. Y. Cho, “Optically pumped 1.55- μm double heterostructure $\text{Ga}_x\text{Al}_y\text{In}_{1-x-y}\text{As}/\text{AluIn}_{1-u}\text{As}$ lasers grown by molecular beam

- epitaxy,” Appl. Phys. Lett. **42**, 254-256 (1983).
- [10]. W. T. Tsang and N. A. Olsson, “New current injection 1.5- μ m wavelength Ga_xAl_yIn_{1-x-y}As/InP doubleheterostructure laser grown by molecular beam epitaxy,” Appl. Phys. Lett. **42**, 922-924 (1983).
- [11]. N. Nishiyama, C. Caneau, B. Hall, G. Guryanov, M. H. Hu, X. S. Liu, M.-J. Li, R. Bhat, and C. E. Zah, Long-wavelength vertical-cavity surface-emitting lasers on InP with lattice matched AlGaInAs–InP DBRgrown by MOCVD,” IEEE J. Sel. Top. Quantum Electron. **11**, 990–998 (2005).
- [12]. L. A. Zenteno, H. Po, and N. M. Cho, “All-solid-state passively Q-switched mode-locked Nd-doped fiber laser,” Opt. Lett. **15**, 115-117 (1990).
- [13]. Y. F. Chen and S. W. Tsai, “Simultaneous Q-switching and mode-locking in a diode-pumped Nd:YVO₄-Cr⁴⁺:YAG laser,” IEEE J. Quantum Electron. **37**, 580-586 (2001)



Chapter 5

Widely Tunable Eye-safe Laser with Photonic Crystal Fiber



Double-cladding rare-earth doped fiber lasers are of great interest due to their good beam confinement, excellent heat dissipation, spatial beam quality, and high efficiency [1]-[7]. In Chapter 4, a 7-m Erbium-Ytterbium-codoped double clad fiber was used to be a gain medium in a fiber laser. Long-length fiber up to 7 m is based on the consideration of sufficient gain, however, it increases the pulse width up to 200 ns and consequently the peak power is lower. In order to effectively narrow down the pulse width, a fiber with higher gain coefficient is desired. This can be achieved by increasing the core size and utilizing active ions with larger stimulated cross section. An Ytterbium doped photonic crystal fiber (PCF) can meet the above-mentioned requirement. Though the radiation is mainly located in the range of 1 μm , we can exploit an AlGaInAs quantum-well (QW) structure and optical parametric oscillator (OPO) configuration to convert the 1- μm radiation into eye-safe regime as described in chapter 4 and chapter 2, respectively.

High-peak-power tunable laser sources have been in demand for the applications in the eye-safe wavelength regime near 1.55- μm such as free-space communication, gas sensing, spectroscopy, and medical treatment [8]-[11]. Because of the broad bandwidth resulted from the amorphous nature of the glass host [12],[13], directly utilizing erbium-ytterbium-codoped double-clad fiber lasers (EYDFL) possess the potential of wavelength tunability. However, traditionally a wavelength-selective element such as grating or etalon is desired in the cavity and thus increases the complexity of laser cavity. An alternative method for flexibility in tuning wavelength is an OPO pumped by a laser source with shorter wavelength [14], [15]. Based on the phase matching condition, the signal output wavelength could be controlled by adjusting the temperature of nonlinear crystal, pump incident direction, or pump wavelength.

For pulsed OPO operation, the passively Q-switch gives the advantage of simplification and compactness in experimental setup. In addition to the mostly used transition metal-doped crystals, semiconductor material with a periodic quantum-well structure has been demonstrated as a saturable absorber in the EYDFL to achieve a 105- μJ passively Q-switched 1.54- μm laser, as reported in chapter 4 and ref. [16], and in the ytterbium doped PCF laser to achieve an 1.1-mJ passively Q-switched 1.03- μm laser [17]. In 2010, the performance of

eye-safe laser with a passively Q-switched PCF laser in an intracavity OPO was firstly reported [18]. In the published work, the fundamental wavelength is fixed at the maximum gain peak and a temperature-insensitive x-cut KTP was used in the OPO, this makes it inflexible to realize a broadly tunable laser. Periodically poled lithium niobate (PPLN) is a powerful QPM nonlinear crystal in OPOs for generating near (NIR) to mid-infrared (MIR) radiation because of its high nonlinear coefficient (~ 15 pm/V), broad transmission spectrum (up to $4.5\mu\text{m}$) [19]. In addition, the high differential refractive-index/temperature coefficient makes a signal wavelength shift up to 0.5 nm/ $^{\circ}\text{C}$ at a pump source of 1030 nm for a grating period of $28 \sim 30$ μm . Therefore, it is well worthy of investigation to utilize the QPM nonlinear crystal in an OPO pumped by a passively Q-switched ytterbium-doped PCF laser to generate broadly tunable eye-safe wavelength radiation.



5.1 Experimental setup and results

The schematic of external-cavity OPO pumped by a passively Q-switched PCF laser is depicted as Fig. 5.1-1. The experimental setup could be separated into two major parts, one is a diode pumped passively Q-switched PCF laser and the other one is a singly resonating OPO. The performance of these two parts will be discussed individually in the following two sections.

5.1.1 Diode pumped PCF laser with AlGaInAs semiconductor absorber

The cavity consists of a 55-cm polarization maintaining (PM) Yb-doped PCF and an external feedback cavity with a saturable absorber. The external cavity incorporates with a focusing lens of 50-mm focal length to focus the fiber output into the saturable absorber and a high reflective mirror behind the saturable absorber for feedback. The detail technical data of the rod-type PCF (DC-200/70-PM-Yb-ROD, NKT Photonics) is shown in Table 5.1-1. The PCF has a large mode field diameter of 55 μm to push the nonlinear threshold up to higher level than conventional single mode fiber. And a low numerical aperture value of 0.02 permits to sustain the operation in single transverse mode and excellent beam quality. The pump cladding of the PCF has a diameter of 200 μm and a high numerical aperture of 0.6. The image of the cross section of the PCF is depicted as Fig. 5.1-2(a). The small ratio between the inner pump cladding and 70- μm core diameters brings about the pump absorption coefficient to be 30dB/m at 976nm. The PCF was surrounded with a 1.7-mm thick outer cladding and was sealed with end-caps for protection. The boron doped stress-applying parts were adopted to induce birefringence that produces diverse spectral losses to form a linearly polarization state for the fundamental mode. The saturable absorber is a structure of AlGaInAs QW/barrier grown on a Fe-doped InP substrate by metalorganic chemical–vapor deposition (MOCVD), as depicted in Fig. 5.1-2(b). The structure consists of 50 groups of AlGaInAs QW/barrier. Each group contains three 8-nm-thick QWs and 10-nm-thick barriers. In order to increase the damage threshold, each group of quantum wells is designed to be located at the nodes of the

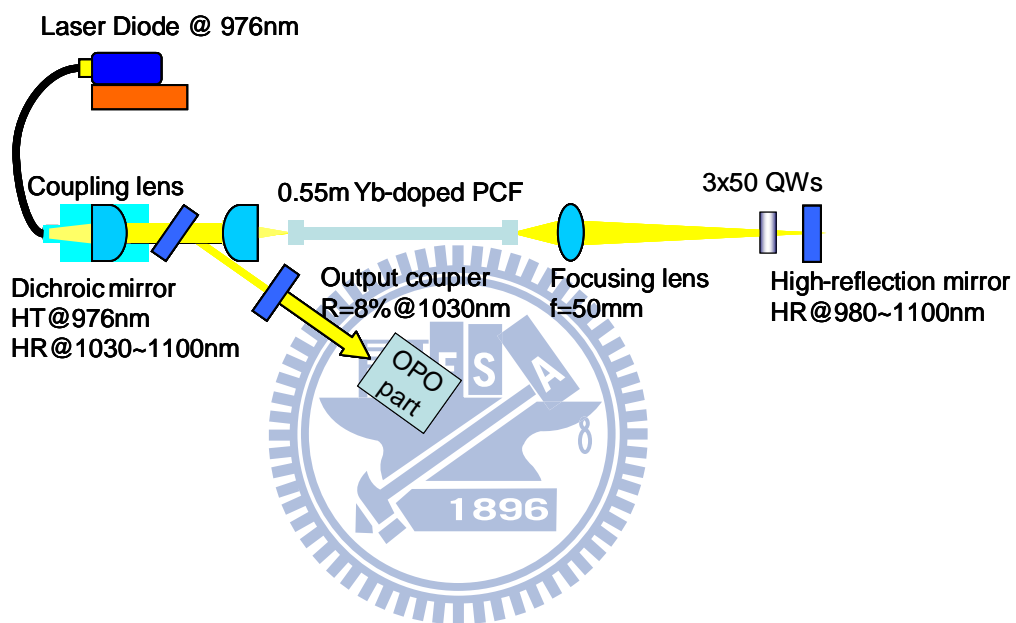


Fig. 5.1-1. The experimental setup of external-cavity pumped OPO with PCF fiber.

Multimode pump core	
Numerical aperture @ 950 nm	0.6 ± 0.05
Pump absorption @ 920 nm	~ 10 dB/m
Pump absorption @ 976 nm	~ 30 dB/m
Slope efficiency	$\sim 60\%$
Physical properties	
Core material	Yb-doped silica
Outer cladding diameter	1.7 ± 0.1 mm
Coating	None
Signal core diameter	70 ± 5 μ m
Pump-cladding diameter	200 ± 5 μ m
Pump-cladding shape	Circular
End cap option	
Material	Pure silica
Length/diameter	8 mm / 8.2 mm
AR coating, R @ 1040-1080 nm	$< 0.1\%$
AR coating, R @ 976 nm	$< 0.5\%$
Spot size at facet ($1/e^2$)	> 140 μ m
Signal return loss	< -35 dB
NA supported	> 0.6
Optical properties	
Signal core	
Single mode	Yes
Mode field diameter	55 ± 5 μ m
Mode field area	2200 ± 200 μ m ²
NA @ 1060 nm	~ 0.02

Table 5.1-1. The property of Yb doped rod-type PCF.

pumping mode, or to have intervals of half-wavelength separated by barriers. A window layer of InP was deposited on the gain structure to prevent surface recombination and oxidation. Both surfaces of the saturable absorber were coated to have anti-reflection coating at 1030 nm ($R < 0.2\%$). The initial transmission of the saturable absorber was measured to be 19%. The mode diameter on the saturable absorber was estimated to be approximately 400 μm . The pump source was a 20-W 976-nm fiber-coupled laser diode with a core diameter of 200 μm and a numerical aperture of 0.2. Focusing lens with 25-mm focal length and 90% coupling efficiency was used to re-image the pump beam into the fiber through the dichroic mirror with high transmission (HT, $T > 90\%$) at 976 nm and high reflectivity (HR, $R > 99.8\%$) within 1030~1100 nm. The pump spot radius was approximately 100 μm , and the pump coupling efficiency was estimated to be around 80%. The pulse temporal behavior was recorded by a digital oscilloscope with a fast InGaAs photodiode.

The output power, pulse energy and output spectrum are shown in Fig. 5.1-3. The maximum output power was obtained to be 4.9 W under the 13.1 W of pump power and it turns out a conversion efficiency over 37%. The central peak of wavelength is dependent on the pump power and distributes from 1031 nm to 1029 nm with the increasing of pump power. The inset of Fig. 5.1-3 shows the output spectrum of PCF laser with the 13.1 W of pump power. The FWHM of bandwidth is around 0.5 nm and the M^2 factor was measured to be less than 1.3 over the complete output power range, owing to the low-NA feature of the fiber. The laser output was measured to be linearly polarized with an extinction ratio of approximately 100:1. Figure 5.1-4 (a) and (b) show the traces of output pulses under a lower and higher pump power level, 6.3W and 13.1 W, respectively. A self-modulation phenomenon inside the Q-switched envelope was obviously observed in pulsed fiber lasers for high pump power. This phenomenon is generally considered to arise from the stimulated Brillouin scattering (SBS) which can provide strong feedback to the cavity together with pulse compression [20]-[23]. The output repetition rate ranges from 1.5 kHz to 6.5 kHz and is related to pump power. The pulses with maximum peak power of 170 kW and pulse energy up to 750 μJ were obtained.

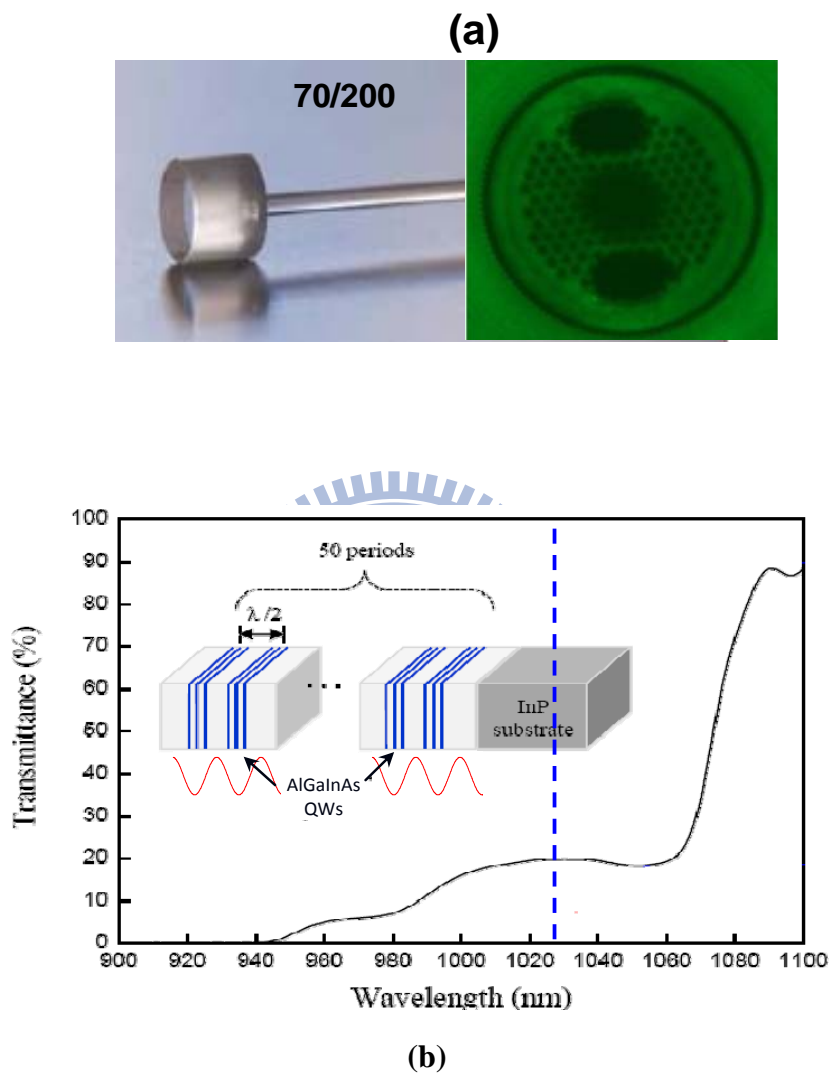


Fig. 5.1-2. (a) The image of cross section of rod-type PCF. (b) The transmission spectrum and structure of AlGaInAs saturable absorber, which consists of 50 groups of three quantum wells

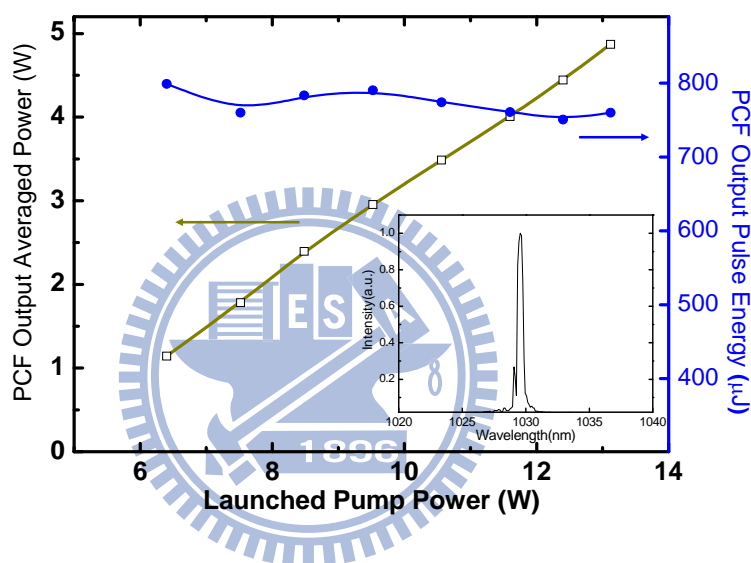


Fig. 5.1-3. The output power of the passively Q-switched PCF laser versus the 976-nm launched pump power. Inset, the lasing spectrum obtained with 12.5 W of pump power.

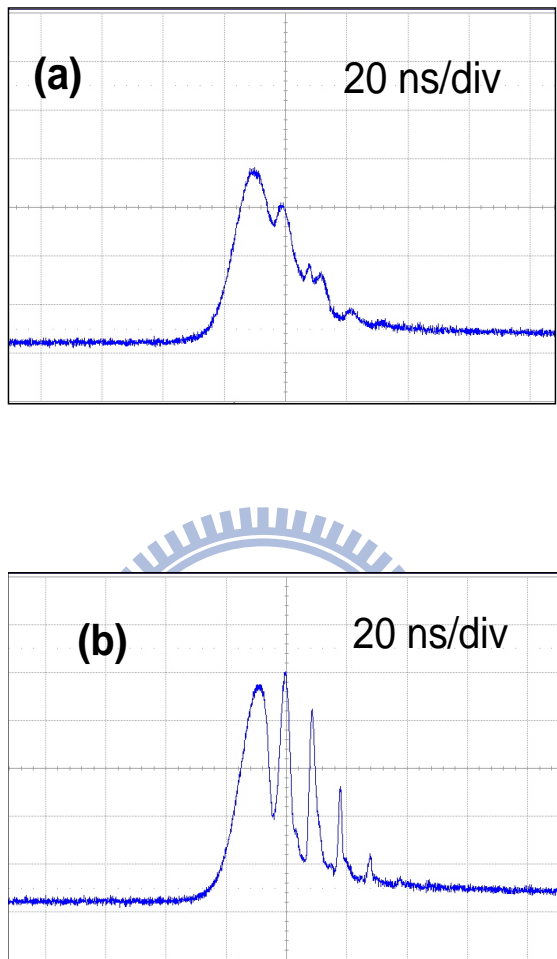


Fig. 5.1-4. Typical oscilloscope traces of output pulses of the passively Q-switched PCF laser. (a) Pulse shape with 6.3 W of pump power. (b) Pulse shape with 13.1 W of pump power.

5.1.2 External-cavity OPO

The 750- μ J passively Q-switched PCF laser at a repetition rate of 6.5 kHz was used as a pump source in the external-cavity OPO, as depicted in Fig. 5.1-5. The nonlinear crystal in is a 0.76-mm thick and 2-cm long congruent PPLN with a poling period of 29.6- μ m. The singly-resonant OPO cavity consists of two BK7 plane mirrors, the front mirror and output coupler. The front mirror is coated with high transmission at pump wavelength ($T > 90\%$) and high reflectivity from 1500 nm to 1600 nm ($R > 99\%$). The output coupler is coated with high transmission at pump wavelength ($T > 90\%$) and partial reflectivity from 20% to 90% corresponding to the wavelength from 1510 to 1590 nm. A focusing lens with 75-mm focal length was used to focus the pump source into the PPLN crystal. The pump spot size inside PPLN was measured to be around 300 μ m. Between the PCF laser and external-cavity OPO, a half-wave plate and a polarization cube were bundled together to control the pump incident power. The maximum average pump incident power was limited to 2.6 W, or the pulse energy limited to 390 μ J for the consideration of photorefractive effect and damage threshold of PPLN. The PPLN was temperature controlled from 20 $^{\circ}$ C to 140 $^{\circ}$ C by an oven to adjust the phase matching wavelength.

The performance of output power of external-cavity OPO pumped by passively Q-switched PCF laser is shown in Fig. 5.1-6(a). The temperature of PPLN was controlled at 100 $^{\circ}$ C. Under the pump power of 2.6 W, the output average power of 0.9W at signal wave was obtained corresponding to a pulse energy of 138 μ J. The conversion is about 35% and the slope efficiency is up to 37.5%. From the temporal pulse traces of pump and signal wave shown in Fig. 5.1-6(b), the signal pulse shape possesses several spikes which were resulted from SBS effect in pump source as mentioned above. Such an effect can be reduced for lower operating power of PCF laser as depicted in Fig. 5.1-4(a). The maximum output peak power of signal wave was estimated to be 19 kW with an effective pulse width of 7.3 ns.

The temperature of PPLN was tuned from 20 $^{\circ}$ C to 140 $^{\circ}$ C in an interval of 20 $^{\circ}$ C. The output wavelength of signal wave shifts from 1513 nm to 1593 nm and total 80-nm tuning

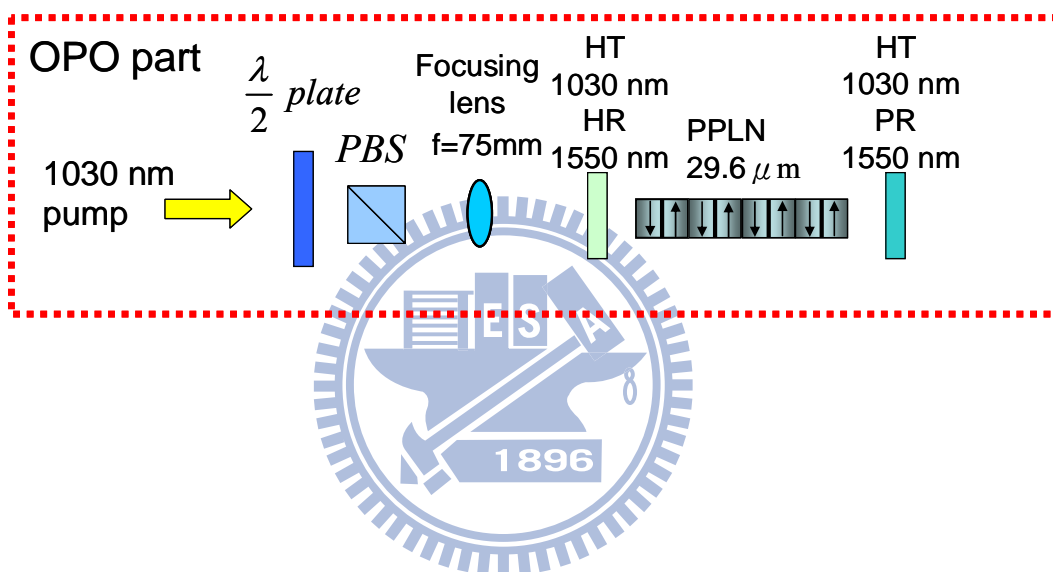
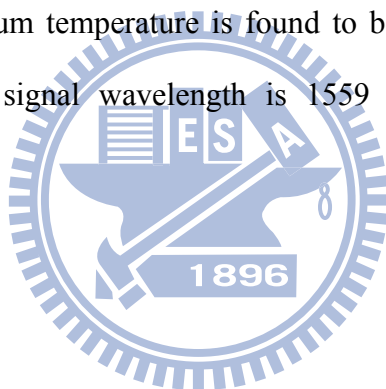


Fig. 5.1-5. The schematics of external-cavity OPO setup. A half-wave plate and polarization beam splitter cube were settled in front of OPO to control the input pump power.

range was obtained. Fig. 5.1-7 shows the wavelength of output signal in different operating temperature. The experimental data with empty circles is in good agreement with theoretical data calculated from Selmier's equations [24],[25]. Higher temperature and larger wavelength is possible. However, the reflectivity of output coupler used is not uniform within the tuning range of wavelength. Besides, with increasing the temperature higher than 140 °C, the idler phase-matching wavelength gradually approaches 2.8 μm which locates at the peak absorption of lithium niobate [26]. As a result, higher loss will be induced in the cavity for operating temperature higher than 140 °C. On the other hand, for lower operating temperature, the photorefractive effect of congruent PPLN will get stronger and limit the output performance. Therefore, there is an optimum conversion efficiency for a specific temperature, as depicted in the inset of Fig. 5.1-7. In this experiment, the conversion efficiency varies from 11% to 35% and the optimum temperature is found to be around 100 °C. At the optimum point, the phase-matching signal wavelength is 1559 nm with a corresponding output reflectivity of 65%.



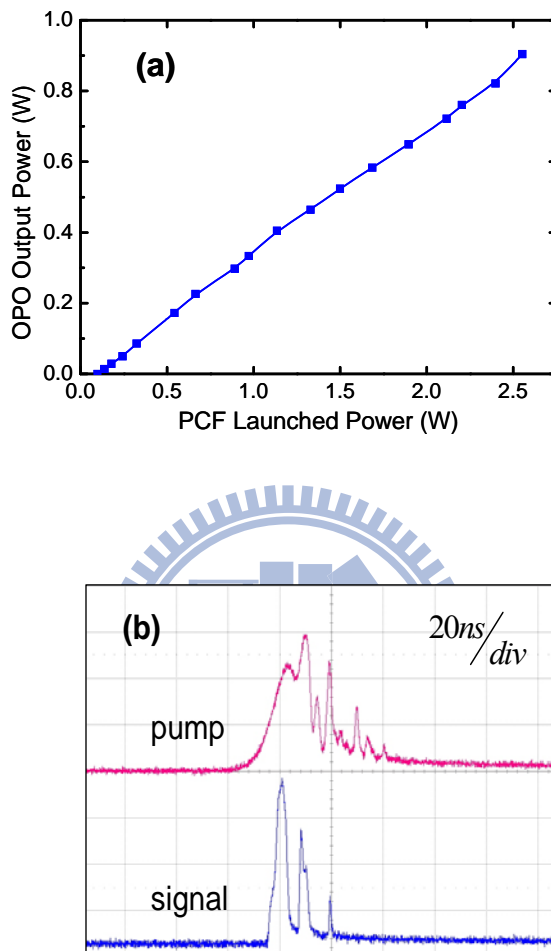


Fig. 5.1-6. The output performance of external-cavity OPO. (a) The averaged output power of signal wave versus averaged power of PCF laser. (b) The temporal traces of pump and signal wave.

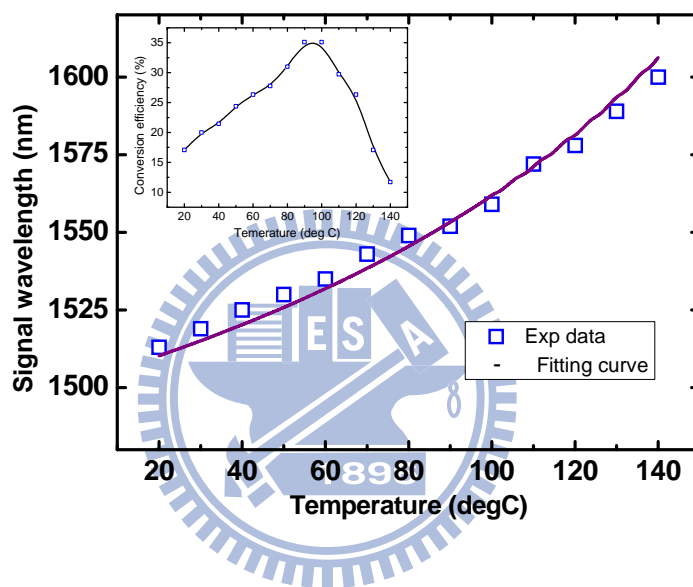
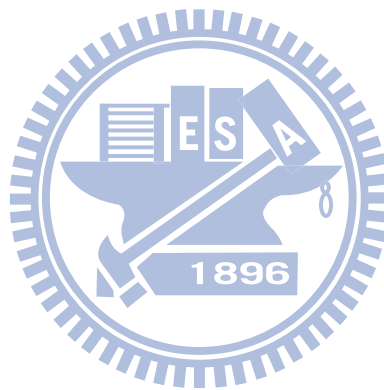


Fig. 5.1-7. The tuning curve of signal wavelength versus different operating temperature. Inset, the conversion efficiency versus operating temperature.

5.2 Conclusion

We achieved a widely tunable passively Q-switched photonic crystal fiber laser by means of an external-cavity optical parametric oscillator. The wavelength tuning range is up to 80 nm. With an AlGaInAs Qs/barrier structure as a saturable absorber in the 1029-nm PCF laser, the fundamental pulse with energy up to 750 μJ was obtained and was incident into the OPO cavity. Under the pump energy of 390 μJ , the maximum output energy and peak power of signal wave was found to be 138 μJ and 19 kW, respectively. By tuning the temperature of nonlinear crystal, PPLN, over 80-nm tuning range of the signal output wavelength from 1513 to 1593 nm was obtained.



References

- [1]. A. Tünnermann, T. Schreiber, F. Röser, A. Liem, S. Höfer, H. Zellmer, S. Nolte, and J. Limpert, “The renaissance and bright future of fibre lasers,” *J. Phys. At. Mol. Opt. Phys.* **38** (9), S681–S693 (2005).
- [2]. Y. Jeong, J. K. Sahu, M. Laroche, W. A. Clarkson, K. Furusawa, D. J. Richardson, and J. Nilsson, “120-W Qswitched cladding-pumped Yb-doped fibre laser,” in Proc. Conference on Lasers and Electro-Optics Europe, 2003. CLEO/Europe, Munich ICM, Germany, June 22–27, 2003, 626–626 (2003).
- [3]. J. Limpert, S. Höfer, A. Liem, H. Zellmer, A. Tünnermann, S. Knoke, and H. Voelckel, “100-W average-power, high-energy nanosecond fiber amplifier,” *Appl. Phys. B* **75**(4-5), 477–479 (2002).
- [4]. Y. Jeong, J. K. Sahu, R. B. Williams, D. J. Richardson, K. Furusawa, and J. Nilsson, “Ytterbium-doped largecore fibre laser with 272 W output power,” *Electron. Lett.* **39**(13), 977–978 (2003).
- [5]. Y. Jeong, J. K. Sahu, D. N. Payne, and J. Nilsson, “Ytterbium-doped large-core fiber laser with 1.36 kW continuous-wave output power,” *Opt. Express* **12**(25), 6088–6092 (2004).
- [6]. A. Liem, J. Limpert, H. Zellmer, A. Tünnermann, V. Reichel, K. Mörl, S. Jetschke, S. Unger, H.-R. Müller, J. Kirchhof, T. Sandrock, and A. Harschak, “1.3 kW Yb-doped fiber laser with excellent beam quality,” in Proc. Conference on Lasers and Electro-Optics 2004, San Francisco, USA, May 16–21, 2004, postdeadline paper CPDD2.
- [7]. A. Fotiadi, A. Kurkov, and I. Razdobreev, “All-fiber passively Q-switched ytterbium laser,” CLEO/Europe- EQEC 2005, Technical Digest, CJ 2–3, Munich, Germany (2005).
- [8]. S. G. Grubb, “High-power fiber amplifiers and lasers,” *Optical Amplifiers and their Applications* **5**, Washington, DC, 42–44 (1996).


- [9]. B. K. Nayar, J. J. Lewandowski, F. J. Wilson, J. A. Chavez, A. B. Grudinin, J. D. Minelly, G. Kennedy, and A. Raven, "High power 1540 nm fiber lasers for surgical applications," Proc. LEOS 98, **2**, Orlando, FL, 397–398 (1998).
- [10]. S. U. Alam, P. W. Turner, A. B. Grudinin, and J. Nilsson, "High-energy, high repetition rate, tunable Er-Yb-codoped Q-switched fiber laser," Tech. Dig. Conf. Lasers and Electro-Optics (LEOS), Baltimore, MD, 218–219 (2001).
- [11]. J. E. Nettleton, B. W. Schilling, D. N. Barr, and J. S. Lei, "Monoblock laser for a low-cost, eyesafe, microlaser range finder," Appl. Opt. **39**, 2428–2432 (2000).
- [12]. G. A. Ball and W. W. Morey, "Continuously tunable single-mode erbium fiber laser," Opt. Lett. **17**, 420–422 (1992).
- [13]. Q. Mao and John W. Y. Lit, "Widely tunable L-band erbium-doped fiber laser with fiber Bragg gratings based on optical bistability," Appl. Phys. Lett. **82**, 1335 (2003).
- [14]. M. E. Klein, C. K. Laue, D. H. Lee, K. J. Boller, and R. Wallenstein, "Diode-pumped singly resonant continuous-wave optical parametric oscillator with wide continuous tuning of the near-infrared idler wave," Opt. Lett. **25**, 490–492 (2000).
- [15]. S. E. Bisson, K. M. Armstrong, T. J. Kulp, and M. Hartings, "Broadly Tunable, Mode-Hop-Tuned cw Optical Parametric Oscillator Based on Periodically Poled Lithium Niobate," Appl. Opt. **40**, 6049–6055 (2001)
- [16]. J. Y. Huang, S. C. Huang, H. L. Chang, K. W. Su, Y. F. Chen, and K. F. Huang, "Passive Q switching of Er-Yb fiber laser with semiconductor saturable absorber," Opt. Express **16**, 3002–3007 (2008)
- [17]. W. Z. Zhuang, W. C. Huang, P. Y. Chiang, K. W. Su, K. F. Huang, and Y. F. Chen, "Millijoule-level Yb-doped photonic crystal fiber laser passively Q-switched with AlGaInAs quantum wells," Opt. Express **18**, 27910–27915 (2010)
- [18]. W. Z. Zhuang, W. C. Huang, Y. P. Huang, K. W. Su, and Y. F. Chen, "Passively Q-switched photonic crystal fiber laser and intracavity optical parametric oscillator," Opt. Express **18**, 8969–8975 (2010)
- [19]. M. M. J. W. van Herpen, S. E. Bisson, and F. J. M. Harren, "Continuous-wave operation of a single-frequency optical parametric oscillator at 4–5 μm based on periodically

- poled LiNbO₃," Opt. Lett. **28**, 2497-2499 (2003).
- [20]. M. Salhi, A. Hideur, T. Chartier, M. Brunel, G. Martel, C. Ozkul, and F. Sanchez, "Evidence of Brillouin scattering in an ytterbium-doped double-clad fiber laser," Opt. Lett. **27**, 1294–1296 (2002).
- [21]. Y. X. Fan, F. Y. Lu, S. L. Hu, K. C. Lu, H. J. Wang, G. Y. Zhang, and X. Y. Dong, "Narrow-linewidth widely tunable hybrid Q-switched double-clad fiber laser," Opt. Lett. **28**, 537–539 (2003).
- [22]. A. A. Fotiadi, P. Mégret, and M. Blondel, "Dynamics of a self-Q-switched fiber laser with a Rayleigh-stimulated Brillouin scattering ring mirror," Opt. Lett. **29**, 1078–1080 (2004).
- [23]. Z. J. Chen, A. B. Grudinin, J. Porta, and J. D. Minelly, "Enhanced Q switching in double-clad fiber lasers," Opt. Lett. **23**, 454–456 (1998)
- [24]. G. J. Edwards and M. Lawrence, "A Temperature-Dependent Dispersion for Congruently Grown Lithium Niobate," Opt. Quantum Electron., **16**, 373-374 (1984)
- [25]. D. H. Jundt, "Temperature-dependent Sellmeier equation for the index of refraction, n_e , in congruent lithium niobate," Opt. Lett. **22**, 1553-1555 (1997).
- [26]. Y. Kong, W. Zhang, X. Chen, J. Xu and G. Zhang, "OH⁻ absorption spectra of pure lithium niobate crystals," J. Phys.: Condens. Matter **11** 2139-2143 (1999)

Chapter 6

Optically Pumped

Semiconductor Laser

A circular logo in the background, featuring a gear-like border. Inside the circle, there is a stylized building or structure with the letters 'FSA' and the year '1896' at the bottom.

6.1 OPSL with barrier-pumping

In the previous chapters I have reported several methods for generating eye-safe lasers including the optical parametric oscillators (OPO), stimulated Raman scattering (SRS) pumped by Nd-doped lasers and Er/Yb fiber laser, and an external-cavity OPO pumped by a Yb³⁺-doped PCF fiber laser.

In this chapter I propose another more compact structure for eye-safe laser sources which is based on AlGaInAs quantum-well (QW) materials. Recently, a high-peak-power AlGaInAs laser at 1.36 μm has been designed with a diode-pumped actively Q-switched Nd:YAG laser as a pump source [1]. We will demonstrate in this chapter a high-peak-power optically pumped semiconductor laser (OPSL) with AlGaInAs QWs structure in eye-safe region.

6.1.1 Device fabrication and laser structure

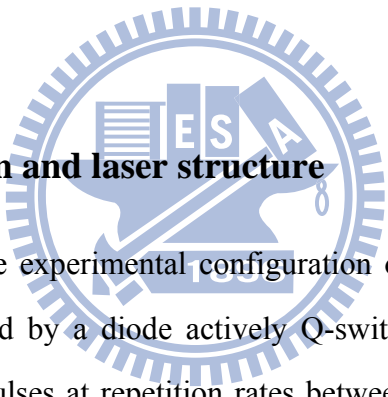


Figure 6.1-1 shows the experimental configuration of the high-peak-power AlGaInAs QWs 1570-nm laser pumped by a diode actively Q-switched Nd:GdVO₄ laser. The pump source provides 20–60 ns pulses at repetition rates between 20 and 60 kHz. The pump spot diameter was controlled to be 480 ± 20 μm for efficient spatial overlap with the fundamental transverse mode. The laser resonator is a linear flat–flat cavity that was stabilized by the thermally induced lens in the gain medium. This concept was found nearly simultaneously by Zayhowski and Mooradian [2] and by Dixon et al. [3]. A linear flat–flat cavity is an attractive design because it reduces complexity and makes the system compact and rugged. When the average pump power is between 0.5 and 1.5 W, the mode-to-pump ratio is experimentally found to be in the range of 1.0–1.5. The input mirror was a flat mirror with antireflection coating on the entrance face at 1064 nm ($R < 0.2\%$), high-reflection coating at 1570 nm ($R > 99.8\%$), and high-transmission coating at 1064 nm on the other surface ($T > 90\%$). The reflectivity of the flat output coupler is 95% at 1570 nm. The overall laser cavity length is approximately 10 mm.

The gain medium is an AlGaInAs QW/barrier structure grown on a Fe-doped InP substrate by metalorganic chemical-vapor deposition. Note that the conventional S-doped InP substrate has large absorption in the 1.0–2.0 μm spectral region, while the Fe-doped InP substrate is chosen because of its transparency at the lasing wavelength. The gain region is made up of thirty groups of two 8-nm-thick 1570-nm AlGaInAs QWs with 10-nm-thick barriers. Each QW group is spaced at a half-wavelength interval by an AlGaInAs barrier layer with the band-gap wavelength approximately 1064 nm to absorb the pump light as well as to locate the QWs in the antinodes of the optical standing wave. An InP window layer was deposited on the gain structure to avoid surface recombination and oxidation. The backside of the substrate was mechanically polished after growth. The both sides of the gain chip were antireflection-coated (AR-coated) to reduce back reflections and the couple-cavity effects. For simplicity, we used a single layer of coating on the gain medium. As a result, the total residual reflectivity of the AR-coated sample is approximately 5%. Figure 6.1-2 depicts the room-temperature spontaneous emission spectrum obtained by pulse excitation at 1064 nm. It can be seen that the emission is quite broad with a peak at around 1570 nm and has a long tail extending to shorter wavelength. In the laser experiment, the semiconductor chip was simply mounted on a water-cooled copper block and the water temperature was feedback maintained.

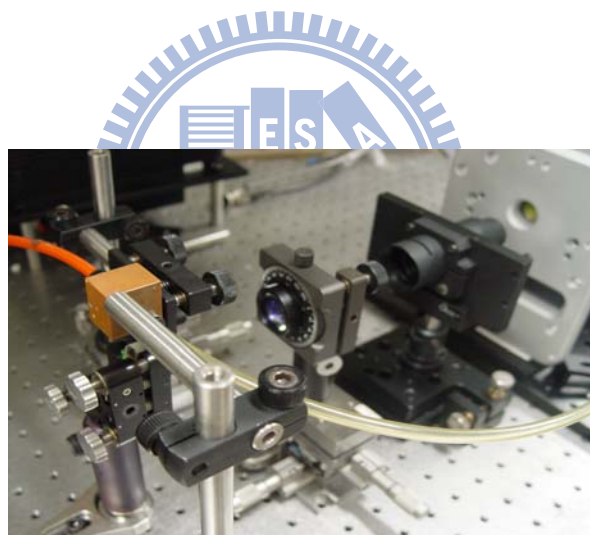
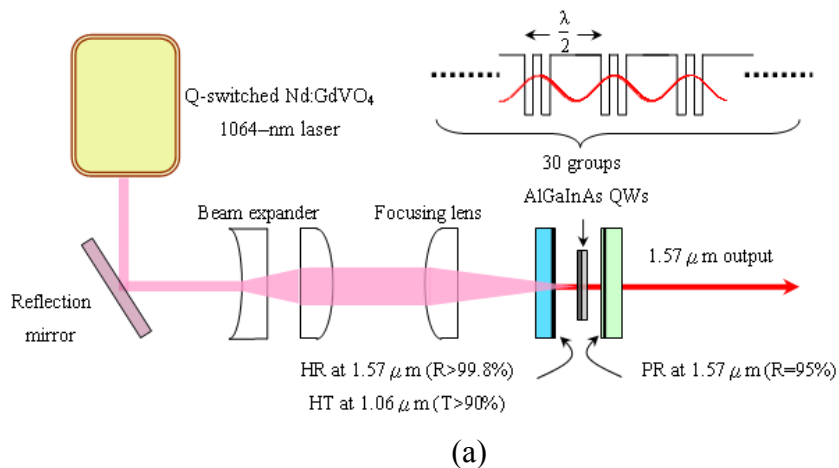


Fig. 6.1-1. (a) Experimental configuration of the high-peak-power AlGaInAs QWs 1570-nm laser pumped by a Q-switched Nd:GdVO₄ laser; HR: high reflection, HT: high transmission, PR: partial reflection. (b) Actual setup.

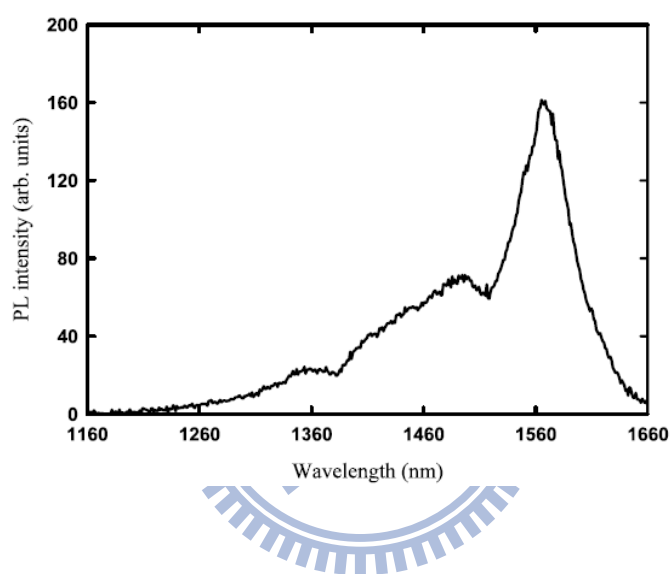


Fig. 6.1-2. Room-temperature spontaneous emission spectrum of the AlGaInAs QWs pumped by a Q-switched Nd:GdVO₄ 1064-nm laser.

6.1.2 Experimental results and discussion

Figure 6.1-3 shows the performance of the optically pumped AlGaInAs laser operated at the water temperature of 10°C at four repetition rates of 20, 30, 40, and 60 kHz. The pump pulse widths for the repetition rates of 20, 30, 40, and 60 kHz are approximately 20, 25, 30, and 40 ns, respectively. The transverse mode was measured to be the fundamental mode over the complete output power range. The beam quality factor was determined by a Gaussian fit to the laser beam waist and the divergence angle, and was found to be less than 1.3 indicating fundamental transverse-mode operation. Spectral information of the laser was monitored by an optical spectrum analyzer (Advantest Q8381A). The spectrum analyzer with a diffraction monochromator can be used for high-speed measurement of pulse light with a resolution of 0.1 nm. It was found that the bandwidth of the lasing spectrum initially increases linearly with the pump power but varies slowly at the higher pump power. The lasing spectrum has the highest peak approximately at 1570 nm with maximum bandwidth up to 18 nm. The typical lasing spectrum shown in the inset of Fig. 6.1-3 was obtained with 1.0 W of average pump power at repetition rate of 30 kHz. The lasing spectra generally comprised dense longitudinal modes and their bandwidth were up to 20 nm at the average pump power greater than 200 mW. The temporal shapes for pump and output pulses were recorded by a LeCroy digital oscilloscope (Wave pro 7100, 10 G samples/s, 1 GHz bandwidth). Typical oscilloscope traces of pump and output pulses are shown in Fig. 6.1-4. With the finest alignment, the pulse-to-pulse amplitude fluctuation was found to be within $\pm 10\%$, which is mainly attributed to the instability of the pump beam.

As shown in Fig. 6.1-3, the average output power at a repetition rate of 30 kHz initially increases with the pump power and begins to saturate at 135 mW at an average pump power greater than 1.25W. Similarly, the conversion efficiency at a repetition rate of 20 kHz is reduced significantly at the average pump power greater than 1.0W and the maximum average output power is saturated at approximately 115mW. The reduction of the conversion efficiency at higher pump powers mainly comes from the gain-saturation effect. Figure 6.1-5(a) shows the output peak power as a function of pump peak power at a repetition rate of

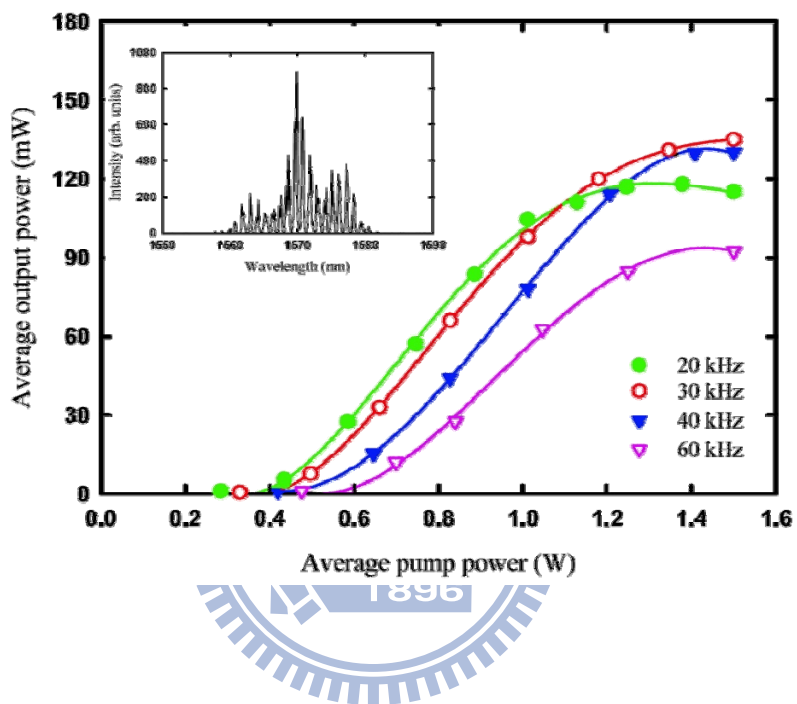


Fig. 6.1-3. Experimental results for the optically pumped AlGaInAs 1570-nm laser operated at the water temperature of 10°C at pump repetition rates of 20, 30, 40, and 60 kHz. Inset shows typical lasing spectrum obtained with 1.0 W of average pump power at a repetition rate of 30 kHz.

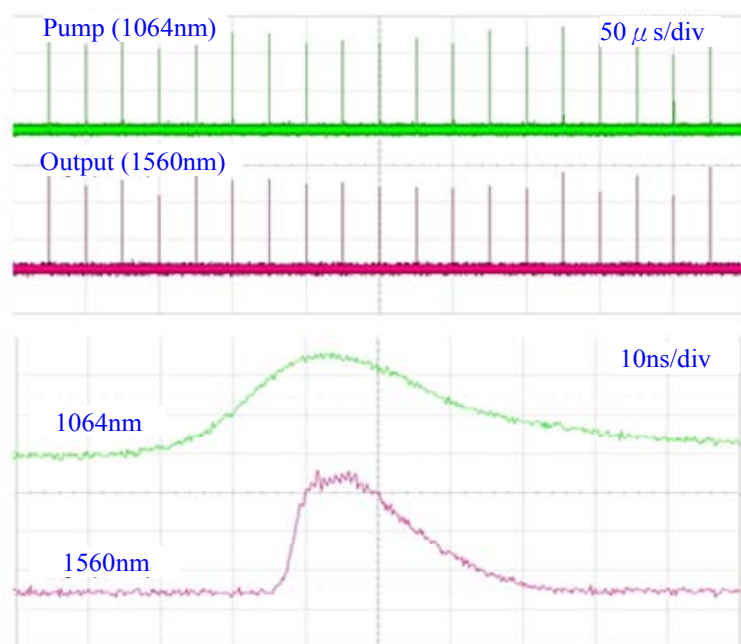


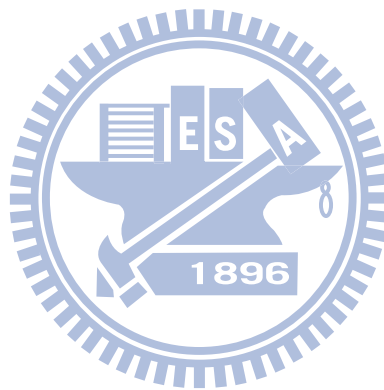
Fig. 6.1-4. Typical oscilloscope traces of pump and output pulse.

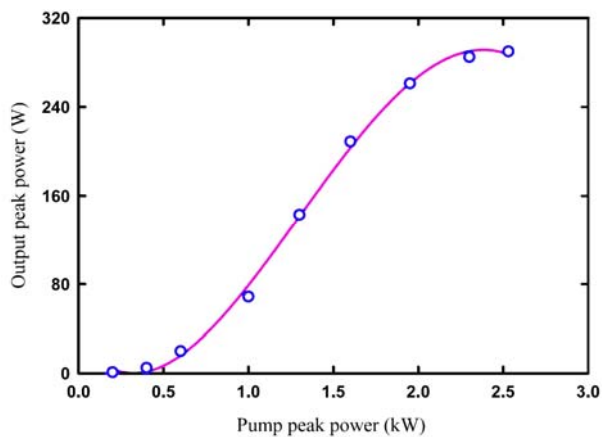
20 kHz. The maximum output peak power is found to be 290 W at a pump peak power of 2.3 kW. With the transmission of the output coupler of 5%, the maximum intracavity lasing power can be calculated to be 5.8 kW. Using lasing mode size $\omega_L = 250 \mu\text{m}$, the lasing mode area $A = \pi\omega_L^2$ and the saturation intensity of the gain chip can be found to be 0.002 cm^2 and 2.9 MW/cm^2 , respectively. This value was two orders of magnitude higher compared to conventional solid-state laser crystals because of its shorter fluorescence decay time. To confirm the gain-saturation effect we used a pulsed semiconductor laser at $1.57 \mu\text{m}$ to measure the transmittance versus the excitation intensity with the z-scan method. The excitation pulse energy and pulse width were $3 \mu\text{J}$ and 50 ns , respectively. The pump radius was varied from 0.01 to 0.1 cm . As a consequence, the excitation fluence was in the range of 0.1 – 10 mJ/cm^2 and was comparable to the fluence in the present laser cavity. As shown in Fig. 6.1-5 (b), the transmittance of the gain material exceeds 85% at the excitation intensity higher than 3.0 MW/cm^2 . Therefore, the number of QWs in the gain chip needs to increase to overcome the gain saturation effect for scaling up the output peak power.

On the other hand, the lower conversion efficiency at 60 kHz is speculated to arise from the longer pump pulse width at this repetition rate leading to the heavier heating effect. We examined the dependence of lasing efficiencies on the water temperature to investigate the influence of the thermal effect. Figure 6.1-6 depicts the input–output characteristics for the water temperatures of 10, 15, 20, and 25°C at a repetition rate of 30 kHz. Increasing temperature can be seen to lead to a certain reduction in the lasing efficiency. Compared with the experimental results shown in Fig. 6.1-3, it can be found that the maximum output power at 20°C at a repetition rate of 30 kHz is almost comparable with that at 10°C at a repetition rate of 60 kHz. As a result, we estimate the overall temperature of the gain chip at 60 kHz to be approximately 10° higher than that at 30 kHz. However, further investigation is required to analyze the influence of the heating dynamics on the conversion efficiency.

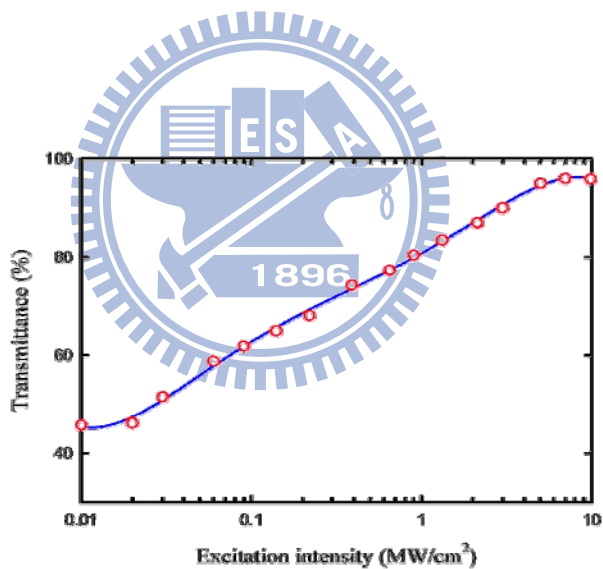
It is worthwhile mentioning that even though the present slope efficiency is not better than the methods based on the nonlinear wavelength conversion, the present pump threshold is generally lower than of the approaches with SRS and OPO processes [4],[5]. Furthermore,

there is some room for optimizing the output performance. One promising way for improving the slope efficiency is to reduce the quantum defect by using a pump laser with longer wavelength and gain chip and with a proper absorption barrier as described in next section.





(a)



(b)

Fig. 6.1-5. (a) Experimental results for the peak output power versus peak pump power at a repetition rate of 20 kHz; (b) the transmittance of the gain chip versus the excitation intensity at 1.57 μm

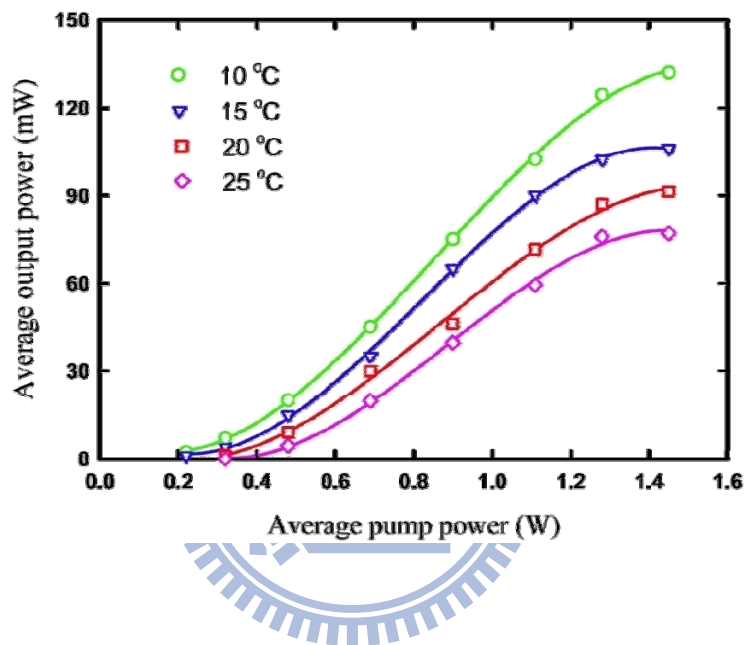


Fig. 6.1-6. Input–output characteristics for the water temperatures of 10, 15, 20, and 25°C at a repetition rate of 30 kHz

6.2 OPSL with in-well-pumping

In the previous section, an optically pumped high-peak-power AlGaInAs eye-safe laser at 1.57 μm pumped by an actively-Q-switched 1064-nm laser was demonstrated. In the gain region of AlGaInAs QW/barrier, the electrons are excited from the ground state to an excited state in the barrier region with band-gap wavelength around 1064 nm, and emit photons with wavelength of 1.57 μm in the QW region. Such a scheme could generate high peak power of hundreds of watt with quite low lasing threshold. However, the quantum defect between the pump photon and lasing photon would give rise to heat generation and influence the performance for the operation of high repetition rate and high pump power.

Recently, the quantum defect and the thermal load were confirmed to be significantly reduced by pumping the QW directly [10],[11]. In this section, we employ the in-well pumping scheme to excite AlGaInAs QWs for efficient eye-safe emission at 1.56 μm . The gain medium is an AlGaInAs QW structure grown on a Fe-doped InP transparent substrate and is pumped by an actively Q-switched 1342 nm laser which directly excites the electrons to an excited state in the QW region rather than in the barrier region. As depicted in Fig. 6.2-1, electrons are excited in the QW region and the quantum defect between pump photon and lasing photon is reduced from 32% to 14% compared with a pump source at 1064 nm. As a result, the thermal effect is significantly reduced.

6.2.1 Device fabrication and experimental setup

Figure 6.2-1 shows the experimental configuration for the AlGaInAs QWs 1555-nm laser pumped by a diode-pumped actively Q-switched Nd:YVO₄ laser at 1342 nm. The pump source provides 20~110-ns pulse width between 20 kHz and 100 kHz. For comparison, a 1064-nm Q-switched laser was used in barrier-pumping scheme. The pump spot radius was controlled to be 70-100 μm by a focusing lens to maintain the spatial overlapping between lasing mode and pump mode. To simplify the cavity structure, the resonator is designed to be a flat-flat cavity stabilized by thermal lens effect of gain medium [22,23]. Although the

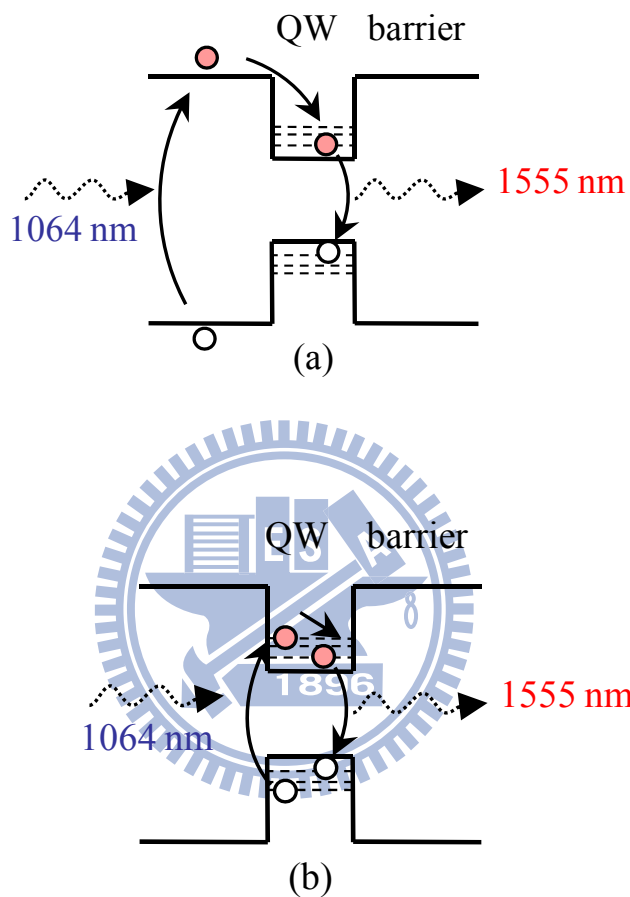


Fig. 6.2-1. Schematic explanation of energy diagrams of (a) barrier pumping and (b) in-well pumping.

thermal lens is reduced in in-well pumping, the effect is still strong enough to stabilize the cavity. For the pump power between 0.4 W and 1.7 W, the mode to pump size was experimentally measured to be 0.6-0.9. The front mirror of resonator is a flat mirror coated with anti-reflection coating at pumping wavelength ($R < 0.2\%$) on the entrance surface, and with high-reflection coating at 1555 nm ($R > 90\%$) as well as high-transmission coating at pumping wavelength ($T > 80\%$) on the other surface. The output coupler is a flat mirror with partial reflection of 90% at 1555nm and 60% at pumping wavelength. The overall laser cavity length is approximately 5 mm.

The gain medium is a structure of AlGaInAs QW/barrier grown on a Fe-doped InP substrate by metalorganic chemical–vapor deposition. The optically active region consists of 30 pairs of AlGaInAs QW/barrier. Each pair contains two 8-nm-thick QWs and 10-nm-thick barrier. The band-gap wavelength of barrier is around 1064 nm and of quantum well is around 1555 nm. In order to get a resonant periodic gain, each group of quantum wells is designed to be located at the antinodes of the lasing mode, or to have intervals of half-wavelength separated by barriers. A window layer of InP was deposited on the gain structure to prevent surface recombination and oxidation. Both surfaces of the gain chip were coated to have antireflection coating at pumping and lasing wavelength. The active gain medium was adhered to a water-cooled copper heat sink and the temperature was controlled by water feedback. Figure 6.2-2(a) depicts the transmission spectrum of the gain medium and Fig. 6.2-3 (b) shows the room temperature spectrum of photoluminescence (PL) obtained by pulse excitation at 1342 nm. It can be seen that there is a high absorption at the pump wavelength of 1342 nm and the spectrum of emission extends more than 200 nm with a peak at the wavelength of 1555 nm.

It is worthwhile to mention that due to the shorter effective thickness of quantum well, the active gain region has lower absorption at 1342-nm pump wavelength than at 1064 nm which has single pass absorption higher than 95%. In order to increase the absorption efficiency, double chips were further used in the serial experiments. The advantage of directly using multiple chips is that could reduce the difficulty of fabrication of gain medium with

more quantum wells. The experimental result shown in Fig. 6.2-3(c) reveals that the single pass absorption efficiency was increased from 45% to 65% when double chips were employed. Total effective absorption efficiency in the cavity could be estimated to be 60% and 79%, respectively. On the other hand, the effective absorption efficiency for single chip could be up to 70% by using an output coupler with retro-reflection at pump wavelength.



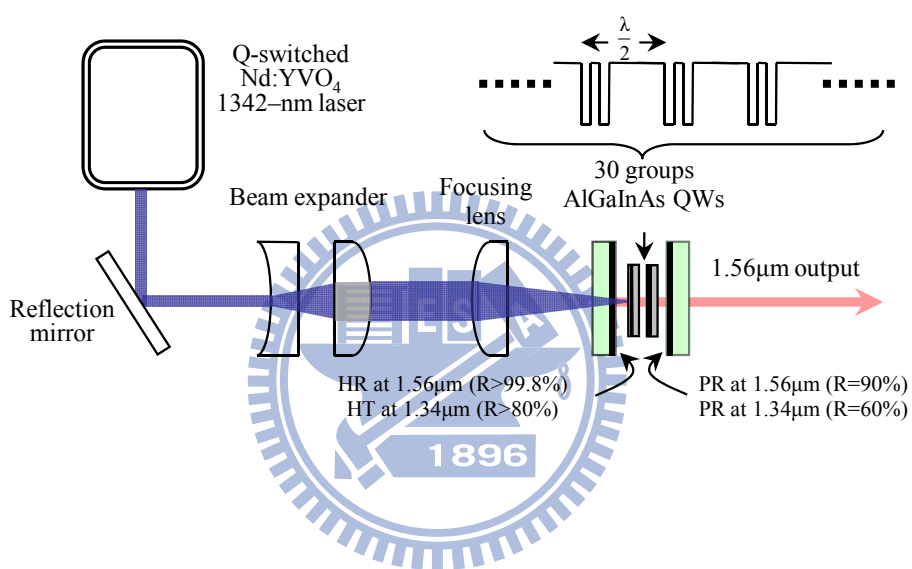


Fig. 6.2-2. The schematic of the AlGaInAs/InP eye-safe laser at 1555 nm. HR: high reflection; HT: high transmission; PR: partial reflection.

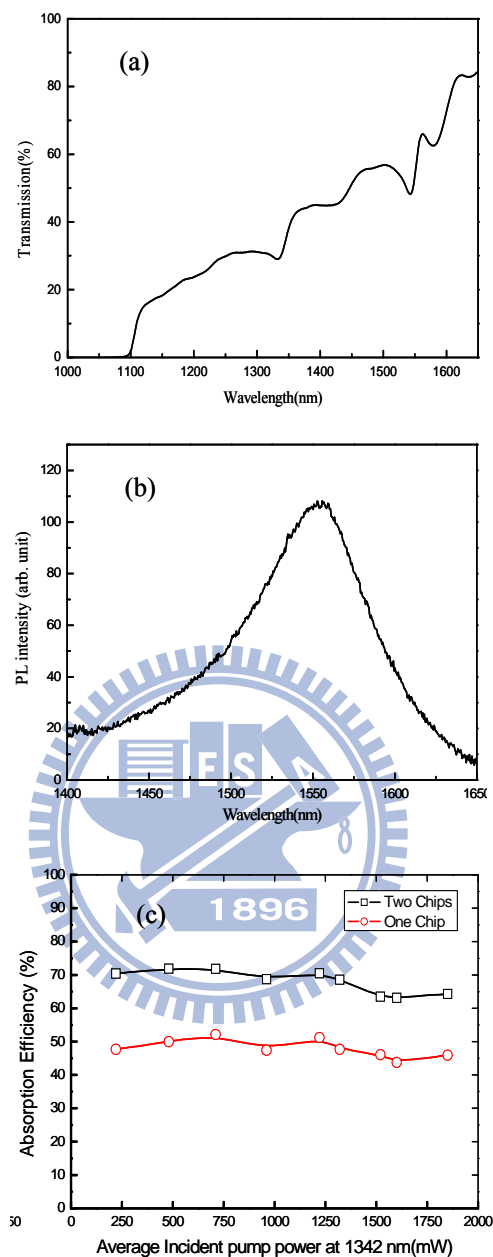


Fig. 6.2-3. (a) The transmission spectrum of AlGaInAs/InP quantum-well/barrier structure. (b) the room-temperature spectrum of photoluminescence pumped by an actively Q-switched Nd:YVO₄ 1342-nm laser. (c) The single pass absorption efficiency of single and double AlGaInAs QW chips.

6.2.2 Experimental results and discussions

Figure 6.2-4 shows the comparison of average output power of single gain chip with in-well and barrier pumping for the operation of 40 kHz repetition rate and 12°C temperature. The maximum values shown in the two curves were measured for the comparable incident pumping power. The solid lines are fourth order polynomial fitting curves. It can be seen that employing the 1342-nm laser as a pump source exhibits good performance in conversion efficiency. This significant improvement result is contributed from the heat reduction by lowering the quantum defect which is diminished from 32% to 14%. However, since the absorption efficiency of gain medium at 1342 nm is lower than at 1064 nm, the available pump power is restricted. Double gain chips, accordingly, were investigated to improve the absorption efficiency. The earlier onset of thermal rollover in in-well pumping shows that further thermal management may be desired to delay the thermal rollover such as lower operating temperature or bonding a diamond heat spreader.

Figure 6.2-5(a) shows the performance of the optically pumped AlGaInAs eye-safe laser with double gain chips operated at 12°C for different pump repetition rate from 20 kHz to 100 kHz in 20 kHz interval. The corresponding average pump pulse width ranges from 20 ns to 110 ns with increasing repetition rate and therefore a decreasing peak power of pulse is corresponded. In the process of increasing the repetition rate for the given cavity and absorbed pump power, the conversion efficiency was limited by instantaneous high peak power which resulted in a rapid temperature rise in low repetition rate and limited by high average power which resulted in an average temperature rise in high repetition rate. Therefore, there was an optimum repetition rate for obtaining the maximum average output power. This conclusion is coincident to the result of the experiment and the published research [19]. From the experimental results shown in Fig. 6.2-5(a), the optimum repetition rate was between 40 kHz and 60 kHz. Figure 6.2-5(b) shows the typical lasing spectrum for the operation of 40-kHz repetition rate with average pump power of 0.65 W. The spectral bandwidth was approximately 17 nm. The filamented spectrum may result from multiple interferences between cavity mirrors and chips and it could also be observed in single chip operation.

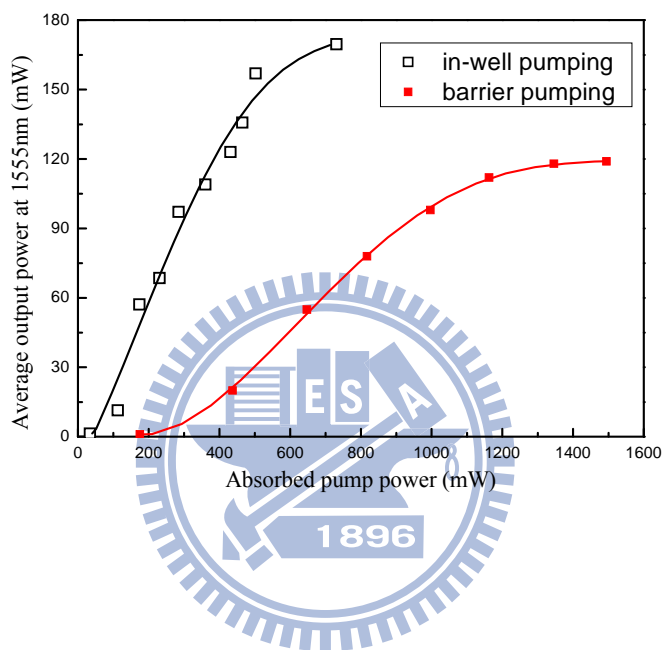
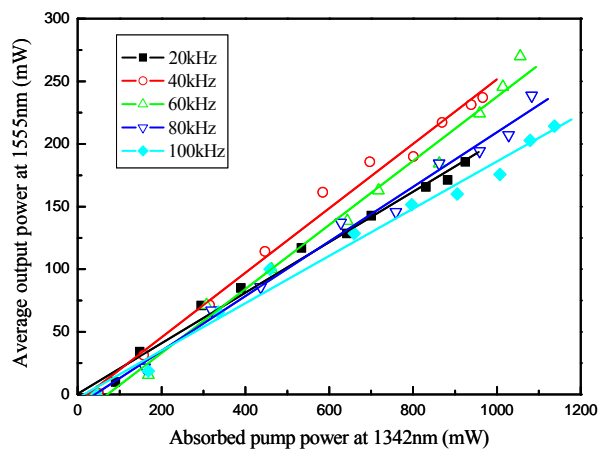
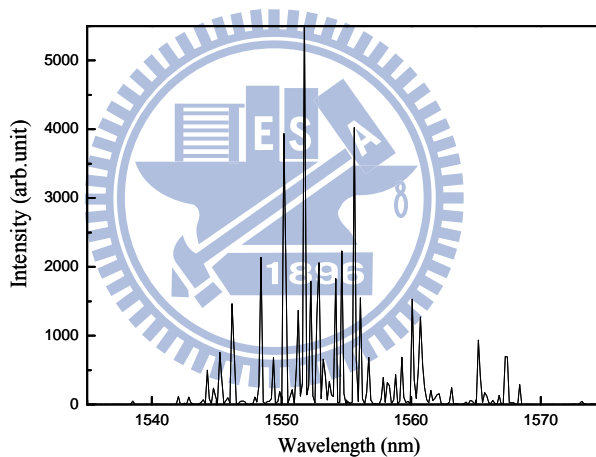


Fig. 6.2-4. The performance of single-chip AlGaInAs 1555-nm laser for 40 kHz and 12°C operation in the scheme of barrier and in-well pumping, respectively. The solid lines are fourth order polynomial fitting curves. The in-well pumping scheme exhibits good performance in conversion efficiency



(a)

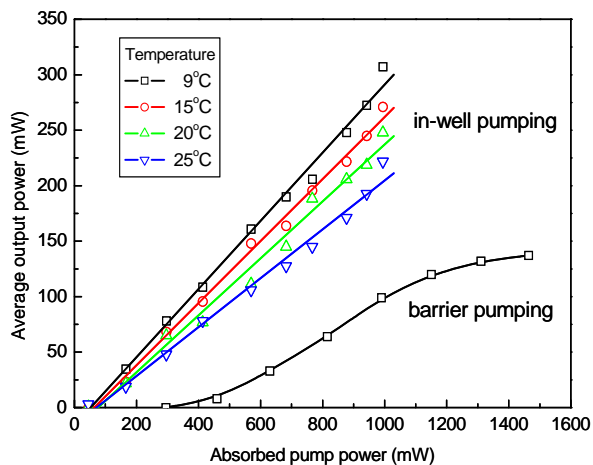


(b)

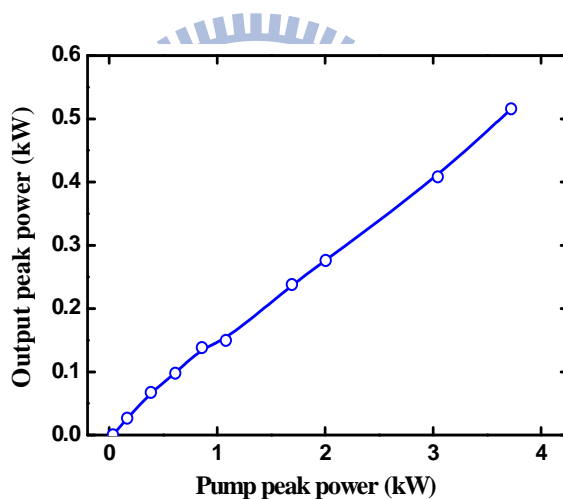
Fig. 6.2-5. Performance of double chips: (a) Experimental results for the optically pumped AlGaInAs eye-safe laser operated at 12 °C for several pulse repetition rates. The repetition rate for optimum performance of conversion efficiency was between 40 kHz and 60 kHz. (b) Typical lasing spectrum at repetition rate of 40 kHz and average pump power of 0.65 W.

In order to further realize the influence of thermal effect, the average output power versus pump power was measured for different operating temperature, 9°C, 15°C, 20°C, and 25°C, at 50 kHz repetition rate and the result was shown in Fig. 6.2-6(a). Increase of temperature leads to the reduction of conversion efficiency and this result demonstrates the reduction of quantum defect is a practical way to improve optical conversion efficiency. The optical conversion efficiency could be up to 30% under the operating temperature of 9°C. Compared with barrier pumping which shows an optimum efficiency in 30 kHz repetition rate, the optical conversion efficiency exceeds 3 times and over 20% of enhancement was obtained. The operation of 20-kHz pulse repetition rate was chosen to evaluate the performance of output peak power due to shorter pulse and available maximum pump peak power. For the operation at the temperature of 9 °C, the output peak power from double chips at 1555 nm versus the absorbed pump power at pulse repetition rate of 20 kHz was measured and shown in Fig. 6.2-6(b). At the pump peak power of 3.7 kW, the maximum output peak power up to 0.52 kW was generated.

The typical pump and output pulse train as well as extended pulse shape of single pulse was recorded by a Lecroy digital oscilloscope (Wave pro 7100, 10G samples/sec, 1 GHz bandwidth) and shown in Fig. 6.2-7. The output pulse with long tail follows in the characteristic of pump source. But the turn-on time of output pulse is slightly different between in-well and barrier pumping (Fig. 6.1-4), where the former has a nearly 10-ns advance. The output peak power fluctuates within 10% variation and it mainly comes from the fluctuation of pump source. Experimental result shows that the output beam possesses an excellent beam quality. The half divergence angle of output beam was measured by using knife-edge method to be approximately 0.01 rad. Consequently, the M square value was estimated to be smaller than 1.3.



(a)



(b)

Fig. 6.2-6. (a) The output characteristics of double chips in in-well pumping (50 kHz) and of single chip in barrier pumping (30 kHz) were measured for the operation of different temperature. (b) The output peak power of double-chip in-well pumping AlGaInAs laser at the repetition rate of 20 kHz.

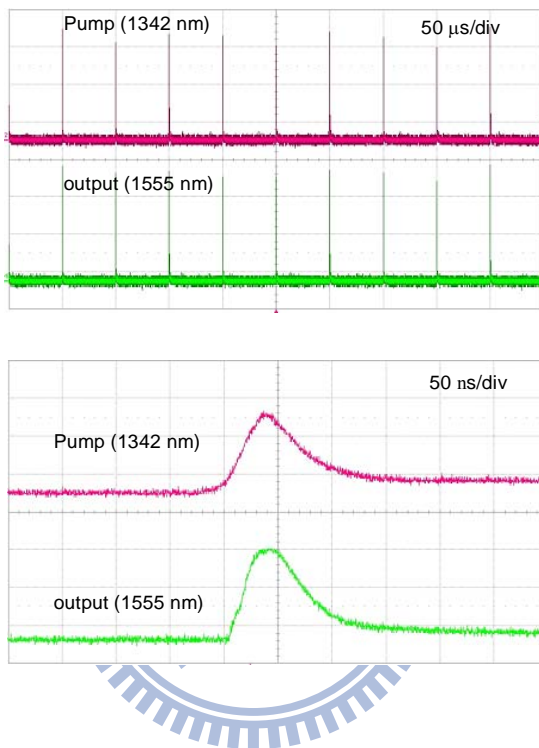
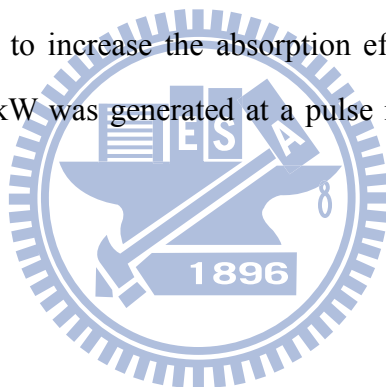


Fig. 6.2-7. The typical pump and output pulse train and the expanded pulse shape of a single pulse.

6.3 Conclusion

We first demonstrated an optically pumped semiconductor laser with barrier pumping scheme. A high-repetition-rate high-peak-power AlGaInAs 1.57- μm TEM₀₀ laser driven by a diode-end pumped actively Q-switched 1.06- μm laser was realized. With an average pump power of 1.25 W, an average output power of 135 mW was produced at a repetition rate of 30 kHz. The maximum peak power was up to 290 W at a peak pump power of 2.3 kW and a pulse repetition rate of 20 kHz. In order to further enhance the conversion by reduce the thermal effect, the pumping scheme was modified from barrier pumping into in-well pumping where an actively Q-switched 1.342- μm laser was used as pumping source. With lower quantum defect, the thermal effect in gain medium decreases and results in improvement of optical conversion efficiency. The conversion efficiency is enhanced over three times. By means of double gain chips to increase the absorption efficiency of pump laser and a high peak output power of 0.52 kW was generated at a pulse repetition rate of 20 kHz and peak pump power of 3.7 kW.

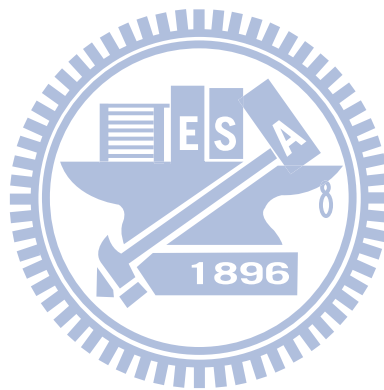


References

- [1]. K.W. Su, S.C. Huang, A. Li, S.C. Liu, Y.F. Chen, K.F. Huang, "High-peak-power AlGaInAs quantum-well 1.3- μm laser pumped by a diode-pumped actively Q-switched solid-state laser," *Opt. Lett.* **31**, 2009–2011 (2003)
- [2]. J.J. Zayhowski, A. Mooradian, "Single-frequency microchip Nd lasers," *Opt. Lett.* **14**, 24–26 (1989)
- [3]. G.J. Dixon, L.S. Lingvay, R.H. Jarman, "Properties of close coupled monolithic, lithium neodymium, tetraphosphate lasers," *Proc. SPIE* **1104**, 107 (1989)
- [4]. Y.F. Chen, "Compact efficient all-solid-state eye-safe laser with self-frequency Raman conversion in a Nd:YVO₄ crystal," *Opt. Lett.* **29**, 2172–2174 (2004)
- [5]. Y.F. Chen, "Efficient 1521-nm Nd :GdVO₄ Raman laser," *Opt. Lett.* **29**, 2632–2634 (2004)
- [6]. C. E. Zah, R. Bhat, B. N. Pathak, F. Favire, W. Lin, M. C. Wang, N. C. Andreadakis, D. M. Hwang, M. A. Koza, T. P. Lee, Z. Wang, D. Darby. Flanders, and J. J. Hsieh, "High-performance uncooled 1.3- μm Al Ga In As/InP strained-layer quantum-well lasers for subscriberloop applications," *IEEE J. Quantum Electron.* **30**, 511–521 (1994).
- [7]. N., J. M. Hopkins, A. J. Kemp, N. Schulz, M. Rattunde, J. Wagner, M. D. Dawson, and D. Burns, "Pulsed pumping of semiconductor disk lasers," *Opt. Express* **3**, 3247-3256 (2007)
- [8]. S. Calvez, N. Laurand, H. D. Sun, J. Weda, D. Burns, M. D. Dawson, A. Harkonen, T. Jouhti, M. Pessa, M. Hopkinson, D. Poitras, J. A. Gupta, C. G. Leburn, C. T. A. Brown, and W. Sibbett, "GaInNAs(Sb) surface normal devices," *Phys. Status Solidi* **205**, No 1, 85-92 (2008).
- [9]. S. C. Huang, H. L. Chang, K. W. Su, A. Li, S. C. Liu, Y. F. Chen, and K. F. Huang, "AlGaInAs/InP eye-safe laser pumped by a Q-switched Nd:GdVO₄ laser," *Appl. Phys. B* **94**, 483-487 (2009).
- [10]. M. Schmid, S. Benchabane, F. T. Goudarzi, R. Abram, A. I. Ferguson, and E. Riis,

“Optical in-well pumping of a vertical-external-cavity surface-emitting laser,” Appl. Phys. Lett. **84**, 4860-4862 (2004).

- [11]. J. Wagner, N. Schulz, M. Rattunde, C. Ritzenthaler, C. Manz, C. Wild, and K. Köhler, “Barrier- and in-well pumped GaSb-based 2.3 μm VECSELs,” Phys. Status Solidi **4**, No 5, 1594-1600 (2007).



Chapter 7



Summary

7.1 Contribution of this dissertation

The contributions of this dissertation are as follows.

1. I confirm the threshold of a passively Q-switched intracavity OPO pumped in a shared resonator is essentially determined by the bleach of the saturable absorber not by the signal output reflectivity. As a result, the output performance such as pulse energy or peak power can be optimized by optimizing the reflectivity without considering the threshold. An eye-safe laser at 1572 nm with 1.5 MW peak power and 3.3 mJ pulse energy was obtained with 15% signal output reflectivity. A 10-mJ eye-safe laser was further achieved by scaling up the cross section of element and pump power. In addition, I integrated the influence of depolarization of electric fields into the rate equations of Q-switched and OPO process to analyze the output dynamics in time domain. The depolarization induced by the thermally induced birefringence effect in the gain medium, Nd:YAG, results in parasitic and multi-peak pulse. The experimental result shows a good agreement with the numerical analysis indicates that the theoretical model is ascertained.
2. A double-end diffusion-bond Raman crystal, Nd:YVO₄, was first employed in the self-SRS. The thermal lensing effect was greatly decreased and consequently the output performance including the slope efficiency, available maximum power and the lasing threshold was improved. With an input pump power of 17.2 W, the maximum average power at 1525 nm is 2.23 W at a pulse repetition rate of 40 kHz, corresponding to conversion efficiency of 13%. The pulse width of Raman pulse is about 3.2 ns corresponding to a peak power of 17.4 kW. The maximum average output power with the composite crystal is found to be nearly 40% higher than that with a conventional Nd:YVO₄ crystal at the same pulse repetition rate.
3. A periodic AlGaInAs semiconductor saturable absorber in an Er/Yb codoped double cladding fiber laser at 1560 nm was firstly proposed and demonstrated. Greater than 1.26 W of an average output power at a repetition rate of 12 kHz was generated with a 13.5-W diode pump power. It turns out a pulse energy more than 100 μ J was obtained. The

maximum peak power is higher than 500 W. The remarkable performance confirms the prospect of using AlGaInAs QWs as saturable absorbers in passively Q-switched eye-safe lasers. Moreover, the present result indicates that the output peak power can be significantly enhanced by using a fiber with a larger core size and a saturable absorber with a lower initial transmission.

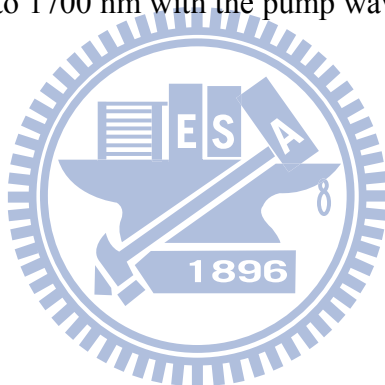
4. I realized a widely tunable eye-safe laser from 1513 nm to 1593 nm by incorporating a passively Q-switched photonic crystal fiber laser and an external-cavity optical parametric oscillator. The wavelength tuning range is up to 80 nm. The passively Q-switched PCF laser utilized an AlGaInAs Qs/barrier structure as a saturable absorber and output a 1029-nm fundamental pulse with energy up to 750 μJ . The output pulse was incident into an external OPO cavity. Under the pump energy of 390 μJ at 1029 nm, the maximum output energy and peak power of signal wave was found to be 138 μJ and 19 kW with repetition rate up to 6 kHz.
5. I accomplished a high-peak-power optically pumped semiconductor disk laser pumped with an actively Q-switched laser in two pump configurations. The gain medium is an AlGaInAs quantum well/barrier structure consisting thirty groups of two 1550~1570-nm AlGaInAs QWs. In the first configuration, referred to as barrier-pumping, the carriers were pumped by the 1064 nm Q-switched laser in the barrier region and radiate in QWs. An average output power of 135 mW with a pulse width of 30 ns at a pulse repetition rate of 30 kHz was obtained with an average pump power of 1.5 W. The optical-to-optical conversion efficiency is around 9%. The maximum peak power was up to 290 W at a pulse repetition rate of 20 kHz. In the second configuration, referred to as in-well pumping, the carriers were pumped by an actively Q-switched 1342-nm laser directly in the QWs to reduce the quantum defect. With lower quantum defect, the thermal effect in gain medium decreases and results in improvement of optical conversion efficiency. The conversion efficiency is enhanced over three times compared with barrier pumping. A high peak output power of 0.52 kW was generated at a pulse repetition rate of 20 kHz and peak pump power of 3.7 kW. The output power was limited by the available pump power

and roll-over has not been observed. For both barrier-pumping and in-well pumping configurations, the high beam quality was obtained with M^2 smaller than 1.3.



7.2 Future work

In Chapter 5 I report a widely tunable eye-safe laser by means of an OPO with PPLN nonlinear crystal. The tuning range distributes from 1513 nm to 1583 nm with increasing the temperature of PPLN from 20°C to 140°C. The average shift coefficient is around 0.58 nm/°C. In the future, I will focus on the research of the tunable wavelength of eye-safe laser with narrow line width by utilizing a grating inside an intracavity OPO pumped with Yb doped PCF (Fig. 7.2-1(a)). Due to the broad emission band, the pump wavelength can be selected by a grazing incident grating in the cavity. A broader wavelength tunable laser could be more efficiently achieved by tuning the cavity mirror instead of the phase matching temperature of nonlinear crystal. In the premise of uniform output reflectivity, the wavelength of signal wave can be tuned from 1550 nm to 1700 nm with the pump wavelength from 1020 nm to 1070 nm (Fig. 7.2-1(a)).



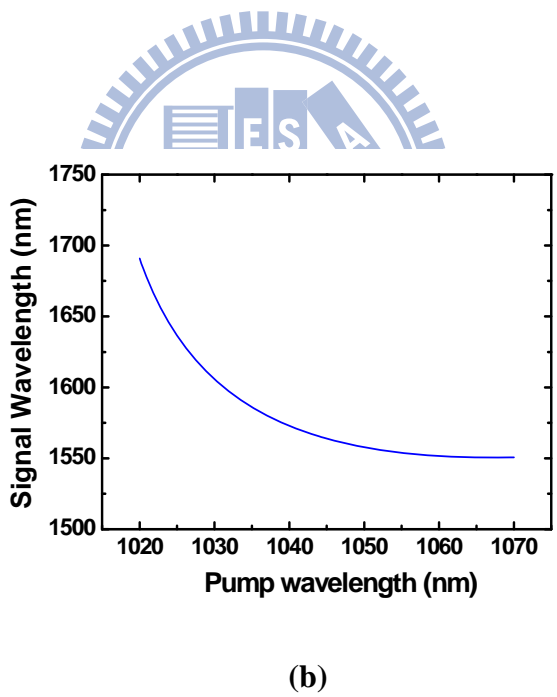
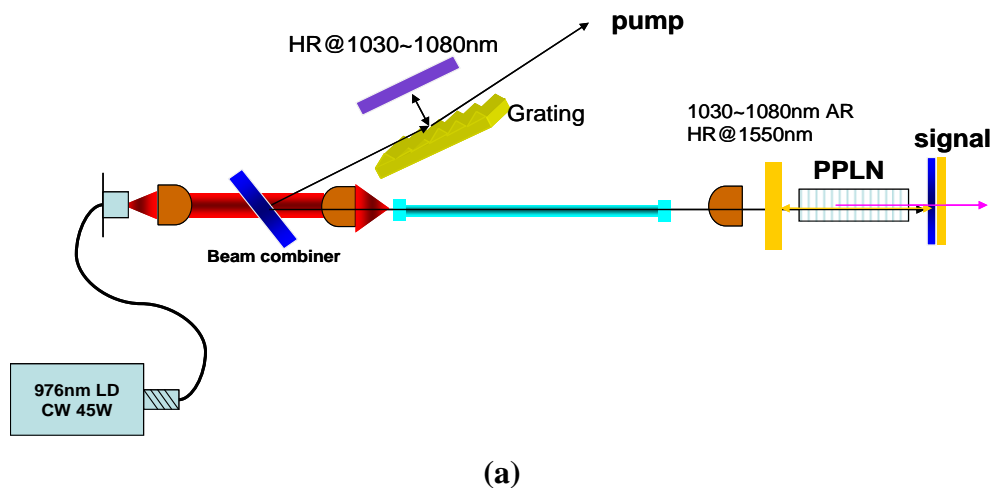


Fig. 7.2-1. (a) The concept of narrow-linewidth tunable eye-safe laser. (b) The simulated result of signal output wavelength pumped by tunable PCF laser.

Publication List

A. International journal papers

- [1]. J. Y. Huang, S. C. Huang, **H. L. Chang**, K. W. Su, Y. F. Chen, and K. F. Huang, "Passive Q switching of Er-Yb fiber laser with semiconductor saturable absorber," *Opt. Express* **16**, 3002-3007 (2008)
- [2]. S. C. Huang, **H. L. Chang**, K. W. Su, A. Li, S. C. Liu, Y. F. Chen, K. F. Huang "AlGaInAs/InP eye-safe laser pumped by a Q-switched Nd:GdVO₄ laser," *App. Phys. B*, Vol. 94, 483-487 (2009)
- [3]. H. C. Liang, **H. L. Chang**, W. C. Huang, K. W. Su, Y. F. Chen and Y. T. Chen, "Self-mode-locked Nd:GdVO₄ laser with multi-GHz oscillations: manifestation of third-order nonlinearity," *App. Phys. B*, Vol. **97**, 451-455 (2009)
- [4]. Y. P. Huang, **H. L. Chang**, Y. J. Huang, Y. T. Chang, K. W. Su, W. C. Yen, and Y. F. Chen, "Subnanosecond mJ eye-safe laser with an intracavity optical parametric oscillator in a shared resonator," *Opt. Express* **17**, 1551-1556 (2009)
- [5]. Y. T. Chang, K. W. Su, **H. L. Chang**, and Y. F. Chen, "Compact efficient Q-switched eye-safe laser at 1525 nm with a double-end diffusion-bonded Nd:YVO₄ crystal as a self-Raman medium," *Opt. Express* **17**, 4330-4335 (2009)
- [6]. **H. L. Chang**, S. C. Huang, Yi-Fan Chen, K. W. Su, Y. F. Chen, and K. F. Huang, "Efficient high-peak-power AlGaInAs eye-safe wavelength disk laser with optical in-well pumping," *Opt. Express* **17**, 11409-11414 (2009)
- [7]. Y. T. Chang, **H. L. Chang**, K. W. Su, and Y. F. Chen, "High-efficiency Q-switched dual-wavelength emission at 1176 and 559 nm with intracavity Raman and sum-frequency generation," *Opt. Express* **17**, 11892-11897 (2009)
- [8]. S. C. Huang, **H. L. Chang**, Yi-Fan Chen, K. W. Su, Y. F. Chen, and K. F. Huang, "Diode-pumped passively mode-locked 1342 nm Nd:YVO₄ laser with an AlGaInAs quantum-well saturable absorber," *Opt. Lett.* **34**, 2348-2350 (2009)
- [9]. **H. L. Chang**, W. Z. Zhuang, W. C. Huang, J. Y. Huang, K. F. Huang, and Y. F. Chen, "Widely tunable eye-safe laser by a passively Q-switched photonic crystal fiber laser and an external-cavity optical parametric oscillator, " *Laser Phys. Lett.* Vol **8**, 678-683 (2011).

B. International conference papers

- [1]. Y. C. Huang, **H. L. Chang**, and A. C. Chung, “Beat-wave laser driven photoinjector for superradiance free-electron laser,” 28 th International Free-electron Laser Conference, THPPH50, Berlin , Germany , Aug. 27- Sep. 1, 2006.
- [2]. T. D. Wang, **H. L. Chang**, A. C. Chiang, Y. C. Huang, “Narrow-line, high-repetition-rate THz-wave Generation from Collinearly Phase-matched Periodically Poled Lithium Niobate,” OSA Topic Meeting: Optical THz Science and Technology, March 18-21, 2007, Orlando, Florida, USA.
- [3]. T. D. Wang, **H. L. Chang**, S. T. Lin, Y. Y. Lin, A. C. Chiang, and Y. C. Huang, “Narrow-Line, High-Repetition-Rate THz-Wave Generation from Collinearly Phase-Matched Difference-Frequency Mixing in Periodically Poled Lithium Niobate,” CLEO2007 (JWA98), May 6-11, 2007, Baltimore, Maryland, USA.

C. Domestic conference papers

- [1]. **H. L. Chang**, A. C. Chiang, Y. H. Lin, Y. Y. Lin, and Y. C. Huang, “Miniature superradiance free-electron laser,” PSROC-2007 oral presentation, CL0-06, Chungli, January 23-25.
- [2]. **H. L. Chang**, S. C. Huang, Y. F. Chen, and K. F. Huang, “Optically pumped AlGaInAs quantum-well 1.36 μ m laser with a diode-pumped actively Q-switched solid-state laser,” PSROC-2008 poster presentation, PE-08, Hsinchu, January 28-30.
- [3]. **H. L. Chang**, Chih-Min Liao, Shin-I Ma, Chin-Der Hwang, Wen-Cheng Huang, Yi-Yuh Hwang, Chun-Hao Chen, Tin-Wei Chiang, and Mau-Ran Wang, “The method for maintaining optical speckle shape-invariant in a broad range of motions,” PSROC-2011 poster presentation, EP-103, Taipei, January 25-27.